Heavy Metal Detection in Crops and Soil Clay Mineral Abundance Mapping using Hyperspectral Data

by

SWATI PRIYA
201621014

A Thesis Submitted in Partial Fulfilment of the Requirements for the Degree of

DOCTOR OF PHILOSOPHY

to

DHIRUBHAI AMBANI INSTITUTE OF INFORMATION AND COMMUNICATION TECHNOLOGY

December, 2023

Declaration

I hereby declare that

i) the thesis comprises of my original work towards the degree of Doctor of Philosophy in at Dhirubhai Ambani Institute of Information and Communication Technology and has not been submitted elsewhere for a degree,

ii) due acknowledgment has been made in the text to all the reference material used.

Swati Priya

Certificate

This is to certify that the thesis work entitled HEAVY METAL DETECTION IN CROPS AND SOIL CLAY MINERAL ABUNDANCE MAPPING USING HYPERSPECTRAL DATA has been carried out by SWATI PRIYA for the degree of Doctor of Philosophy in at *Dhirubhai Ambani Institute of Information and Communication Technology* under our supervision.

Prof. Ranendu Ghosh
Thesis Supervisor

Dr. Srimanta Mandal
Thesis Co-Supervisor

Acknowledgments

First and foremost, I am extremely grateful to Dr. Ranendu Ghosh, my research supervisor, for his guidance, support and motivation throughout this work. He inculcated in me the much required analytical approach towards problem-solving. It has been a great learning journey working under his guidance. I am also thankful to my Co-supervisor Dr. Srimanta Mandal, who was always approachable for expert guidance throughout my research.

I offer my sincere thanks to Dr. Bimal Bhattacharya, Senior Scientist, SAC, Ahmedabad and Dr. Pankaj Kumar, Professor DA-IICT, for their constructive scientific inputs during the research progress seminar.

I am also thankful to the Vice Chancellor of SDAU, Dantiwada for their support in completing the pot experiment and for providing the necessary facilities at their labs. My sincere gratitude to Dr. B T Patel, Head of Central Instrumentation Lab, SDAU, for his valuable guidance in completing the pot experiment and preparation of soil samples. Thanks are also due to Mr. Jayesh, Assistant at SDAU, for helping during pot experiment. I also want to thank Mr. V. G. Vyas, Food Testing Laboratory, JAU, Junagadh for carrying out analysis of soil and plant samples.

I sincerely thank SAC (ISRO), Ahmedabad for providing the hyperspectral data under the AVIRIS-NG AO project and for facilitating the ASD instrument during the control pot experiment. I also thank IIT Gandhinagar for providing the necessary infrastructure to carry out the XRD analysis of clay samples.

I am deeply thankful to Viral Dave, Megha Pandya and Srikumar Sastry, co-researchers at Geospatial Lab, DA-IICT, Gandhinagar for their constant encouragement and support during this research work.

Contents

Abstract

Presence of heavy metal in crops is an indicator of environmental pollution. The heavy metals found in the plant indicate that the specific metal exists in the terrestrial environment. These metals affect leaves' spectral characteristics and interfere with plants' biochemical features, such as chlorophyll concentration and photosynthesis. Accurate detection of heavy metals in plants is necessary for agricultural management and to preserve ecological balance. Field spectroscopy techniques are used to measure the spectral changes triggered due to contamination with heavy metals. The advantage of these remote sensing approaches to assess heavy metal contamination is that they can frequently collect data across a wide geographic area.

The study mainly focuses on detecting different levels of heavy metal pollution from airborne hyperspectral data using reference data from *in situ* controlled pot experiments. We constructed a training set spectrum from a controlled experiment on cotton and tobacco for two important heavy metals, Lead (Pb) and Cadmium (Cd). Cotton and tobacco crops were grown in pots after artificially contaminating the soil with four Pb and Cd heavy metal treatments. The hyperspectral and biochemical data generated spectra of heavy metal concentrations at different crop growth stages. Standard reflectance spectra at different contamination levels do not show significant changes at different wavelengths due to the presence of heavy metal. These spectra were further decomposed using wavelet transform at different levels to capture the subtle changes in spectra using the detailed component of wavelets. The reconstructed detailed wavelet reflectance at the third level of decomposition was found to be significant with heavy metal stress. The correlation analysis established that the wavelength range of 651-742

nano meter (nm) in cotton was sensitive to Pb stress, and 631-802 nm was sensitive to Cd stress in tobacco. The reconstructed detail reflectance at a particular wavelength was then further used as reference spectra with different heavy metal levels to map heavy metal pollution.

The AVIRIS-NG data obtained for the study area was first classified to identify the tobacco crop in the Anand region and the cotton crop in the Surendranagar region using a combination of Autoencoder (AE) for feature extraction followed by an artificial neural network for classification. The training data obtained from the pot experiment were utilized to map Pb and Cd pollution from classified airborne hyperspectral data from Airborne Visible InfraRed Imaging Spectrometer - Next Generation (AVIRIS-NG) using a spectral matching algorithm known as Dynamic Spectral Warping (DSW). The results confirm the efficiency of the developed algorithm in estimating Cd content in tobacco and Pb content in cotton crops. The model was validated by collecting the exact field points and heavy metal concentration, which shows a promising result for this algorithm.

Diverse soil minerals may be easily identified through modern hyperspectral technology for remote sensing. The aerial hyperspectral sensor's enhanced spatial and spectral resolution can identify the abundance of several clay minerals, such as Kaolinite, Montmorillonite, and Illite. This study maps the clay mineral distribution in the Udaipur area of Rajasthan and the Ambaji region of Gujarat using hyperspectral data acquired by the AVIRIS-NG sensor on an airborne platform.

The representative soil sampling sites were selected from hyperspectral data using the Spectral Feature Fitting (SFF) algorithm. X-ray Diffraction (XRD) analysis was carried out to find different clay minerals in the samples. Then the regression analysis was carried out to find the relation between Absorption Peak Depth (APD) extracted from hyperspectral data corresponding to the actual location of sampling sites and the corresponding clay percentage obtained from XRD analysis. Regression analysis between absorption peak depth values estimated from hyperspectral data at 2205 nm – 2214 nm spectral region of soil sampling sites and corresponding clay content value showed a significant relationship. The regression line obtained for the known pixel is used to prepare the mineral abun-

dance map over the study area. The study over the Udaipur region shows the dominance of montmorillonite clay minerals, and the Ambaji region showed an abundance of kaolinite.

List of Figures

List of Tables

Acronyms

μM Micromolar

AE Autoencoder

ANN Artificial Neural Network

APD Absorption Peak Depth

AVIRIS-NG Airborne Visible InfraRed Imaging Spectrometer - Next Generation

Cd Cadmium

Co Cobalt

Cr Chromium

CRD Completely Randomized Design

Cu Copper

DAS Days After Sowing

DAT Days After Transplanting

DSW Dynamic Spectral Warping

FCC False Color Composite

FOV Field of View

Hg Mercury

ICA Independent Component Analysis

ICDD International Centre for Diffraction Data

ICP-AES Inductively coupled plasma-atomic emission spectroscopy

IIT Indian Institute of Technology

JPL Jet propulsion Laboratory

LLE Linear Local Embedding

MCARI Modified Chlorophyll Absorption Ratio Index

Mn Manganese

MNF Minimum Noise Fraction

MTMF Mixture Tuned Matched Filtering

NDRE Normalized Difference Red Edge Index

Ni Nickel

NIR Near Infrared

nm nano meter

NN Neural Networks

Pb Lead

PCA Principle Component Analysis

REP Red Edge Position

RMSE Root Mean Square Error

RMSEP Root Mean Square Error of Prediction

SDAU Sardarkrushinagar-Dantiwada Agricultural University

SEM Scanning Electron Microscopy

SFF Spectral Feature Fitting

Sn Tin

SWIR Short wave Infrared

TF Transfer Factor

USGS United States Geological Survey

WT Wavelet Transform

XRD X-ray Diffraction

Zn Zinc

CHAPTER 1

Introduction and Literature Survey

1.1 Presence of heavy metal in vegetation

The recent era of modernization has increased the risk of heavy metal pollution due to the upscaling of developmental activities like mining, smelting, manufacturing, and processing industries. Anthropogenic activities and weathering of parent material result in the release of heavy metals in soils [3]. As per the reports, industrial, agricultural, and automobiles are various sources accounting for heavy metals in the environment [4][5]. The indiscriminate use of these heavy metals in industries, agriculture, and day-to-day applications has made them significant contaminants of the environment [6].

Heavy metals are naturally occurring elements in trace quantities throughout the earth's crust with a specific density greater than 5 $g.cm^{-3}$, for example, Lead (Pb) , Cadmium (Cd), Chromium (Cr), Mercury (Hg), Zinc (Zn), Manganese (Mn), Cobalt (Co), Nickel (Ni),Copper (Cu) and Tin (Sn) among others [7]. Some heavy metals are considered essential, like Cu, Mn, Fe, Zn, and Ni due to their requirement for the growth of plants and animals. At the same time, some heavy metals like Pb, Cd, and Hg are classified as non-essential due to their lack of a prominent role in the growth and metabolic processes of organisms. These non-essential heavy metals are harmful as they are highly toxic, easily absorbed by plants, and not biodegradable [8][9].

In the past few years, there has been an increase in public awareness related to ecological safety and human health due to heavy metal pollution. Furthermore, heavy metal contamination has become a topic of primary environmental con-

cern due to its impact on agricultural soil and the plant produce, affecting food quality and safety. Agriculture soil is more frequently exposed to heavy metals because of innovations in farming techniques and the existence of heavy metals in pesticides, fertilizers, and manures. The agricultural land adjacent to various industries is more susceptible to heavy metal pollution due to industrial effluent's movement through water and soil. However, a few heavy metals like Cu, Zn, Co, and Mn are helpful for plant growth when applied in trace amounts, as they are constituents of several vital enzymes for their metabolic activities. The excessive accumulation of toxic and non-essential heavy metals, such as Pb, Hg, Cr, and Cd, in agricultural soils not only results in environmental contamination but also elevates heavy metal uptake by crops and increases its concentration in plant tissues causing a significant reduction in plant growth [10].

Among the various non-essential heavy metals, Pb and Cd are the most common heavy metal in the environment, which are considered highly toxic to plant and human health. Pb is the leading environmental pollutant released from car exhaust and fertilizers containing heavy metal contaminants [11]. It accumulates in various parts of plants, such as roots, stems, and leaves, from contaminated soil, and accumulation increases with increasing Pb contamination [12] [13]. It affects plant growth due to its effect on photosynthesis and other enzymatic activities [10]. Excessive Pb exposure results in mental retardation and behavioral disorders in humans [14]. Similarly, cadmium is a heavy metal of significant environmental concern, particularly for crops, due to its high toxicity, relative mobility, and high-water solubility. The primary source of Cd in the earth's crust is rock phosphate, which contains about 15 $mg.kg^{-1}$ Cd [15]. Agricultural soils are contaminated with Cd through the indiscriminate use of phosphate fertilizers [16]. The plants absorb heavy metals through contaminated soil, adversely affecting plant growth and animals and humans consuming such plants. It enters the food chain and threatens human and animal life due to various health risks [17].

Heavy metals directly affect crops by altering the plant's metabolic, physiological, and biochemical processes. The response of plants differs due to different heavy metal concentrations depending on factors such as soil, type of heavy

metal, and plant growth conditions. The excessive buildup of heavy metals in plants may adversely affect their development by interfering with cellular function and deteriorating photosynthetic pigments, resulting in a reduction of chlorophyll pigment and other enzymatic activities [18] [12] [19].

Heavy metals and plants interact in a specific manner. Plants exhibit the ability to absorb heavy metals from the soil, accumulate in different parts, and serve as a critical indicator of heavy metal pollution in a particular region. Therefore, vegetation plays a vital role in studying the presence of these heavy metals in the environment and their interaction with plants and animals. Few plants can survive in the presence of heavy metals without early signs of degradation, making them an effective tool for monitoring heavy metal pollution before further damage occurs in the contaminated area. Effective prevention measures can reduce heavy metal contamination in suspected areas and early recovery in the areas where accumulation has already occurred [20]. Presently, the field-based analytical method is used for detecting the presence of heavy metals in plants by sample collection and chemical analysis. The process is relatively costly and time-consuming so it can be utilized on a small scale [21].

1.2 Relevance of remote sensing for detection of heavy metal pollution in vegetation

Traditional field sampling and laboratory analysis methods are expensive and inefficient for the investigation of large areas [22]. Besides, it cannot be used for early detection and is concentrated over mining or industrial area where there is a possibility of heavy metal contamination but not in general fields, which also get polluted by heavy metal due to excessive use of fertilizers or accidental contact with industrial effluents. In comparison, remote sensing can be effectively used for wide-scale and rapid monitoring of heavy metal contamination. Remote sensing is defined as the science of obtaining information about any object or area by remotely capturing electromagnetic radiation reflected from the target [23]. Remote sensors provide timely coverage of large areas, which is helpful in sur-

veying natural resources and monitoring the environment. In recent years, it has become an increasingly important science with an improved understanding of environmental processes, conditions, and changes affecting both human and ecological health [24]. In recent years, advanced remote sensing techniques such as hyperspectral technology have been used for assessing crop biophysical and biochemical properties [25], crop health [26], water content [27] as well as detecting heavy metal pollution [28] [29].

Remote sensing is being widely used for mapping heavy metal contamination of plants. The presence of heavy metal may not be so high to trigger a direct effect on vegetation, so these studies rely on hyperspectral remote sensing with advanced technology and high resolution. Hyperspectral images provide continuous spectral information over a wide range of electromagnetic spectra, which provide more detailed changes in spectral properties of the plant under heavy metal stress and can be used for mapping and monitoring heavy metal contamination. Hyperspectral indices and derivatives enhance the signal of the target metals by optimizing the noise. The most used wavebands lie within the visible-near infrared portion of the spectrum. In comparison, mid- and far-infrared wavelengths are used far less frequently [30]. Depending on the material's spectral response, reflectance spectroscopy is also relatively less expensive and faster than traditional wet chemical measurements.

1.2.1 Effect of heavy metal on vegetation spectral signatures

Every material on the earth has a unique way of reflecting electromagnetic radiation called its spectral signature. The spectral signature of vegetation is mainly a function of pigment, cellular structure, tissue's optical properties, water present, and viewing geometry and illumination angle and provides essential information about the biophysical and biochemical properties of plants [31]. The study of spectral reflectance by the researcher can give an insight into plant condition and health as well as any stress on plants [32]. Figure 1.1 shows the spectral signature of vegetation in detail.

The spectral signature of a healthy leaf follows a bimodal reflectance pat-

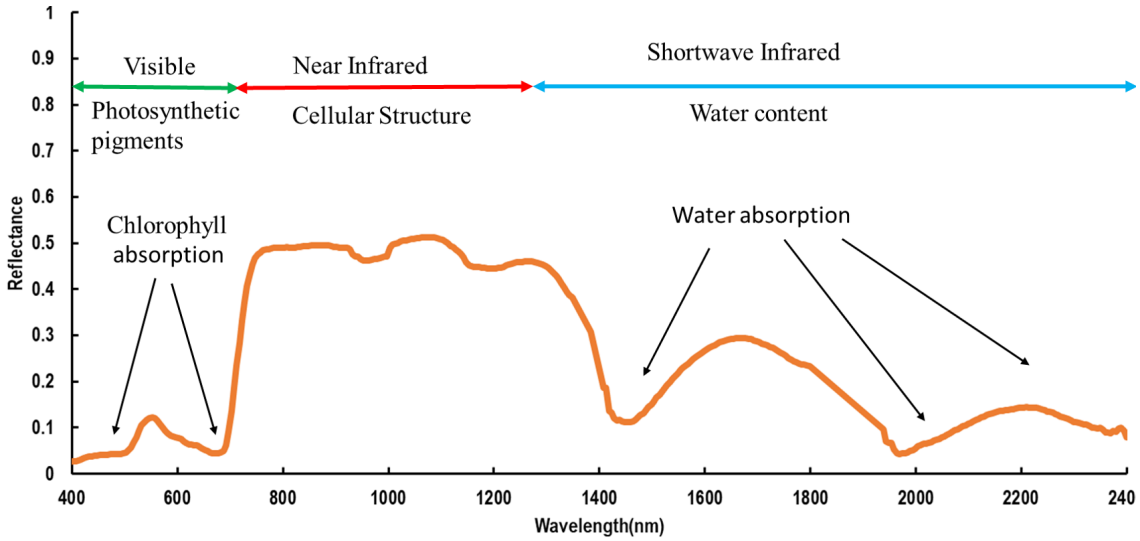

Figure 1.1: Spectral signature of vegetation[1]

tern across the electromagnetic spectrum, falling in the visible, near-infrared, and shortwave infrared regions [1]. The significant factors affecting vegetation reflectance are photosynthetic pigments, mainly chlorophyll, cellular structure, leaf water, and the presence of other biochemicals such as lignin and cellulose [33]. In the visible region, strong absorption occurs due to photosynthetic pigments like chlorophyll a and b in blue ($450nm$) and red ($680nm$) bands, followed by strong reflectance in the Near Infrared (NIR) region due to scattering of light by leaf mesophyll tissues and absorption features due to leaf water in Short wave Infrared (SWIR) region (at about 1400 and 1900nm) of the electromagnetic spectrum [1]. During leaf stress, as chlorophyll decreases, the spectral response of leaves shows a reduction in the absorption in the red region as well as the shift in absorption peak in the red region (red edge position) toward shorter wavelengths, known as blue shift [34]. The response of vegetation under heavy metal exposure has been examined to understand the importance of spectral reflectance in detecting plant stress. The presence of heavy metals causes changes in the internal structure of the leaf, directly and indirectly, influencing the reflectance. Elevated levels of heavy metals affect plant metabolisms and photosynthetic processes, causing a reduction in chlorophyll content by inhibition of chlorophyll biosynthesis. In some cases, the substitution of the central Mg ion occurs with the absorbed metal ion in chlorophyll molecules, resulting in a breakdown of photosynthesis which

ultimately affects plant growth [30][35].

Plants exposed to heavy metals have subtle differences in the spectra compared to healthy plants. These differences mainly occur in the visible and near-infrared regions of the electromagnetic spectrum[27]. Most of the studies the heavy metal concentration in leaves is concerned with various vegetation indices (ratios or linear combinations of two or more spectral wavelengths[35]and red edge position (a sharp transition between red and NIR wavelengths; positively related to chlorophyll concentration to study the stress [36]. Little research was carried out to find the effect of heavy metal pollution on the leaf reflectance by identifying optimal wavelengths to monitor a particular heavy metal. Heavy metal concentrations in plant leaves are not so much high as to cause significant changes in reflectance spectra under normal field conditions, and it is essential to diagnose metal-induced vegetation stress before any stress-related damage occurs [37] [38]. In this context, an integrated approach using in-field spectroscopy data from control experiments and hyperspectral data to detect heavy metal pollution has yet to be carried out. The proximal sensing for two primary heavy metals, Cd and Pb, was done to study their effect on leaf spectra of cotton and tobacco crops in a control pot experiment for generating reference spectra. These training sets obtained from controlled experiment was used for heavy metal detection in tobacco crop and cotton crop from airborne hyperspectral data over the Surendranagar and Anand region of Gujarat, respectively. This research utilizes a combined biochemical and spectral characteristics approach to evaluate crop performance under different heavy metal stress after artificial contamination with metal under study by integrating the in-field spectroscopy data with airborne hyperspectral data. Such a study can provide a theoretical basis for remote sensing of heavy metal-contaminated areas.

1.3 Literature survey

Given the impact of heavy metal, many researchers have conducted trials on various crops to test heavy metal stress on various biophysical and biochemical prop-

erties of plants.

1.3.1 Review of the effect of Pb and Cd on crop

Pb and Cd are non-essential hazardous elements for plants but can accumulate in different plant parts and hamper the growth and physiological processes [39]. Various studies revealed the harmful effects of high concentrations of heavy metals on the germination, growth, and physiological processes of plants [40] [41]. Among all the metabolic processes, photosynthesis is one of the most significant physiological traits of plants reported to be negatively impacted by heavy metals [42]. Photosynthetic inhibition during heavy metals stress is one of the prominent actions in plants because the presence of toxic element influences the biosynthesis of photosynthetic pigments like chlorophyll and carotenoids and affect different photosynthetic apparatus and their functions [43]. Various studies have examined the harmful effect of Pb and Cd on plant growth parameters in pot studies and greenhouse experiments by artificially contaminating the soil with various heavy metals.

Pb has been reported to be phytotoxic due to its harmful effects on different plant growth parameters and photosynthesis [44][45][46]. In a laboratory-scale experiment conducted to determine the toxic effects of different concentrations of Pb (2, 4, and 6 $mg.l^{-1}$) on the total chlorophyll $(a + b)$ content of aquatic plant tissues *Ceratophyllum demersum*., it was found that the content of total chlorophyll decreased noticeably, with increasing initial concentrations of Pb compared to control plants [47]. In a field experiment conducted on the effect of Pb stress on cotton plants, it was established that Pb toxicity caused a sharp decline in photosynthetic pigments such as chlorophyll a, chlorophyll b, total chlorophyll, and carotenoids values at both levels of Pb ($50\ and\ 100\ \mu M$)) [48]. A greenhouse study to determine Pb's phytotoxic effect on *Helianthus* revealed that various growth parameters were affected due to the accumulation of different levels of Pb in the soil compared to the control [49]. Similar studies on the phytotoxic effect of Pb on various species, including *Triticum aestivum* and *Spinacia oleracea* [50], *Solanum Melongena* [51], *Helianthus annuus* [52], *Brassica juncea* [53] [54], *Nicotiana tabacum*

[55], has also reported a decrease in chlorophyll content as well as growth due to presence of Pb. A pot experiment established that Pb metal has an adverse effect on chlorophyll content and photosynthetic efficiency of two cotton genotypes (Desi cotton and *Bt* cotton)[56]. Pb metal ions can accumulate in plants when their content increases in soil and have a very high transfer rate from soil to plants [57]. Various studies have been carried out to study the mechanism of accumulation of Pb in different plant species. Angelova et al. investigated the pollution level and how heavy metals enter the fiber crops by taking soil and plant samples from the heavy metal-polluted regions and a distinct pattern in the accumulation of heavy metals in the vegetative and reproductive organs of flax, hemp, and cotton was revealed. The distribution of heavy metals like Pb, Zn, Cu and Cd showed a selective preference in the plant parts, with more accumulation in the cotton leaves than in other parts [58]. Wang et al., in a study, found that Cotton cultivars can survive Pb concentration up to $200 mg/l$ with little effect on growth [59]. The accumulation of Pb in plants from soil varies in different species and increases or decreases with the amount of Pb in soil [60] [61].

Among toxic heavy metals, Cd is the most persistent in soil and harmful to plants when absorbed by plants. Cd toxicity severely inhibits crop yield and quality by affecting critical physiological and biochemical processes, such as inhibition of photosynthesis, cell wall biosynthesis, and remodeling. Various studies have observed the effect of heavy metals on physiological and biochemical parameters [62][63]. The presence of Cd affects photosynthesis as it interferes with enzymatic activities and the synthesis of photosynthetic pigments like chlorophyll. Cd toxicity in plants can decrease chlorophyll synthesis, resulting in yellowing leaves [64] [65]. Various studies and experiments have been conducted to study the harmful effect of Cd. The presence of Cd caused a decrease in chlorophyll concentration in different plants. The deleterious effect of Cd on chlorophyll has been observed in lady's finger [66], [67], Chinese mustard [68], [69], maize [70], seagrass [71], and *Brassica campestris* [72]. The uptake and accumulation of Cd in plants from the contaminated soil mainly depend on the type of plant and its ability to accumulate Cd present in the soil [73] [74].

Various research has established a distinct ability of tobacco plants to absorb Cd and act as an efficient accumulator of Cd among various heavy metals. Typically, heavy metals accumulate in roots due to their less mobility, but in the case of the tobacco plant, Cd Concentration is higher in leaves. Tobacco can accumulate more Cd in leaves even under low exposure conditions than other plants [75] [76]. Cd concentration in tobacco leaves is affected by soil conditions, climatic conditions, and tobacco varieties [77][78]. A pot experiment conducted in a greenhouse demonstrates that Cd concentrations in tobacco leaves increased by 48.89% ($P < 0.05$) in tobacco grown in soil severely contaminated with Cd ($30 mg/kg$) [79]. Halil et al. reported that higher doses of Cd concentration in soil harm tobacco growth. The study revealed that among various Cd levels ($0, 0.25, 2.5$, and $10 mg/kg$), even a lower dose of Cd up to $0.25 mg/kg$ significantly affects the tobacco plant [80]. A study conducted at Anand showed that the tobacco plant has higher heavy metal extraction efficiency than other field crops like sunflower and castor [81].

1.3.2 Review of hyperspectral remote sensing techniques for heavy metal detection

Heavy metal pollution is increasing worldwide, having an adverse effect on plants as well as human health. This problem can be efficiently addressed and managed by properly mapping the heavy metal-contaminated areas. Plants are essential for monitoring heavy metal's presence due to their ability to grow in heavy metal-polluted soils. Field-based methods for effectively mapping heavy metal contamination are costly, labor-intensive, and feasible for a small area. Remote sensing provides a good alternative for fast and effective real-time mapping over large areas. Remote sensing studies are vital in assessing vegetation's biotic and abiotic stress [82]. Various researchers reported that specific changes in spectral patterns, like the shift in red edge (680 nm to 730 nm) and other vegetation indices, are related to plant health and stress and can be used to study the quality of vegetation growth and health [83]. The presence of heavy metals like Pb and Cd causes physiological changes in leaves, which can lead to variations in the spectral

properties of leaves. These changes usually occur in the visible and near-infrared regions of the electromagnetic spectrum and cannot be captured by a multispectral sensor. Hyperspectral or imaging spectroscopy has recently emerged as a promising tool for heavy metal detection in a relatively wide area. Many spectral bands at minimum spectral intervals give an excellent spectral continuity with lots of spectral information and make it easy to measure slight differences in features of plants like disease detection [84], water content [85], heavy metal stress [86][87] and biophysical and biochemical properties [88][89]. Advanced hyperspectral technology has shown high potential in the early monitoring of heavy metal stress in vegetation due to its high spectral resolution and increased spectral sensitivity [90]. Several studies have also focused on in-field spectroscopy for rapid and non-destructive mapping of the heavy metal status of the crop based on in situ and high-efficiency monitoring of the spectral changes due to heavy metals. These studies have been used in controlled laboratory conditions or specific field environments for monitoring crops under heavy metal stress [91] [92][92]. Rosso et al. studied the effect of Cd stress on the reflectance of *Salicornia virginica* and showed a strong relationship between spectral response and heavy metal stress [93]. Various study shows researchers are using these techniques for early detection of heavy metal-induced stress to monitor overall vegetation health. In a controlled experiment, Ren et al. found that the spectral response due to changes in chlorophyll content and photosynthesis can be used to monitor heavy metal stress in paddy plants grown in contaminated soil [94]. Yang and Li conducted a series of pot experiments to study the effects of Cd. The findings show the chlorophyll concentration decreases with increasing Cd levels and higher tolerance of Brassica Juncea to increased concentration of Cd level in soil [95]. Rathod et al., in their controlled experiment with artificially contaminated soil, studied the changes in leaf reflectance spectra (350nm – 2500 nm) in barley plants grown in metal-spiked soils (3 levels of Cd, Pb, As and their metal-mixture treatments). The result shows heavy metal's adverse effect on barley growth [96].

Several researchers have also used vegetation spectral indices to characterize the variation in vegetation response to heavy metal stress. The spectral indices

such as normalized difference vegetation index, Modified Chlorophyll Absorption Ratio Index (MCARI), red-edge chlorophyll index, Red Edge Position (REP), and Normalized Difference Red Edge Index (NDRE) are effective in heavy metal assessment owing to their correlation with various metals [94] [97]. Ren et al. derived normalized vegetation indices for the detection of Pb, As, Zn, and Cu using different wavelengths [94]. Gu et al. predicted the Cd content in leaves of *Brassica rapa chinesis* growing on soils treated with Cd of different concentrations by incorporating the ratio of different wavebands, which reflects the changes in photosynthetic pigment and cell structure [98]. Wu et al. used REP to study the presence of Cd in rice [99]. Various spectral derivatives, and vegetation indices, such as absorption depth and distance of red edge position, showed a relationship with leaf heavy metal concentration [96][97]. In a previous study, Liu et al. proposed a hyperspectral index to monitor the subtle changes in the canopy chlorophyll content of rice due to arsenic stress. The proposed index performed better than the random forest model and other indices [100]. Also, many a time, the vegetation indices fail to distinguish heavy metal stress due to very minute changes in spectral signal [101].

To overcome these problems, various researchers have used methods to enhance the spectral signals, such as spectral absorption depth [96], the first and second derivative of spectra [102], and principal components [103] to extract useful spectral information from stressed vegetation. Only some studies focused on regression analysis, such as step-wise linear regression and partial least square regression, to build empirical models that quantify the relationship between spectral variables and biochemical and biophysical vegetation parameters under heavy metal stress [104][105]. Regression and correlation analysis using various spectral parameters has been used to determine the heavy metal content in plant leaves. Nowadays, researchers use sophisticated machine learning techniques such as Neural Networks (NN) in heavy metal studies [106] [107]. Liu et al. used a back-propagation neural-network model to quantify the relationship between the chlorophyll content of rice and Cd content [108].

Heavy metal concentrations in plant leaves are not high enough to cause sig-

nificant changes in reflectance spectra under normal field conditions. So various researchers have employed different methods like derivative or continuum-removed reflectance that can enhance the potential subtle spectral changes. Wavelet transform has been used in several studies to overcome such problems. It can preserve the peaks and valleys among spectral signatures to magnify subtle spectral features by decomposing a signal into a set of shifted and scaled versions of the original signal producing approximation (low-pass filter) coefficients and detail (high-pass filter) coefficients at various decomposition levels [109][110]. WT finds its use in spectral dimension reduction and denoising research [111] and is also successfully utilized in many fields of remote sensings for quantification of biochemical parameters in plant leaves, such as chlorophyll concentration [112], water content [113], and heavy metal concentrations [114]. Liu et al. used spectral parameters derived from wavelet analysis of leaf reflectance to estimate the concentration of Cd and Cu in rice leaves [114]. Wang et al. developed a wavelet-based area parameter in the wavelength region 605-720 nm sensitive to Cu stress. They used it for estimating the Cu concentration in *Carex* leaves using hyperspectral data [115]. In a recent study, Wavelet Transform (WT) was used to decompose the visible-near infrared (400 nm – 1000 nm) to extract features for prediction of heavy metals content by deep learning in lettuce leaves [116]. Findings of various research show that WT performs well in extracting weak spectral signals by suppressing spectral noises and can perform well in selecting characteristic wavelengths associated with heavy metal stress. The wavelet coefficients of hyperspectral reflectance are less sensitive to external environments, instrument noise interference, and leaf structures, thus enhancing their correlation with biochemical and biophysical vegetation parameters [116]. Conversely, research utilizing sensitive spectral features and determining effective characteristic wavelengths for heavy metal stress is still being determined.

The main challenge in heavy metal detection over a wide area is upscaling non-imaging in-field spectroscopy data to classify airborne hyperspectral data. The use of classification techniques like SVM (support vector machine) and Neural networks has limitations like a large amount of training data and computa-

tional cost. In this regard, the wavelet decomposition method can help determine the optimal wavelength region affected by heavy metal stress. The spectral matching of the training spectra with those obtained from airborne hyperspectral can provide insight into the level of heavy metal in the vegetation. This study proposes a new approach to trace the changes in reflectance patterns using dynamic spectral warping (DSW) based on conventional dynamic time warping (DTW) to overcome the challenges in heavy metal detection. In the past, DTW has been utilized for speech and biomedical signal recognition [117][118]. Also, several researchers have used DTW in the field of remote sensing. Maus et al. [119] used this algorithm for land use and land cover mapping, and Petitjean [120] used the DTW method for time series analysis using satellite data. Moola et al. used DTW to map vegetables from time series of Sentinel 1a images [121]. The researchers are yet to try mapping heavy metal presence by spectral pattern matching using wavelength intervals instead of the time interval.

1.4 Soil clay mineralogy

Soil is a dynamic and vital element of the natural ecosystem. It supports a diverse spectrum of species and is essential for plant development, breakdown, and the recycling of microbial biomass. Knowledge of different constituents of soil plays a vital role in various activities like agricultural planning and urban development.

Clay minerals, with less than two μm sized particles, are one of the critical constituents of the soil. They are formed due to hydrothermal alteration and weathering of the rocks [122]. Clay minerals influence different chemical and physical properties of soil, like the availability of nutrients, water retention capacity, and soil permeability [123]. These are secondary minerals defined as aluminosilicate or aluminum phyllosilicate with SiO_4 tetrahedra sheet as basic structural units [124]. The major groups of clay minerals present in the soil environment include layer and chain silicates based on the number of tetrahedral and octahedral sheets and their arrangements. Kaolinite, illite, and montmorillonite are the principal clay minerals influencing soil properties. They are layer silicates with

1 : 1 arrangement in kaolinite and 2 : 1 in montmorillonite and illite. Among them, montmorillonite is expanding clay belonging to the smectite group of clay minerals, and illite is non-expanding clay. The expanding clays have some prominent characteristics like high cation exchange capacity, swelling, and shrinkage capacity, which improves the soil structure and fertility, thus increasing crop productivity. The illite has a cation exchange capacity lower than montmorillonite but higher than kaolinite [122]. The study of the relative distribution of clay minerals in agricultural soil is of utmost importance for agricultural policy-making and land use planning. It is also crucial for ecological conservation as the soil is under tremendous strain from pollution, and soil deterioration makes it vulnerable to erosion [125].

Practical methods are required for mapping different clay minerals and their characterization. Traditional field and laboratory analyses are costly, tedious, and time-consuming and are usually limited to a few samples and fields, and lack information on the spatial variability of soil [126]. Remote sensing techniques are fast and cost-effective for retrieving soil properties for better soil interpretations. Remote sensing data facilitates soil mapping over large areas, even with rugged terrain otherwise inaccessible through field surveys. Researchers have used remote sensing techniques for soil studies in recent decades due to broader coverage of inaccessible areas and less cost [127]. The advancement to hyperspectral remote sensing or imaging spectroscopy has widened the scope of remote sensing in mapping earth surface features due to its improved spectral and spatial resolution [127][128]. A hyperspectral sensor that provides detailed information about the surface features at various wavelengths helps to map soil mineralogical features [126] like clay minerals [129][130]. Various soil scientists and researchers have tried to quantify the information about clay minerals from reflectance spectra using different methods.

1.4.1 Review of the work done in clay mineralogy

Remote sensing is an effective tool for monitoring soil and its constituents over a large area at a timely interval [131]. Continuous reflectance data with a small

spectral interval from hyperspectral sensors contains information about different soil properties [131]. The specific absorption features at a particular wavelength determine the characteristics of the soil [132] [133]. Various researcher has utilized these advanced remote sensing techniques to quantitatively estimate soil properties such as soil calcium carbonate [134], soil organic matter [135], exchangeable potassium [136], soil organic carbon [137] and soil clay minerals [138][139]. Gilles et al. analyzed the abundance of different soil clay minerals. They compared XRD measurements with estimations from spectroscopy to estimate the potential of field spectroscopy for geotechnical applications [140]. The most critical spectral features for identifying and mapping clay minerals occur at the wavelengths 1200nm, 1400nm and 2200nm due to the metal-OH bonds [136][141] [142]. The spectral features 1400 nm and 1900nm are influenced by water, making it difficult to use [142]. To relate the observed spectra to clay mineral abundances, it is also critical to understand the relationship between absorption strength and volume or weight abundance of the clay minerals in the observed pixel [130]. The complexity of reference spectra makes it challenging to quantify the information present, so various statistical approaches are required [130][143]. Linear regression models help to produce more accurate and updated soil property maps through large-scale studies to relate field-measured variables such as clay content to surface reflectance [143][144]. Mulder et al. tried to find the mineral abundances through regression tree analysis using a range of 2100-2300 nm [145]. Garfangoli et al. utilized high-resolution imagery from data from SIM-GA sensors to produce a high-quality clay map [143]. These strategies, however, fall short in terms of providing quantitative data. Moreover, difficult terrain, vegetation, and moisture variations complicate this process over large areas. Therefore, integrated efforts to overcome these challenges by combining airborne data with exact ground data from the laboratory are a requisite for clay mineral abundance mapping for specific regions.

1.5 Motivation of the work

Heavy metal pollution, especially in agriculture, has attracted considerable attention for sustainable development [10]. Heavy metals being non-degradable, migrate and accumulate in agricultural soils and get transferred into the food chain through crops grown on such soil. Heavy metal's presence in food chains endangers food safety and public health [20]. Furthermore, some contaminants accumulate in leaf tissues, bringing stress and interrupting photosynthetic processes in plants [82]. Due to the dynamic nature of these effects, early monitoring of contaminants can allow suppressive interventions before severe and irreversible vegetation and soil damage happens. In addition, vegetation spectral properties are functions of plant bio parameters, and plants reveal sensitivity to these properties in different spectral ranges (VIS, NIR, and SWIR). By linking this relationship, variation in the spectra of stressed vegetation can be remotely distinguished from healthy vegetation using different methods. Remote sensing allows plant–metal interaction studies and detects stress early, thus avoiding inevitable soil and plant damage. It is necessary to detect and monitor the types of heavy metal pollutants in a timely and effective manner for better crop management and environmental protection. Traditionally, heavy metal stress was assessed through soil testing, crop tissue analysis, and long-term field trials, sequentially increasing the cost. Remote sensing technology provides an efficient and economical means for heavy metal detection over large areas [146] [147].

Many studies have shown that remote sensing monitors crops in controlled laboratory conditions or specific field environments under heavy metal stress [28] [29]. The spectral response of vegetation under heavy metal stress highlights the importance of remote sensing in managing heavy metal-contaminated soils and plants [30] [32]. These responses may be less prominent, but the spectrally sensitive bands can be established through various analytical methods, including stepwise multi-linear regression, partial least squares regression, and wavelet analysis [83][96]. In-situ measured spectral reflectance forms the basis of hyperspectral sensing of heavy metals. The close correlation between reflectance features and

stress highlights the potential of using remote sensing to assess the type and degree of damage. There has been significant progress in detecting heavy metals in vegetation. However, findings acknowledge that more sensitive spectral parameters are needed to identify the precise level of heavy metal pollution in plants. Most studies in this crucial regime have widely used ground-based hyperspectral reflectance data for plant heavy metal detection through control experiments. These data are used to develop spectral indices sensitive to heavy metal stress in vegetation. However, most field-based experiments are confined to the local ecosystem. Conversely, hyperspectral imaging sensors can provide broad spatial and spectral information for large-scale vegetation monitoring across a region. Literature shows that spectral information about vegetation biochemical and biophysical parameters under heavy metal pollution obtained from laboratory or controlled experiments are more accurate and sensitive [94][95][96]. These field-scale approaches need more universality for stress monitoring over a vast geographical area. None of the researchers have tried to integrate the higher accuracy of field-level data with broad coverage of air-borne or space-borne sensors in detecting the level of pollutants in "real-world" ecosystems. The questions about using these field-scale approaches for monitoring heavy metal pollution in vegetation still need to be explored. Most remote sensing methods can estimate relatively severe plant stress, and field-based studies have limited scope, making it difficult to develop general prediction mechanisms. Integrating field-based studies with the airborne hyperspectral imaging technique can accurately assess the heavy metal pollution in vegetation over a large spatial extent. This study tries to develop an integrated method for detecting heavy metal pollution from the field and hyperspectral data.

Soil consists of various chemically active components that affect the spectral response pattern in different wavelengths. One of the vital constituents of soil is clay minerals such as kaolinite, illite, and montmorillonite. The distribution and dominance of various clay minerals affect soil's chemical and physical properties, like plasticity and cation exchange capacity, thereby affecting its overall quality [148]. Hyperspectral remote sensing from airborne or space-borne platforms uti-

lizing better spatial and spectral resolution can provide abundant clay minerals over a geographical region [149]. Clay minerals exhibit specific absorption patterns around 2210 nm, utilized for specific absorption studies [145]. The study establishes that the depth of absorption peaks is related to the dominance of different clay minerals [134][142]. These absorption features are resistant to different observation conditions and scales and provide a reasonable estimate of soil clay minerals. Integrating hyperspectral datasets with lab-based data allows a quantitative approach to map the abundance of different clay minerals. Most of the research in this field has tried to quantify total clay minerals in the soil, not concentrating on the distribution of different types of clay minerals. So, this study explores the possibility of mapping the distribution of dominant clay minerals in soil using high-resolution hyperspectral imagery obtained from the AVIRIS-NG sensor. The main objective of the current research is to map the distribution of dominant clay minerals present in the agricultural soils in the Udaipur region in the Rajasthan and Ambaji region of Gujarat using airborne hyperspectral data.

1.6 Research objectives

The two primary research objectives defined for the thesis are:

1. Heavy metal mapping in cotton and tobacco crops using biochemical and spectral information derived from hyperspectral data.

2. Clay mineral abundance mapping using a combination of hyperspectral data and X-Ray Diffraction (XRD) analysis data.

1.7 Scope and accomplishments of the thesis

In this thesis, we have defined two primary objectives. Our first objective is monitoring heavy metal pollution in vegetation, accomplished in three steps. The first step is to study the biochemical and spectral behavior in cotton and tobacco contaminated with Pb and Cd heavy metals through the control experiment. This study will provide the basis for further heavy metal mapping using satellite data.

The second goal is to classify the hyperspectral data for the crops under study using the airborne hyperspectral data for the Anand and Surendranagar district of Gujarat. Based on the dominance of specific crops for the particular study area, tobacco, and cotton were classified for Anand and Surendranagar, respectively, using an autoencoder and artificial neural network. The third objective is to map Cd pollution in tobacco in the Anand region and Pb pollution in cotton in the Surendranagar region using airborne AVIRIS-NG data. Heavy metal pollution mapping was done using the dynamic spectral warping technique. The training set with different heavy metal levels from the pot experiment was compared with unknown crop pixels from the study area. The second objective is clay mineral abundance mapping which is completed in three different steps—the first step is the identification of dominant clay mineral zones from AVIRIS -NG data for selecting soil sampling sites: the second step is ground truth collection and XRD of collected soil samples to identify the proportion of dominant minerals. The third step includes statistical analysis that relates the absorption peak depth with the dominance of various clay minerals from airborne hyperspectral data to prepare a mineral abundance map for the study area. The findings are discussed in subsequent chpaters in this thesis.

1.8 Organization of thesis chapters

The thesis is structured in nine chapters, as represented in Figure 1.2.

Chapter 1

This includes the introduction of the thesis, primary research objectives, and motivation of the work, with a detailed literature survey on heavy metal detection in vegetation and soil clay mineral mapping using hyperspectral data.

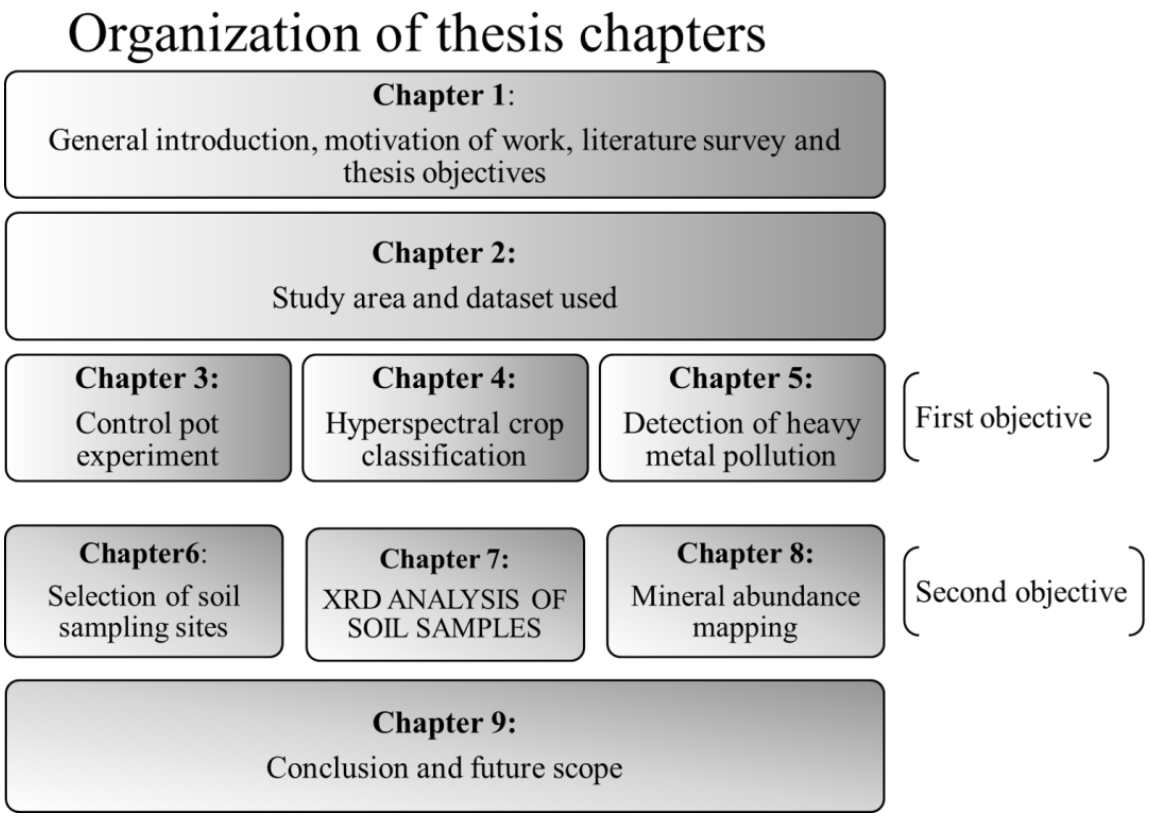

Figure 1.2: Organization of thesis chapter

Chapter 2

This covers the study area and datasets used for different objectives. It also covers the methodology of both research objectives.

Chapter 3

This presents the control pot experiment and results from different biochemical and spectral analyses and their correlation.

Chapter 4

This focuses on the classification of airborne hyperspectral data for the crops under investigation using the AE - Artificial Neural Network (ANN) approach and the classification results.

Chapter 5

This covers heavy metal pollution mapping using airborne hyperspectral data. DSW algorithm is used in this chapter to map the Pb pollution in cotton at Surendranagar and Cd pollution in tobacco at Anand.

Chapter 6

This describes the sampling site selection for soil clay mineral mapping using hyperspectral data.

Chapter 7

This covers the preliminary laboratory analysis and XRD of soil clay minerals in the selected samples.

Chapter 8

This discusses Mineral abundance mapping for Udaipur and Ambaji regions.

Chapter 9

This includes the conclusion, general remarks and future scope of work.

CHAPTER 2

Study area and dataset used

This research has two different objectives. The study area was selected considering the goals of different objectives and the availability of hyperspectral data. For the first objective, Pb is selected as the target heavy metal in the cotton crop at Surendranagar and Cd for contamination in tobacco crops to study heavy metal contamination. Figure 2.1 represents the Anand and Surendranagar study areas for heavy metal pollution detection in tobacco and cotton, respectively. Similarly, for the second objective, montmorillonite, kaolinite, and illite were selected as target clay minerals in Ambaji and Udaipur areas, as shown in Figure 2.2. Table 2.1 summarizes different study areas and data used for different objectives.

2.1 Study area

2.1.1 Anand

The study area for Cd pollution in tobacco is Anand district, between 22° 30′ 43″ N to 72° 56′ 56″ E and 22° 33′ 14″ N to 72° 59′ 22″ E, in Gujarat, popularly known as the milk capital of India. It is also known for its industrial belt, with different industries contributing to heavy metal pollution. The region has a semi-arid to arid climate with tobacco as a major crop and is well known for exporting products with the finest quality of tobacco.

Table 2.1: Study areas and Data used for different research objectives

Study area	**Target**	**Heavy Metals/ Clay minerals**	**Data**
Anand	Heavy metal contamination in Tobacco plants	Pb and Cd	AVIRIS-NG Data and Biochemical Data
Surendranagar	Heavy metal contamination in cotton plants	Pb and Cd	AVIRIS-NG Data and Biochemical Data
Ambaji	Clay mineralogy	Montmorillonite, Kaolinite, Illite	AVIRIS-NG Data and XRD Data
Udaipur	Clay mineralogy	Montmorillonite, Kaolinite, Illite	AVIRIS-NG Data and XRD Data

2.1.2 Surendranagar

The study area selected for detecting heavy metal pollution in cotton crops is part of the Surendranagar district, situated in the very center of Gujarat state of India, between 22° 32′ 51″ N to 71° 35′ 16″ E and 22° 43′ 42″ N to 71° 38′ 16″ E. It is an agricultural district with a subtropical climate, and cotton is the major cash crop grown here.

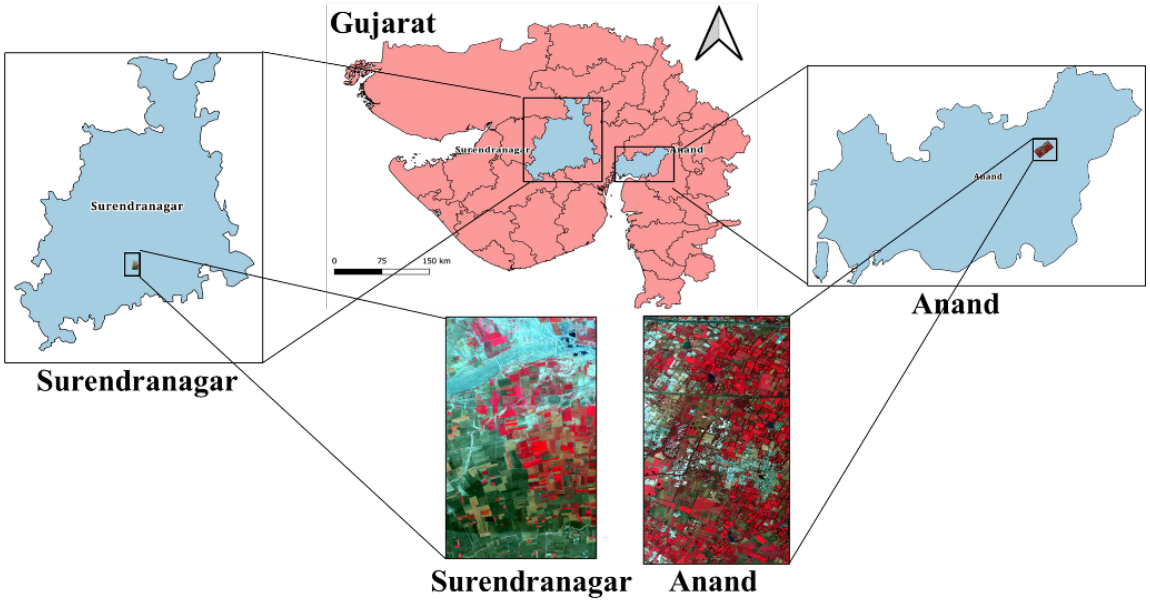

Figure 2.1: Study area for heavy metal detection in crops of Surendranagar and Anand district of Gujarat

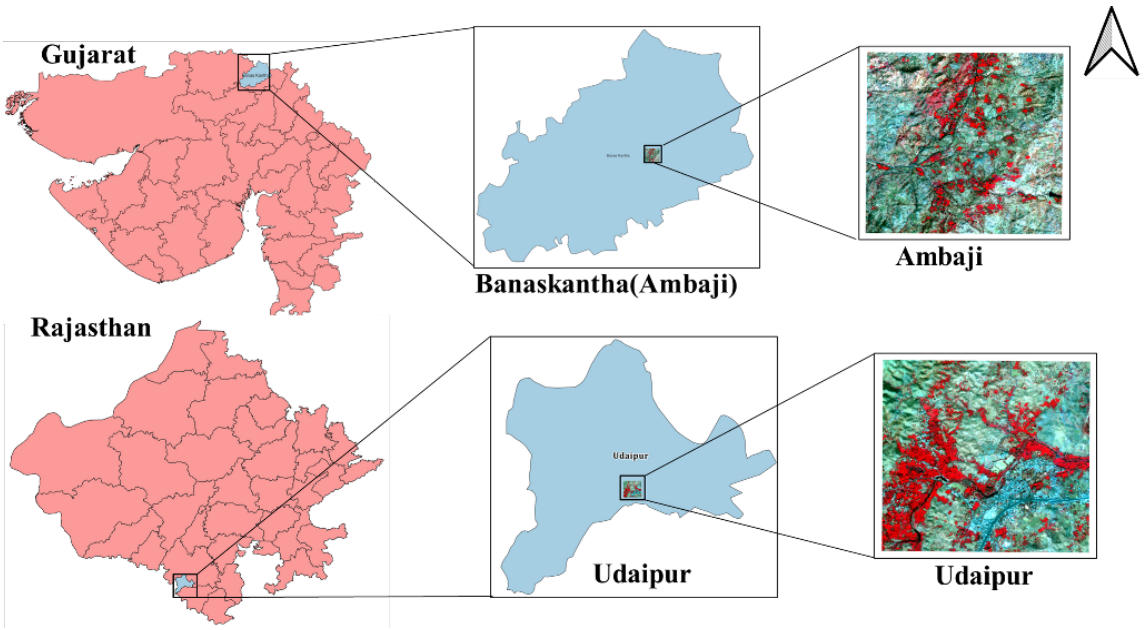

Figure 2.2: Study area for clay mineral abundance mapping at Ambaji in Banaskantha district of Gujarat and Udaipur district in Rajasthan

2.1.3 Udaipur

The study area is a part of Udaipur District, Rajasthan, India, between 23° 58′ 71″ N to 73° 31′ 45″ E and 24° 1′ 47″ N to 73° 38′ 26″ E. Geologically, the study area is a part of the Aravalli Supergroup [150]with an abundance of minerals like talc, iron, and clay minerals. It has a semi-arid climate with a dominant land use category consisting of agricultural (crops and orchards) and fallow land (uncultivated and wastelands).

2.1.4 Ambaji

The study area for mineral mapping is a part of the Ambaji region, between 24° 13′ 22" N to 72° 30′ 12" E and 24° 17′ 10" N to 72° 36′ 52" E, falling under the Banaskantha district in north Gujarat, India. It belongs to Delhi supergroups and is well known for the occurrence of base metals Pb, zinc, and copper [151][150]. Mineralization occurs in metamorphosed magnesian and calc-magnesian rocks. It has a semi-arid climate supporting different crops like maize, bajra, and castor.

Table 2.2: Specifications of AVIRIS-NG

Parameter	**Value**
Wavelength	380-2510 nm
Spectral resolution	5 nm
Spatial Resolution	8 m
Swath	6 km
Altitude of flight	6-7 Km

2.2 Dataset

2.2.1 Hyperspectral data

This study uses hyperspectral data from AVIRIS-NG sensor on an airborne platform acquired between 4-10 February 2016 over different study areas [152]. AVIRIS-NG can be considered the most advanced dataset free from keystone and smile error distortions (Jet propulsion Laboratory (JPL), NASA, 2015) due to its better specifications described in Table 2.2. The dataset contains 425 spectral bands in the wavelength range of 380-2500 nm with 5 nm spectral resolution. We have used the radiometrically and geometrically corrected level-2 AVIRIS-NG data to fulfill different research objectives of this thesis.

2.2.2 Biochemical and X-ray diffraction data

The Pb and Cd content of leaves and soil was measured in the laboratory using Inductively coupled plasma-atomic emission spectroscopy (ICP-AES). X-ray diffraction analysis of soil samples for clay minerals was done in the laboratory using an x-ray diffractometer after processing of samples according to the laboratory manual from US geological survey [153].

2.3 Methodology

We have adopted two different approaches for both the objectives of this thesis.

2.3.1 First objective

Figure 2.3 summarizes the methodology of the first objective, *i.e.*, to detect heavy metal in crops. It was done in three steps. The first step was to generate reference data from pot experiments for the target heavy metals in crops under study. The second step was pre-processing and classifying cotton and tobacco crops from hyperspectral data over the study area. The third and final step was to use the DSW algorithm for spectral matching of pixels from airborne hyperspectral data with reference spectra generated from the pot experiment. The details of each step are provided in different chapters of the thesis.

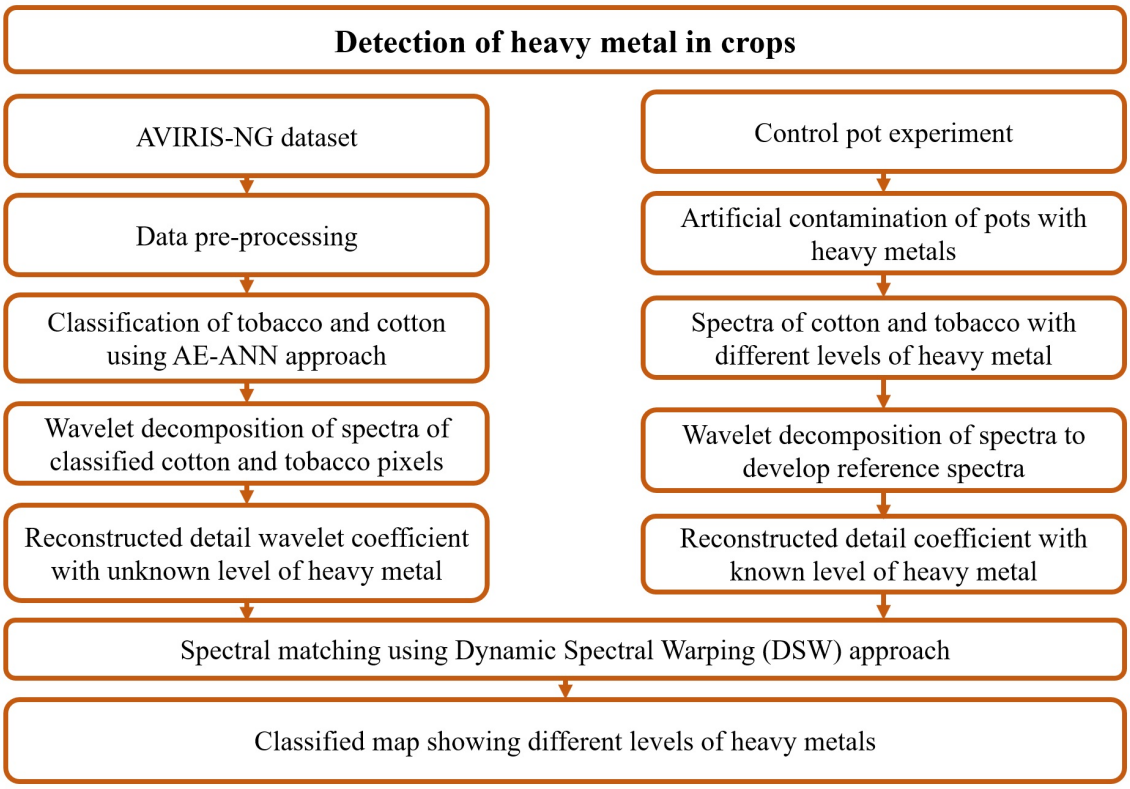

Figure 2.3: Methodology for heavy metal detection in vegetation

2.3.2 Second objective

For clay mineral abundance mapping using hyperspectral data, the adopted methodology is divided into three main parts:

- Identifying clay mineral dominant area from AVIRIS-NG data

- Establishing a relation using ground points
- Mineral abundance mapping

These are discussed in detail in subsequent chapters.

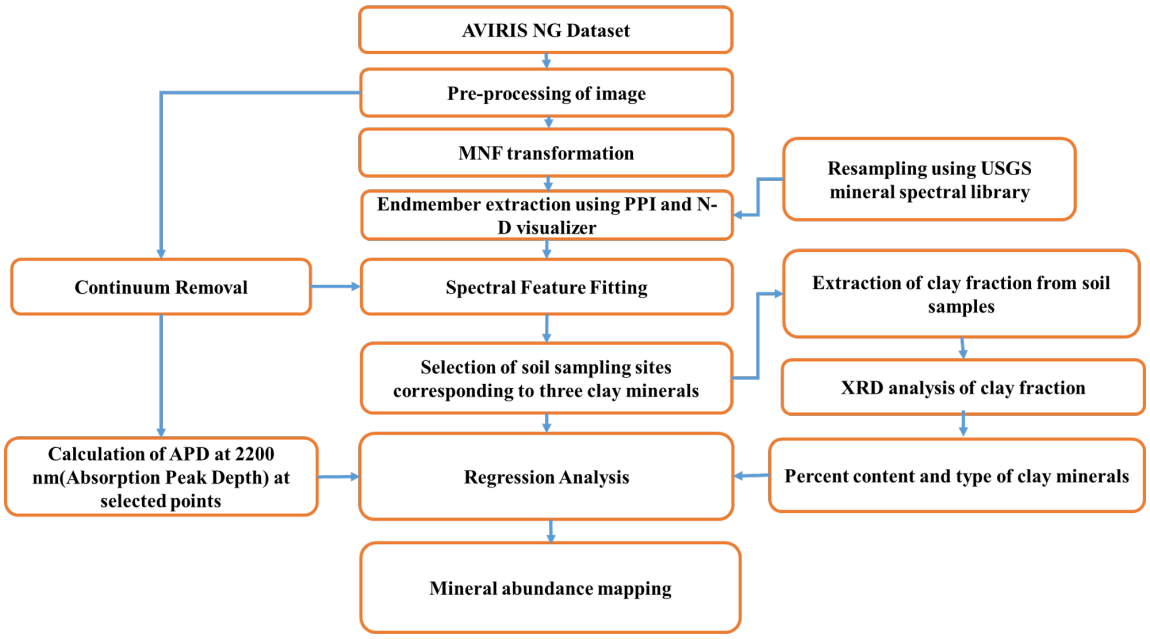

Figure 2.4: Methodology for clay mineral abundance mapping using AVIRIS-NG hyperspectral data

Figure 2.4 depicts the methodology adopted for mineral abundance mapping in various steps. First, sites were selected for soil sample collection corresponding to three dominant clay minerals from AVIRIS-NG data using SFF analysis. Then X-ray diffraction analysis of soil samples was carried out. Furthermore, clay mineral abundance maps are prepared for the study areas using regression analysis between absorption peak depth value and clay mineral content obtained from XRD.

CHAPTER 3

Controlled Pot Experiment[1]

3.1 Problem statement

Cd and Pb heavy metals are non-essential for the growth and metabolism of living organisms. Plants are an essential indicator of heavy metal pollution in a specific region as they absorb and accumulate them. Timely assessment of heavy metals can provide information on plant behavior, which can help to protect the environment. Field-based methods of assessing heavy metal contamination are costly and labor-intensive and can be helpful on a small scale. However, remote sensing methods help real-time heavy metal detection over large areas. Selection of the spectral bands most sensitive to heavy metal content is a prerequisite for the success of heavy metal retrieval from remotely sensed imagery. The most influential bands selected governs the accuracy of predicting and mapping heavy metal concentration. This selection is critical with hyperspectral data as there is a high degree of data redundancy among hundreds of available bands.

Several studies have incorporated pot experiments to study the response of leaf reflectance on the field level [92][154]. Mapping of heavy metal concentration over a large area using this field-level approach is yet to be attempted. Understanding the overall spectral and biochemical response of plants due to the presence of heavy metals is crucial for successful mapping using satellite data. As field level spectra with different levels of heavy metal in tobacco and cotton are

[1]Parts of this chapter is published in the following paper:
Priya, S. and Ghosh, R., "Monitoring effects of heavy metal stress on biochemical and spectral parameters of cotton using hyperspectral reflectance", *Environmental Monitoring and Assessment*, 195(1), p.112, 2023.

not sufficiently available, we conducted this control experiment to generate training sets with different levels of Pb and Cd. The cotton and tobacco crops were selected due to their presence in Surendranagar and Anand districts. The effects of Pb and Cd in cotton and tobacco were established by the crop's biochemical and spectral response after artificially contaminating the soil with different levels of Pb and Cd. The spectral details are further used to detect the level of heavy metal pollution from airborne hyperspectral data.

This experiment aims to determine the sensitivity of cotton and tobacco plant to different levels of Cd and Pb and compare their spectral differences with healthy leaf samples through a combined approach utilizing field-based data and spectral analysis. Altogether, the main aim of this research is to determine (1) the preferential absorption pattern of cotton and tobacco for Pb and Cd, (2) the crop growth stage most sensitive to heavy metal (3) the wavelength region most affected due to heavy metal stress and (4) generating training features for mapping heavy metal pollution.

3.2 Material and methods

A controlled pot experiment using a Completely Randomized Design (CRD) has been conducted at the Sardarkrushinagar-Dantiwada Agricultural University (SDAU), Palanpur to study the effects of Pb and Cd on cotton crops and tobacco crops. Experiments were conducted outdoors in a net house. Cement pots with a soil capacity of 17 kg, which is adequate for crop growth, were selected for this experiment. Pots were filled with well-pulverized and fine-textured soil free from pebbles, leaves, or stones. The soil was artificially contaminated with Analytical Reagent (AR) grade chemicals $CdSO_4$ for Cd and $Pb(NO_3)_2$ for Pb with 0, 5, 10, and 15 ppm of Pb and Cd. The heavy metal levels were decided through soil conditions and literature studies [58][96]. The treatment details are given below:

- T1: Control
- T2: 5 ppm Pb

- T3: 10 ppm Pb
- T4:15 ppm Pb
- T5: 5 ppm Cd
- T6:10 ppm Cd
- T7: 15 ppm Cd

The heavy metals were distributed uniformly through the soil after mixing, and the soil was kept undisturbed for 15 days for stabilization. The sterilized and cleaned cotton seeds are sown in the pots. Small tobacco seeds were first grown in the nursery, and 30 days old, seedlings were used for transplanting. Each treatment was replicated three times. Figure 3.1 shows a schematic of the applied treatments and replications. After the germination of the crops, only two plants were kept in the pots, and others were weeded out. All other agricultural applications, such as watering, fertilization, and pest control, were kept uniform for each treatment to capture the heavy metal effects. These pots were kept in a net house with proper sunlight for better growth, as shown in Figure 3.2a and Figure 3.2b.

Various observations were recorded at the vegetative stage 35 Days After Sowing (DAS), the flowering stage 65 DAS and the harvest stage 95 DAS in cotton and early vegetative stage, 30 Days After Transplanting (DAT), and the maximum growth stage 75 DAT, maturity stage 120 DAT in tobacco.

3.3 Biochemical measurements

3.3.1 Chlorophyll content

The middle portion of the fresh leaves was taken to the laboratory, and chlorophyll was estimated as per the procedure given by Moran [155]. 0.1 g of leaves were weighed with the help of electronic balance and crushed in a mortar and pestle using 80 % acetone. It was filtered with Whatman no 4-filter paper, and the

R_1	R2	R3
T_1	T_5	T_6
T_4	T_3	T_5
T_3	T_7	T_1
T_6	T_1	T_4
T_5	T_2	T_7
T_7	T_6	T_2
T_2	T_4	T_3

Figure 3.1: Schematic design of the treatment for each crop in a pot experiment

(a) Pot experiment for cotton crop

(b) Pot experiment for tobacco crop

(c) ASD readings taken during pot experiment

Figure 3.2: Pot experiment for cotton and tobacco crop

volume was made to 10 ml using 80% acetone. Spectrophotometer was used, and chlorophyll a (chl a), chlorophyll b (chl b), and total chlorophyll (chl a+b)content were measured using the following formula:

$$chl(a) = [12.7 * Ab(663) - 2.69 * Ab(645)]\frac{V}{1000 * W} \tag{3.1}$$

$$chl(b) = [22.9 * Ab(645) - 4.68 * Ab(663)]\frac{V}{1000 * W} \tag{3.2}$$

$$chl(a+b) = [20.2 * Ab(645) + 8.02 * Ab(663)]\frac{V}{1000 * W} \tag{3.3}$$

Where,
$Ab(645)$ = absorbance at 645 nm

$Ab(663)$ = absorbance at 663 nm

V=Volume made up (ml) W=weight of sample taken (g)

The final volume is expressed in $mg.g^{-1}$ fresh weight of leaves.

3.3.2 Heavy metal content

Two sets of leaf samples were taken, one for chlorophyll estimation and the other for heavy metal analysis twice during the complete growth cycle. After washing with distilled water, chlorophyll estimation of the fresh leaves was done in the lab. The oven-dried and ground leaf samples were analyzed for Pb and Cd heavy metals in the laboratory using Inductively Coupled Plasma/Atomic Emission Spectroscopy (ICP/AES) methods. All results are expressed in $mg.kg^{-1}$ of heavy metals of dried samples. After the digestion of dried soil samples, soil samples were also analyzed for Cd and Pb.

3.3.3 Transfer Factor (TF)

The Transfer Factor (TF) is calculated to estimate Pb and Cd uptake in leaves of tobacco and cotton. It is defined as the ratio of heavy metal present in plants to

heavy metal present in soil [156].

$$TF = \frac{Heavy\ metal\ concentration\ in\ plant(mg.kg^{-1})}{Heavy\ metal\ concentration\ in\ soil(mg.kg^{-1})} \tag{3.4}$$

A higher value of TF indicates more absorption of that heavy metal in plants.

3.4 Spectral measurements

Spectral reflectance measurements were done using ASD (Analytical Spectral Devices, Inc., Boulder, CO, USA), as shown in Figure 3.2c. with a 25° Field of View (FOV) through a permanent fiber optic probe. It is sensitive to the wavelength range of 350–2500 nm, having a sampling interval of 1.4 nm between 350 –1000 nm and 2 nm between 1000 –2500 nm and a spectral resolution of 3 nm (@ 350–1000 nm), 8.5 nm (@ 1000–1900 nm), and 6.5 nm (@ 1900–2500 nm). An average of 20 spectra was taken from each pot to study the effects of Pb and Cd on spectral reflectance. After each spectral measurement, those leaves were used for the lab's chlorophyll and heavy metal analysis. The spectral range was limited to 400-1000 nm because the plant responds to stress in this range [157]. Spectral observations were recorded at the vegetative stage 35 DAS, the flowering stage 65 DAS, and the maturity stage 95 DAS. All spectral measurements were taken by placing the pistol above the leaves in the net house between 1000 to 1100 hrs on clear sunny days. All the reflectance spectra were calibrated against a white spectralon panel.

3.4.1 First derivative analysis

The first derivative can strengthen the changes caused by heavy metal stress and minimize the background noise. The first derivative of spectra was calculated as the rate of change for reflectance to change in wavelength [158].

3.4.2 Wavelet analysis

The wavelet transform was used to decompose reflectance spectra to amplify the heavy metal stress. The high pass filter provides detailed coefficients, and the

low pass filter gives approximation coefficients at different levels. Noise is separated from beneficial structural changes carrying viable information by increasing the decomposition levels [115]. Detailed wavelet coefficients can capture minute changes in the spectra to diagnose stress caused by heavy metals. The detail reflectance is reconstructed by upsampling and filtering detail coefficient vectors as per the process described by Misiti et al [159]. The reconstructed detail reflectance having similar dimensions as the original reflectance is used for further efficient spectral analysis.

$$(\phi_(a,b)(t) = \frac{1}{\sqrt{a}}\phi(\frac{t-b}{a}) \tag{3.5}$$

Where wavelet $\phi(t)$ is called the mother wavelet, a is the scaling parameter, and b is the shifting parameter. Based on previous research findings, the Daubechies wavelet ($db5$, 5 is the order) was found to be the most appropriate for reflectance signal analysis [114][115].

3.5 Statistical analysis

The three replications were used for statistical analysis. Biochemical parameters were statistically tested for significance through analysis of variance (ANOVA) in Microsoft Excel. Tukey's HSD test is used for post hoc analysis. Pearson's Correlation coefficient (r) was computed for each treatment between spectral variables (reflectance spectra, its first derivative, and reconstructed detailed wavelet coefficients and leaf-metal concentration to find the sensitive wavelength range due to heavy metal stress [96]. The spectral analysis, like wavelet transforms and first derivative analysis, was done using MATLAB.

3.6 Results and discussion

3.6.1 Chlorophyll content

Chlorophyll pigment plays a vital role in photosynthesis. Chlorophyll a and b are the two major pigments found in higher plants. During the complete lifecycle of a

healthy plant, chlorophyll concentrations are lower at the beginning of the plant's growth cycle, rise during the plant's maximum growth, then fall at maturity due to the yellowing of leaves. Analysis of the chlorophyll concentration in the two crops at different stages of development revealed the same consistent pattern, as illustrated in Figure 3.3 and Figure 3.4, respectively. The pot experiment results revealed that chlorophyll content increased with the plant's growth but significantly decreased in response to rising levels of Cd and Pb. The assessment of cotton and tobacco crops for the impact of Pb and Cd treatments on various chlorophyll pigments at different growth stages yields some distinct results, which are compiled here.

Chlorophyll content in cotton

Chlorophyll content decreased during different stages of cotton growth due to the varying levels of Pb and Cd compared to the control depicted in Figure 3.3. Table 3.1 shows the impact of different Pb and Cd treatments on various chlorophyll pigments in cotton plants at various stages of development.

Table 3.1: Effect of various concentrations of Pb and Cd treatment on Chlorophyll content ($mg.g^{-1}$ of fresh weight) of cotton at different growth stages [1] [2]

Treatments (ppm)		**Vegetative**			**Flowering and Boll formation**			**Harvest**		
		Chl a	Chl b	Chl (a+b)	Chl a	Chl b	Chl (a+b)	Chl a	Chl b	Chl (a+b)
Control	0	1.95^{a}	0.86^{a}	2.81^{a}	2.45^{a}	0.94^{a}	3.38^{a}	1.63^{a}	0.66^{a}	2.30^{a}
Pb	5	1.74^{c}	0.79^{bc}	2.53^{c}	2.07^{c}	0.87^{b}	2.94^{c}	1.54^{c}	0.60^{bc}	2.14^{c}
	10	1.43^{e}	0.67^{d}	2.10^{e}	1.98^{d}	0.82^{c}	2.79^{d}	1.46^{e}	0.57^{cd}	2.04^{d}
	15	1.28^{f}	0.59^{e}	1.95^{f}	1.73^{e}	0.74^{d}	2.47^{e}	1.32^{g}	0.53^{e}	1.85^{e}
Cd	5	1.81^{b}	0.83^{ab}	2.64^{b}	2.26^{b}	0.87^{b}	3.13^{b}	1.57^{b}	0.62^{b}	2.20^{b}
	10	1.78^{bc}	0.77^{c}	2.55^{c}	2.17^{b}	0.77^{cd}	2.94^{c}	1.48^{d}	0.58^{c}	2.07^{d}
	15	1.60^{d}	0.65^{d}	2.25^{d}	2.06^{cd}	0.73^{d}	2.79^{d}	1.35^{f}	0.54^{de}	1.90^{e}

[1] *Mean of three replicates are shown*

[2] *Significance at $p < 0.05$ is indicated by different letters in the same column using Tukey Honestly Significance Difference (HSD) test*

The findings demonstrate that Pb treatments had a more pronounced impact on cotton's chlorophyll content than Cd treatments. The total chlorophyll concen-

tration at the vegetative stage showed a reduction of 10-30% due to Pb (5 ppm) to Pb (15 ppm) treatments but only 6-20% due to Cd (5 ppm) to Cd (15 ppm) treatments. Even low-concentration Pb treatments had caused a significant decrease in the chlorophyll (chlorophyll a, chlorophyll b, total chlorophyll) content, and the effects intensified as the level of heavy metals increased. Among the two chlorophyll components, the adverse effect of Pb is more significant on chlorophyll a, which serves as the primary pigment in photosynthesis, playing an essential role in electron transport [160].

The lowest chlorophyll a was recorded at the highest Pb level of 15 ppm (34% of control) at the vegetative stage, severely damaging the photosynthetic apparatus. Several studies have reported that the presence of Pb slows down the rate of photosynthesis in plants by modifying the chloroplast's ultrastructure, inhibiting chlorophyll's production, impeding electron transport, and obstructing the Calvin cycle enzymes [161][162]. One of the studies revealed a decrease in chlorophyll concentration due to higher Pb - 800 Micromolar (μM) treatment compared to control in *Citrus aurantium* treated with different levels of Pb [39]. A pot culture with 75, 150, and 300 $mg.l^{-1}$ Pb applications, with three replications, showed a negative effect of Pb on the chlorophyll concentration of eggplant seedlings [51].

Heavy metal-induced reduction of chlorophyll concentration is observed in many plant species [50][52]. Heavy metal's presence reduces chlorophyll biosynthesis by reducing the uptake of essential elements such as magnesium and iron [163]. Several studies showed that stress caused by Pb and Cd could destroy the structure of chlorophyll by substituting the central Mg ion and causing a breakdown of photosynthesis [164][165][166]. A study by Lal et al. revealed the toxic effects of Cd and Pb treatments on two cotton genotypes (Desi cotton and *Bt* cotton)[167]. Malar et al. reported more than 50 % reduction in chlorophyll a and b in 1000 $mg.l^{-1}$ Pb treated water hyacinth plant compared to the control [168]. A laboratory scale experiment conducted on the aquatic plant *Ceratophyllum demersum* L. with different Pb concentrations (2, 4, and 6 $mg.l^{-1}$) showed a noticeable decrease in the chlorophyll with increasing Pb concentration initially [47]. The change in chlorophyll concentration was also analyzed across different

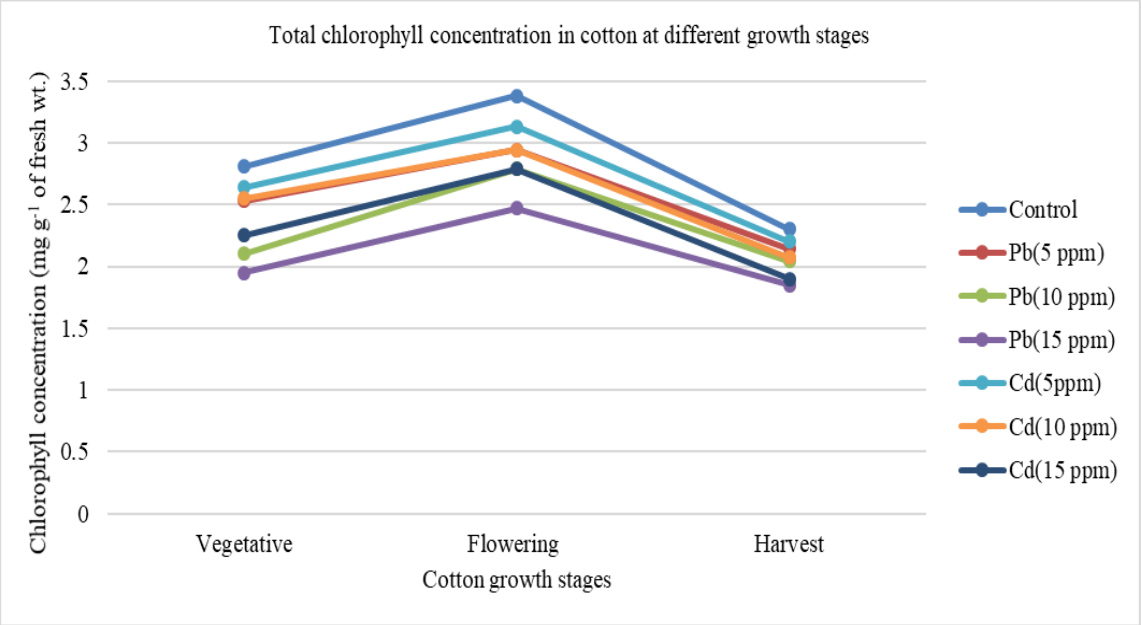

Figure 3.3: Chlorophyll concentration in cotton with different levels of Pb and Cd at different growth stages

plant growth stages.

A diminishing impact of Pb treatment was noticed in chlorophyll concentration from the vegetative to the harvest stage. The reduction in chlorophyll a, b, a+b was higher due to Pb 15 ppm treatment at the vegetative stage compared to the harvesting stage. This reduction was highest in chlorophyll a concentration across the growth stages. This implies that in early growth stages, more Pb is absorbed by leaves than in later stages. Over successive growth stages, as the buildup of Pb in the leaves subsequently diminished, the Pb treatment's impact on the chlorophyll a concentration also dropped significantly [169][170]. The poor solubility of Pb-compounds, which results in less Pb translocation in leaves as crop height rises, is reported to be the cause of the higher initial presence of Pb [171].

Chlorophyll content of tobacco

The chlorophyll concentration in tobacco showed a concentration-dependent response to different levels of Pb and Cd at different growth stages depicted in Figure 3.4. The chlorophyll a, b, and (a+b) content in tobacco leaves decreased under various Pb and Cd treatments, as represented in Table 3.2.

Table 3.2: Effect of various concentrations of Pb and Cd treatment on Chlorophyll content ($mg.g^{-1}$ of fresh weight) of fresh weight) of tobacco at different growth stages [1] [2]

Treatments (ppm)		**Early Vegetative**			**Maximum growth**			**Maturity**		
		Chl a	Chl b	Chl (a+b)	Chl a	Chl b	Chl (a+b)	Chl a	Chl b	Chl (a+b)
Control	0	1.21^{a}	0.72^{a}	1.93^{a}	1.17^{a}	1.20^{a}	2.37^{a}	0.47^{a}	0.58^{a}	1.05^{a}
Pb	5	1.14^{ab}	0.63^{b}	1.77^{b}	1.07^{b}	1.08^{b}	2.15^{b}	0.45^{ab}	0.48^{b}	0.92^{b}
	10	1.03^{c}	0.46^{c}	1.49^{c}	1.03^{bc}	1.04^{b}	2.07^{c}	0.38^{bc}	0.44^{bc}	0.83^{c}
	15	0.92^{d}	0.37^{d}	1.29^{d}	0.86^{d}	0.83^{d}	1.69^{e}	0.33^{c}	0.35^{d}	0.68^{e}
Cd	5	1.05^{bc}	0.49^{c}	1.55^{c}	0.98^{c}	0.95^{c}	1.93^{d}	0.36^{c}	0.40^{cd}	0.76^{d}
	10	0.88^{d}	0.34^{d}	1.22^{d}	0.77^{e}	0.70^{e}	1.47^{f}	0.24^{d}	0.22^{e}	0.46^{f}
	15	0.73^{e}	0.20^{e}	0.93^{e}	0.65^{f}	0.52^{f}	1.16^{g}	0.14^{e}	0.10^{f}	0.24^{g}

[1] *Mean of three replicates are shown*

[2] *Significance at* $p < 0.05$ *is indicated by different letters in the same column using Tukey HSD test*

The response of tobacco plants to changes in chlorophyll concentration with different heavy metal treatments differed remarkably from cotton plants. A reduction was attributable to heavy metal application in chlorophyll a and chlorophyll b. The Cd treatments were more toxic and resulted in a higher reduction in chlorophyll content. There was nearly 24, 35 and 41% decrease in chlorophyll a, chlorophyll b, and Chlorophyll (a+b) with Pb (15 ppm) treatment and a 48, 51 and 72 % decrease in chlorophyll a, chlorophyll b, and chlorophyll (a+b) with Cd (15 ppm) treatment from control pot during the early growth stage. The presence of Cd decreased chlorophyll b concentration by 82 % during the harvesting phase. Various studies have reported the deleterious effects of Cd on chlorophyll content due to the inhibition of enzymes involved in chlorophyll biosynthesis [172][173].

Moreover, when Cd was applied, chlorophyll b concentrations significantly decreased. These findings supported past research that Cd impeded chlorophyll production resulting in senescence [174]. Our findings concur with those of Waheed et al., who confirmed that at 1.5, 3, 6, and 30 $mol.l^{-1}$ of Cd application, the chlorophyll concentration decreased by 25, 27, 35, and 52 %, respectively. In contrast, the Chlorophyll b concentration decreased by 18, 42, 45, and 63 %, respectively, in *E. sativa* plants treated with different levels of Cd [175]. The ad-

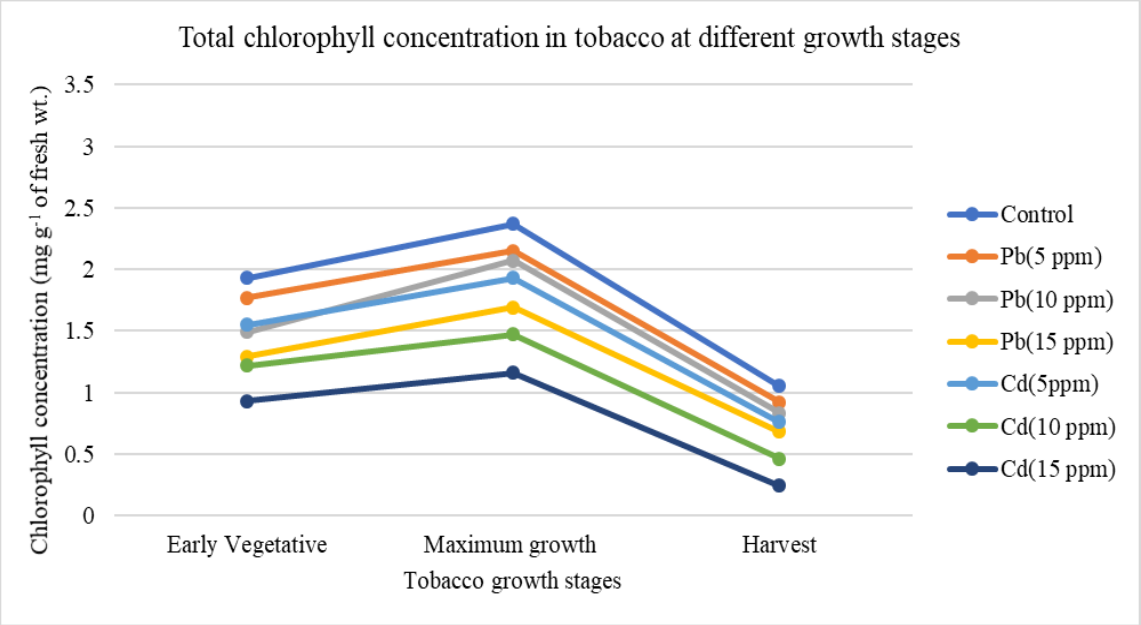

Figure 3.4: Chlorophyll concentration in tobacco with different levels of Pb and Cd at different growth stages

verse effect of Cd on chlorophyll pigments was high during the maturity stage of tobacco compared to the vegetative and maximum growth stage, especially in chlorophyll b, which decreased 83 % from control due to more buildup of Cd in leaves of tobacco during the maturity stage. Photosynthesis is a vital metabolic process negatively impacted by various heavy metals [176][177].

Photosynthetic inhibition during Cd stress is one of the primary actions in plants because they invariably affect photosynthetic apparatus and its functions, diminishing chlorophyll synthesis and inhibiting activities of the Calvin cycle either directly or indirectly, by inhibiting both light and dark reactions of photosynthesis [177]. Various plant species show different patterns of heavy metal uptake, which may influence the biosynthesis of chlorophyll pigment. The heavy metals build up in plants causes damage to photosynthetic machinery and may result in photo-oxidative damage [178]. Therefore, chlorophyll pigments seem to be one of the main reasons for heavy-metal injury in plants. The extent of injury depends on the type and concentration of heavy metal as well as the developmental growth stage of the plant.

3.6.2 Heavy metal accumulation and transfer factor (TF)

The presence of heavy metal above a specific threshold in a plant can be toxic, affecting the plant's growth. Accumulation of heavy metals in plants depends on factors such as the presence of heavy metals in the soil, their availability to plants, and the plant species grown [179]. Plant's uptake of heavy metals is an effective way of responding to their toxic effects [180].

Heavy Metal Accumulation in Cotton

As shown in Table 3.3, exposure to increasing Pb and Cd levels enhanced their accumulation in the cotton leaves.

Table 3.3: Accumulation of various concentrations of Pb and Cd ($mg.kg^{-1}$ of dry weight) in cotton crop and TF [1] [2]

Treatments (ppm)		**Pb in soil**	**Pb in plant**	**TF for Pb**	**Treatments and levels**		**Cd in soil**	**Cd in plant**	**TF**
Control	0	19.87^{d}	12.52^{d}	0.58^{c}	Control	0	0.60^{d}	0.17^{d}	0.28^{a}
Pb	5	26.38^{c}	17.94^{c}	0.67^{bc}	Cd	5	5.43^{c}	1.56^{c}	0.29^{a}
	10	31.20^{b}	22.00^{b}	0.70^{b}		10	11.20^{b}	2.55^{b}	0.23^{b}
	15	38.12^{a}	37.18^{a}	0.97^{a}		15	14.90^{a}	3.14^{a}	0.21^{b}

[1] *Mean of three replicates are shown*
[2] *Significance at* $p < 0.05$ *is indicated by different letters in the same column using Tukey HSD test*

Figure 3.5 and Figure 3.6 shows the accumulation of Pb and Cd at different growth stages in cotton leaves. The Pb accumulation was significantly higher at Pb 15 ppm than the control, while the Cd accumulation was not so affected by a higher level of Cd application clearly indicated in Figure 3.5 and Figure 3.6. Such findings suggest a greater affinity of cotton to absorb higher levels of Pb, also reported by Ramana et al.'s research on cotton plants with various levels of Pb [180]. Various researchers have also reported that the cotton plant has an increased ability to absorb Pb, Cd, and Zn [58][181]. The accumulation of Pb in the cotton plant was highest during the vegetative stage compared to the harvesting stage. The higher accumulation of Pb in the initial growth stages is related to Pb's immobile nature and constraints in Pb's internal movement from roots to shoots

and green leaves. This immobility of Pb is attributed to its strong ability to bind to the carboxyl groups of galacturonic and glucuronic acids in the cell wall, limiting the transport of this metal [182]. The lesser translocation of Pb to leaves due to increased plant height at advanced growth stages can be related to the adaptability of cotton to higher levels of Pb [172][183]. The results demonstrate that Pb absorption is high at the initial growth stage. A similar finding was reported by Rathod et al. showing an increased Pb content at the initial growth stages of barley plants [96].

The TF indicates metals' transmission from soil to plant tissues. The TF was 0.97 for Pb 15 ppm for cotton and significantly differed from control and other Pb treatments. The TF for Cd was very low and did not increase with increasing concentration of Cd in soil, as shown in 3.3. The TF at various Pb levels differed significantly from the control showing a higher uptake of Pb in cotton. At the same time, the TF for Cd was not significant, indicating negligible absorption of Cd in cotton plants. A higher TF value represents a higher metal absorption from the soil by plants and its suitability for bio-monitoring and phytoextraction. The lower values of TF indicate poor metal absorption from the soil [184]. The heavy metals availability in plants is guided by the need for micronutrients and the capacity to eliminate and absorb toxic elements. Different plant species and their adaptation to different environmental conditions also affect the transmission of heavy metals in plants [183] [185]. Cotton plants can be used as a dominant species for studying Pb intake [58][181]; their use in phytoremediation can also be further explored.

Heavy metal accumulation in tobacco

The pot experiment results on tobacco crops revealed a more significant accumulation of Cd than Pb when both heavy metals were applied. Figure 3.7 and Figure 3.8 show the accumulation of Cd and Pb in tobacco leaves. As per Table 3.4, the accumulation of Cd in tobacco leaves increased to 15.97 $mg.kg^{-1}$ with increasing concentration of metal in soil which is not the case with Pb.

In an experiment conducted in Anand by Mistri et al. with different crops,

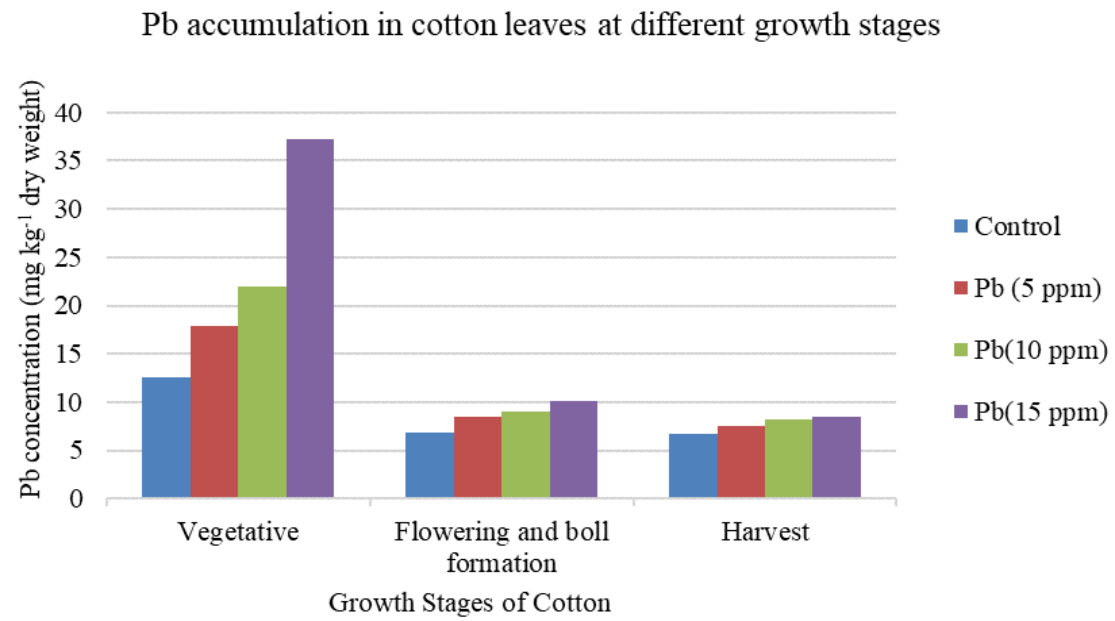

Figure 3.5: Pb accumulation at different growth stages of cotton

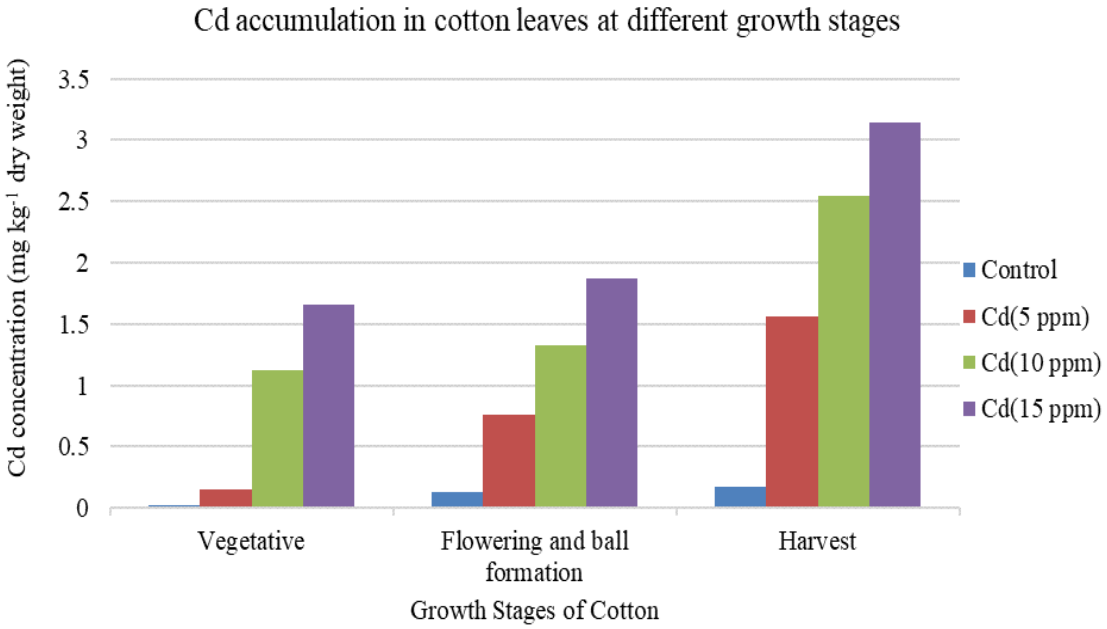

Figure 3.6: Cd accumulation at different growth stages of cotton

Table 3.4: Accumulation of various concentrations of Pb and Cd ($mg.kg^{-1}$ of dry weight) in tobacco crop and TF [1] [2]

Treatments and levels		**Pb in soil**	**Pb in plant**	**TF for Pb**	**Treatments and levels**		**Cd in soil**	**Cd in plant**	**TF**
Control	0	6.22^{d}	1.29^{d}	0.20^{a}	Control	0	1.23^{d}	0.67^{d}	0.54^{c}
Pb	5	11.23^{c}	2.47^{c}	0.22^{a}	Cd	5	7.36^{c}	6.06^{c}	0.83^{b}
	10	16.72^{b}	4.33^{b}	0.25^{a}		10	11.67^{b}	10.77^{b}	0.92^{ab}
	15	20.86^{a}	7.73^{a}	0.30^{a}		15	16.28^{a}	15.97^{a}	0.98^{a}

[1] *Mean of three replicates are shown*

[2] *Significance at* $p < 0.05$ *is indicated by different letters in the same column using Tukey HSD test*

sunflower, cotton, tobacco, and castor, the extraction of heavy metals from soil was highest in tobacco crops compared to other crops [186]. A study conducted by Yang showed similar results in pot and field experiments on tobacco crops with different Cd applications. Results reveal that Cd concentration was higher in tobacco leaves compared to roots and stalks varying from 8.24 $mg.kg^{-1}$ to 15.56 $mg.kg^{-1}$ in tobacco leaves [187]. Various studies revealed that tobacco accumulates higher levels of Cd and is relatively tolerant to this metal [188][189]. A study by Rosen et al. revealed that tobacco leaves could accumulate more than 50% total plant uptake of Cd [190]. Researchers established that migration of Cd from soil to the leaves could be a permanent accumulation mechanism of tobacco plants, describing the role of specific genes in higher accumulation and tolerance of Cd in tobacco irrespective of varieties [75][191]. However, the plant's mechanism of accumulating Cd needs more study [192]. Due to the high accumulation of Cd, the transfer factor of the tobacco plant was found to be significant compared to the control. Its value increased significantly from 0.54 in the control to 0.98 in the highest Cd treatment, as given in Table 3.4. The TF for Pb in tobacco is non-significant as there was no increase in the Pb content of tobacco leaves with an increase in Pb content in the soil. Such high TF of tobacco for Cd has been reported by various researchers [189][190] [193]. Plants with very high TF are considered hyperaccumulators and can play a role in the phytoremediation of soil [187].

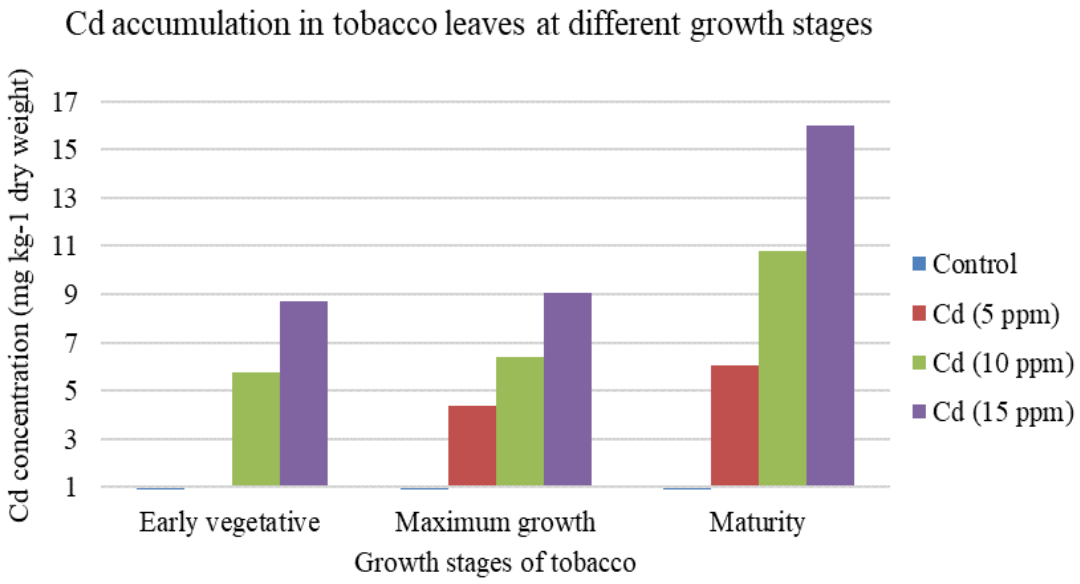

Figure 3.7: Cd accumulation at different growth stages of tobacco

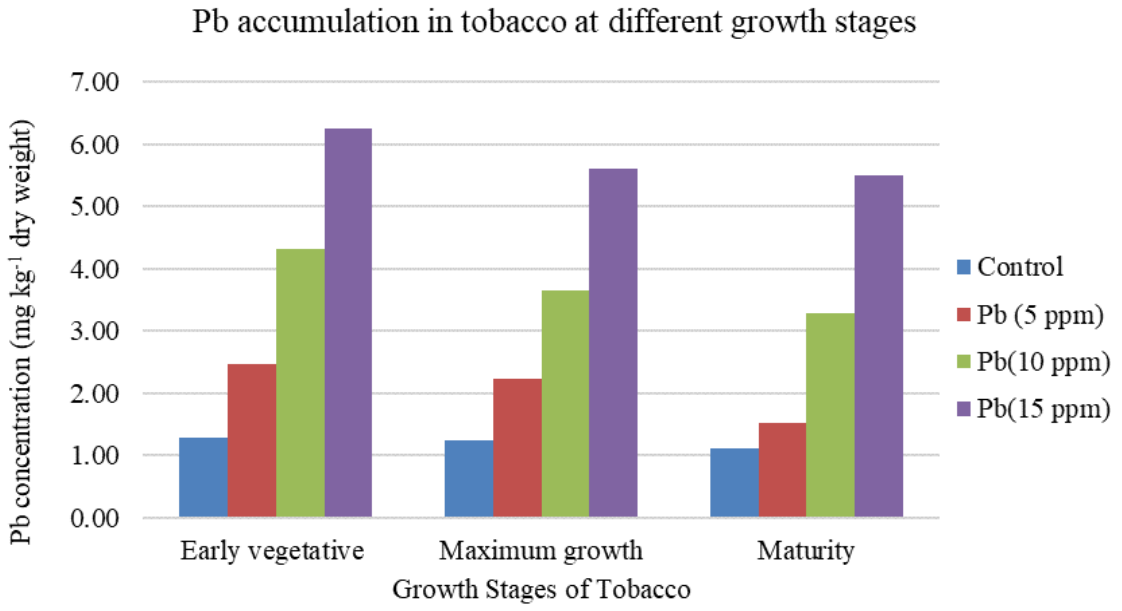

Figure 3.8: Pb accumulation at different growth stages of tobacco

3.6.3 Spectral analysis of cotton and tobacco

Plants acts as an excellent indicator for detecting heavy metal ions present in the soil. Uptake of heavy metal by plants results in some biochemical changes, such as changes in chlorophyll content and in the leaf internal structure, inducing changes in the spectral properties in heavy metal-contaminated plants [194]. The spectral reflectance over a continuous wavelength region provides relevant spectral features to assess changes occurring in vegetation due to heavy metal contamination. Spectral readings were taken for each treatment of cotton and tobacco plants. The readings from the three replication with different levels of Pb and Cd were used for further spectral as well as correlation analysis.The results from the pot experiment revealed more accumulation of Pb in leaves of cotton and Cd in tobacco. In contrast, the accumulation of Cd in cotton and Pb in tobacco was negligible. This result forms the basis for further spectral evaluation of the presence of Pb in cotton and Cd in tobacco.

The pot experiment shows that with increase in levels of Pb and Cd their concentration increases in plant leaves. The chlorophyll content of the leaves decreases accordingly, indicating the effect of Pb and Cd . Such changes affects the reflectance of plant at wavelength regions related to chlorophyll and water content. The findings of previous research shows that the wavelength region in red edge (around 700nm) and NIR (750-1000 nm) shows correlation with the presence of heavy metal [24] [20]. The reflectance spectra collected from each Pb treatment at different growth stages of cotton were indistinguishable. It indicates that the presence of Pb could not induce changes in reflectance spectra at different growth stages of cotton due to lower Pb absorption and higher growth rate at later stages. Owing to the higher accumulation of Pb during the vegetative stage, the cotton spectral observation only at the initial growth stage, i.e., the vegetative stage, was used for further spectral analysis to study Pb contamination. With initial spectral observation at the vegetative stage in cotton, it was evident that the reflectance spectra obtained at different levels of Pb could not capture significant changes due to Pb stress, as depicted in Figure 3.9. The correlation analysis was performed to evaluate the impact of metal concentration on leaf reflectance.

Based on the previous scientific findings strength of correlation was set as weak ($|r| < 0.39$), moderate ($0.40<|r|<0.59$), and strong ($|r|> 0.60$) [195] [196]. The correlation analysis between reflectance spectra at the early vegetative stage of cotton and Pb indicated a non-significant correlation, presented in Figure 3.10.

Pot experiment results for tobacco revealed a higher accumulation of Cd at the maturity stage. So, the maturity stage of tobacco is used for further spectral analysis to study the effect of Cd on spectral properties. The damage due to high Cd levels in tobacco by studying the spectral properties in detail provides an insight into the accurate wavelength region affected by heavy metal. The initial investigation revealed that reflectance spectra do not show any distinct change due to different Cd levels, as visualized in Figure 3.11. The correlation analysis between reflectance spectra and Cd was not significant, as depicted in Figure 3.12.

Reflectance spectra of cotton contaminated with Pb and tobacco contaminated with Cd do not show any distinct changes to assess the effective wavelength of the electromagnetic spectrum affected due to Pb and Cd. Indistinct changes in reflectance can be due to NO_3 salt spiking, which favors chlorophyll biosynthesis resulting in indistinguishable spectra from non-treated plants [96] or relatively lower heavy metal accumulation to produce evident changes in the spectra [115]. Further analysis of spectra was needed to extract meaningful information.

The first derivative of the spectra was used for further spectral analysis to enhance the subtle information about the effect of the heavy metals on spectral properties. Studies have established that changes in peak and the magnitude of first derivative spectra are due to the light scattering by leaf tissues due to chlorophyll absorption [197]. A shift in the red edge position towards a shorter wavelength (blue shift) can indicate heavy metal stress. The first derivative spectra of Pb in cotton and Cd in tobacco, as depicted in Figure 3.13 and Figure 3.15, do not show any changes in peaks obtained between 700 nm and 715 nm. The correlation analysis of the first derivative spectra with heavy metals also showed no significant changes, as represented in Figure 3.14 and Figure 3.16. However, a few researchers have reported that the blue shift might not exist in each case. The absence of this shift can be due to the plant's ability to grow even with heavy

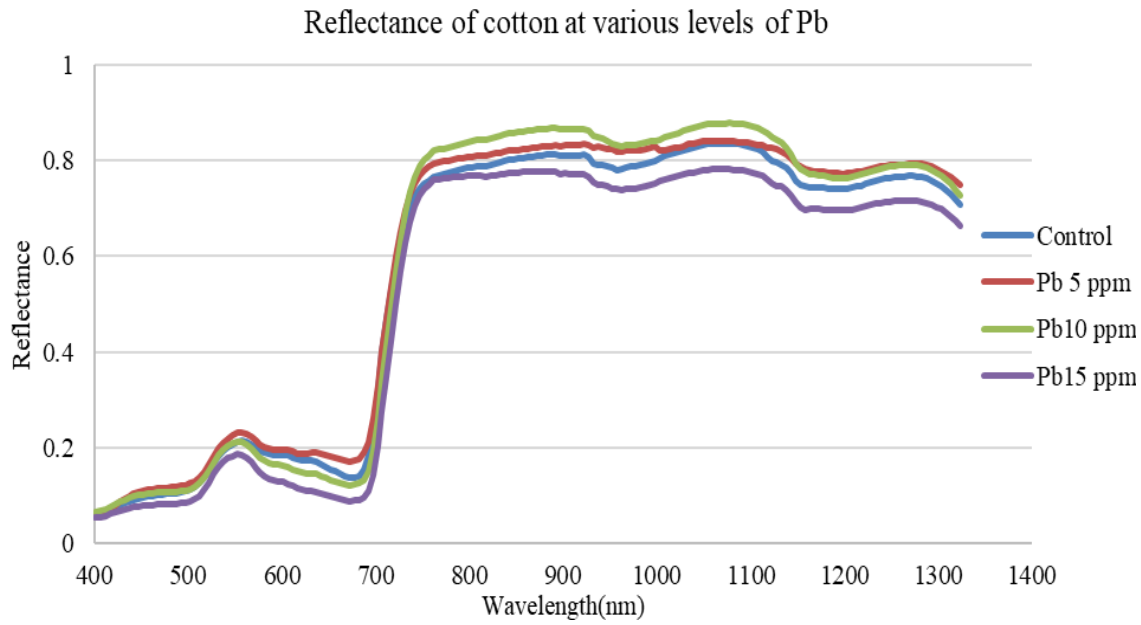

Figure 3.9: Reflectance spectra of cotton at various levels of Pb stress

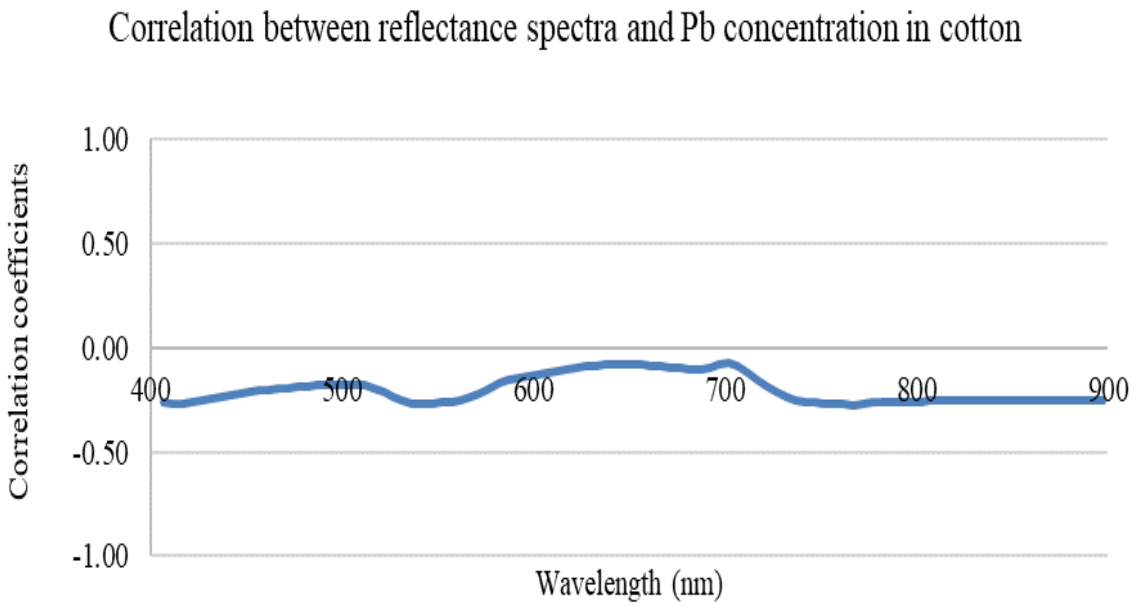

Figure 3.10: Correlation analysis of reflectance with Pb concentration in cotton leaves

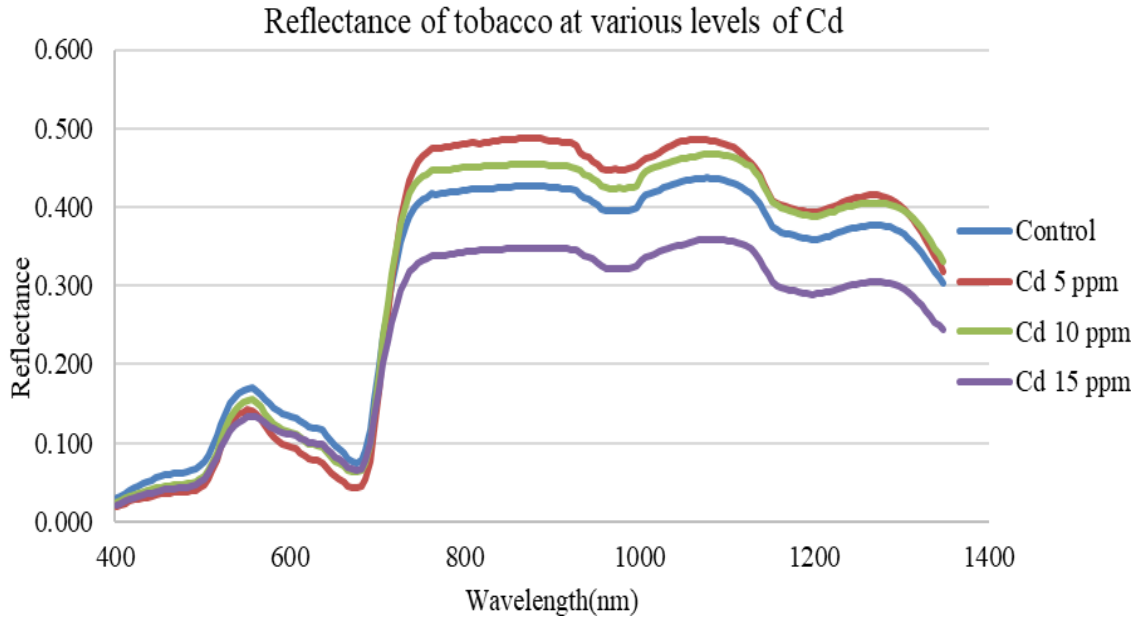

Figure 3.11: Reflectance spectra of tobacco at various levels of Cd stress

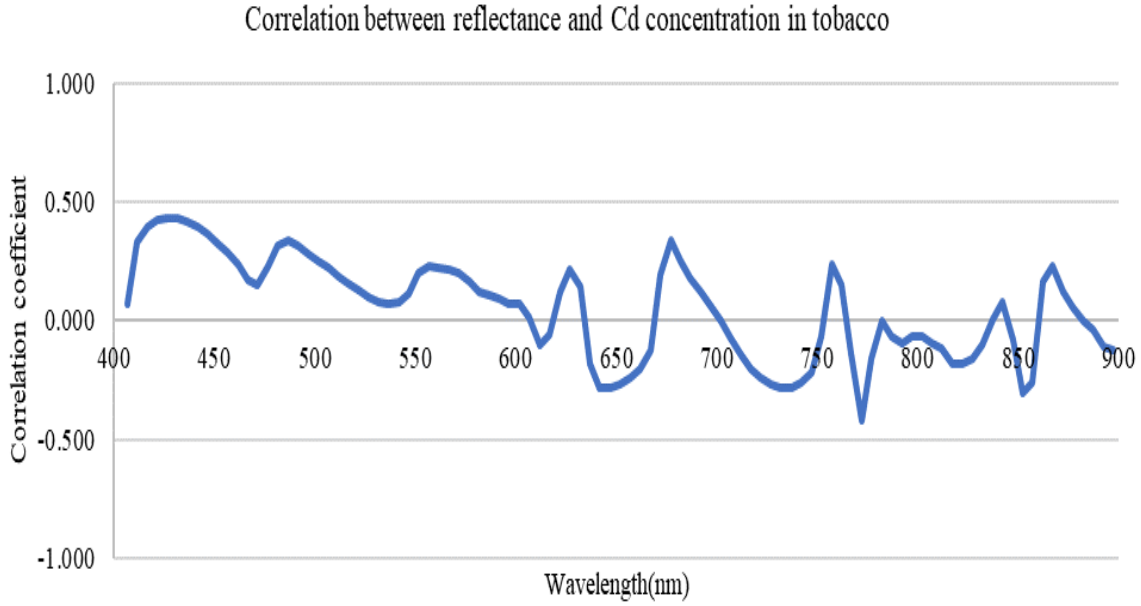

Figure 3.12: Correlation analysis of reflectance with Cd concentration in tobacco leaves

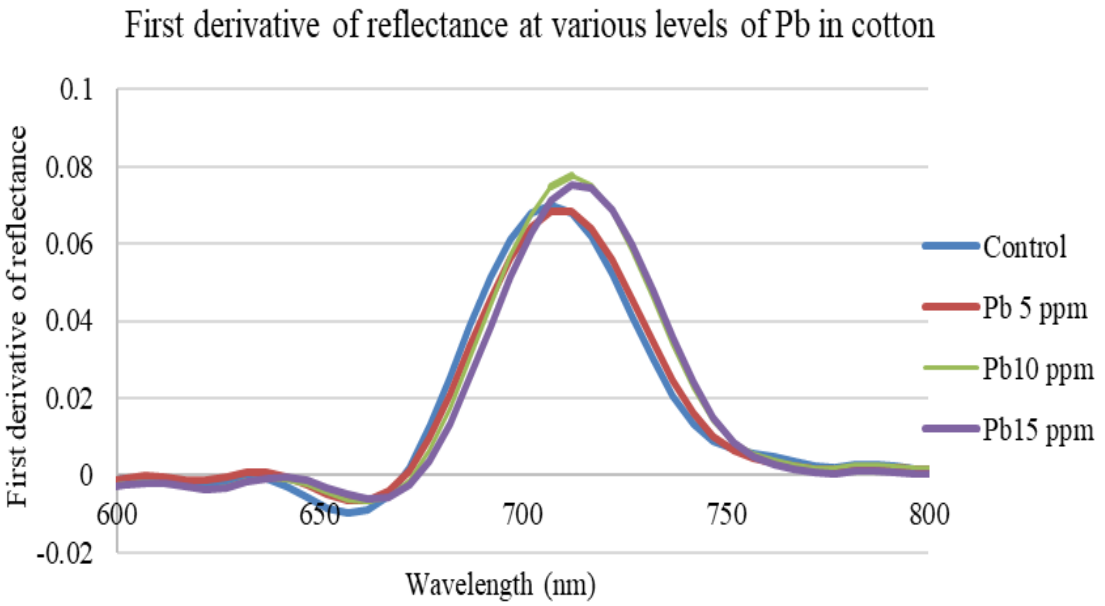

Figure 3.13: The first derivative showing the red edge position of cotton at various levels of Pb

metal stress [198]. No distinct spectral changes were observed in standard reflectance spectra and the first derivative, indicating heavy metal stress in cotton and tobacco. So further spectral analysis by wavelet decomposition of spectra was carried out to estimate the wavelength region sensitive to Pb and Cd in cotton and tobacco, respectively.

3.6.4 Wavelet analysis of spectra

Further wavelet decomposition of the spectra can extract and quantify the heavy metal stress not so evident from the standard reflectance and its first derivative. The wavelet decomposition provides detail and approximation coefficients. Detail wavelet coefficients can capture minute changes present in the reflectance signal. Therefore, the reconstructed detail reflectance obtained from upsampling of detail coefficients having the same dimension as the original spectra were utilized for further spectral analysis [100]. The reconstructed detail reflectance strengthens the spectral variations at the third decomposition level (d3) [115].

The higher decomposition level resulted in a coarser spectral resolution and increased loss of spectral information, while the lower decomposition level might

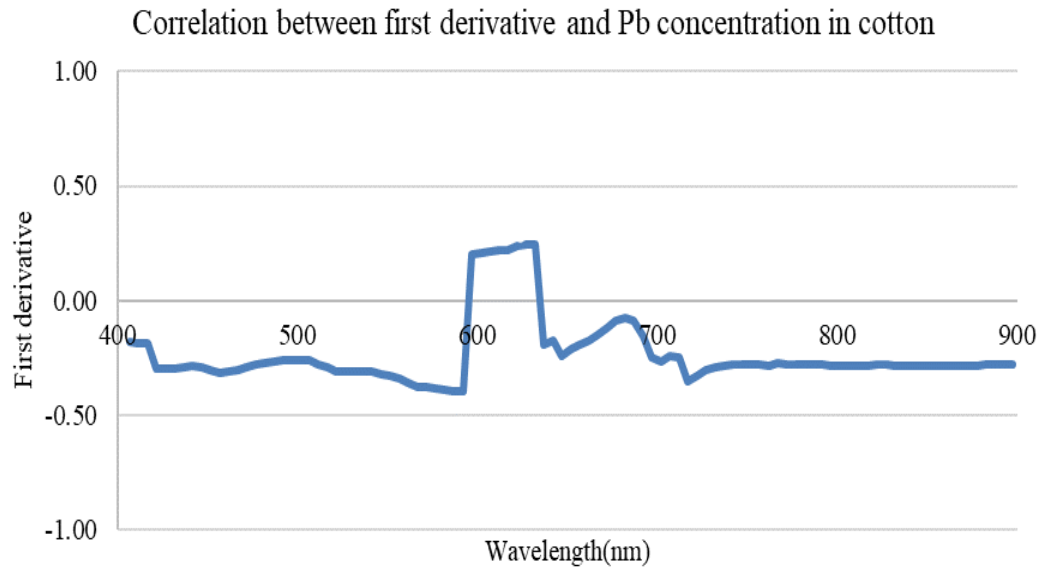

Figure 3.14: Correlation analysis of the first derivative of cotton at various levels of Pb

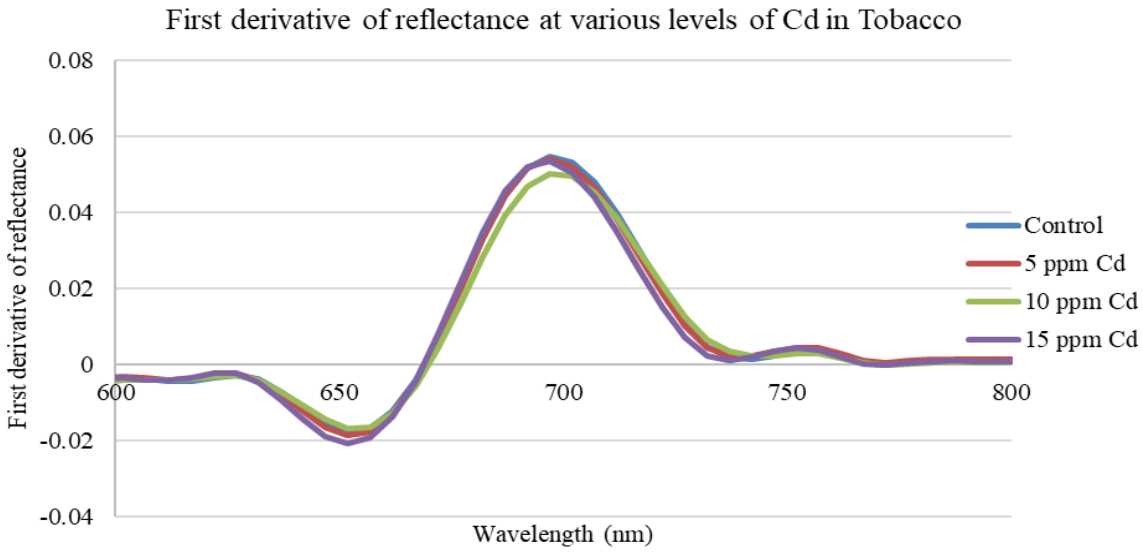

Figure 3.15: The first derivative showing the red edge position of tobacco at various levels of Cd

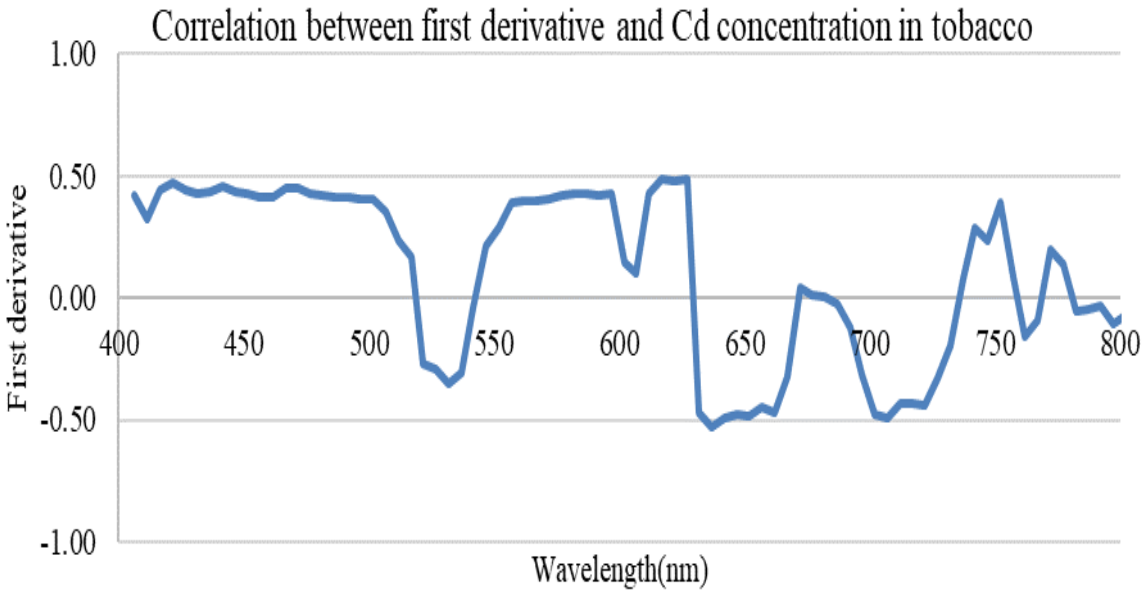

Figure 3.16: Correlation analysis of the first derivative of tobacco at various levels of Cd

have more background noise. Figure 3.17 and Figure 3.19 represent the relationship between Pb concentration in cotton and Cd concentration in tobacco at the third decomposition level. The reconstructed detail reflectance shows a clear pattern in amplitude change due to Pb levels in cotton and Cd levels in tobacco. The large amplitudes of the detail reflectance in the control plant and small amplitude with less discontinuity indicate variations associated with the different levels of Pb in cotton and Cd in tobacco. The correlation analysis at a significance level (alpha = 0.05), further quantifies the relation between the amplitudes of the detail reflectance to find out the optimum wavelength region affected by the presence of Pb in cotton and the presence of Cd in tobacco. The correlation sensitivity analysis shows a significant correlation above -0.70 ($r > -0.70$, $p<0.05$) between 651-742 nm due to Pb stress in cotton, given in Figure 3.18. Similarly, in tobacco, a significant correlation above -0.85 ($r > -0.85$, $p<0.05$) was obtained in the wavelength region between 631 -802 nm showing its sensitivity to Cd, represented in Figure3.20. The correlation analysis revealed that subtle changes in the spectra due to heavy metal not being visible in the original spectra or the first derivative could be quantified by wavelet decomposition.

The spectral analysis establishes the exact wavelength region sensitive to Pb

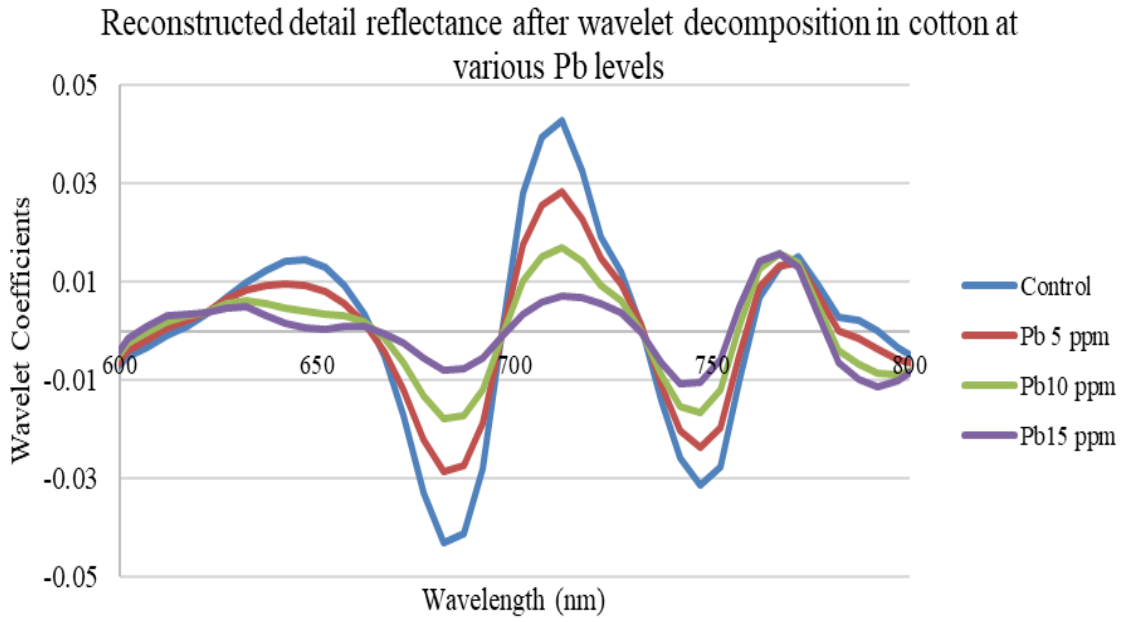

Figure 3.17: Reconstructed detail wavelet coefficients of cotton reflectance spectra at various levels of Pb

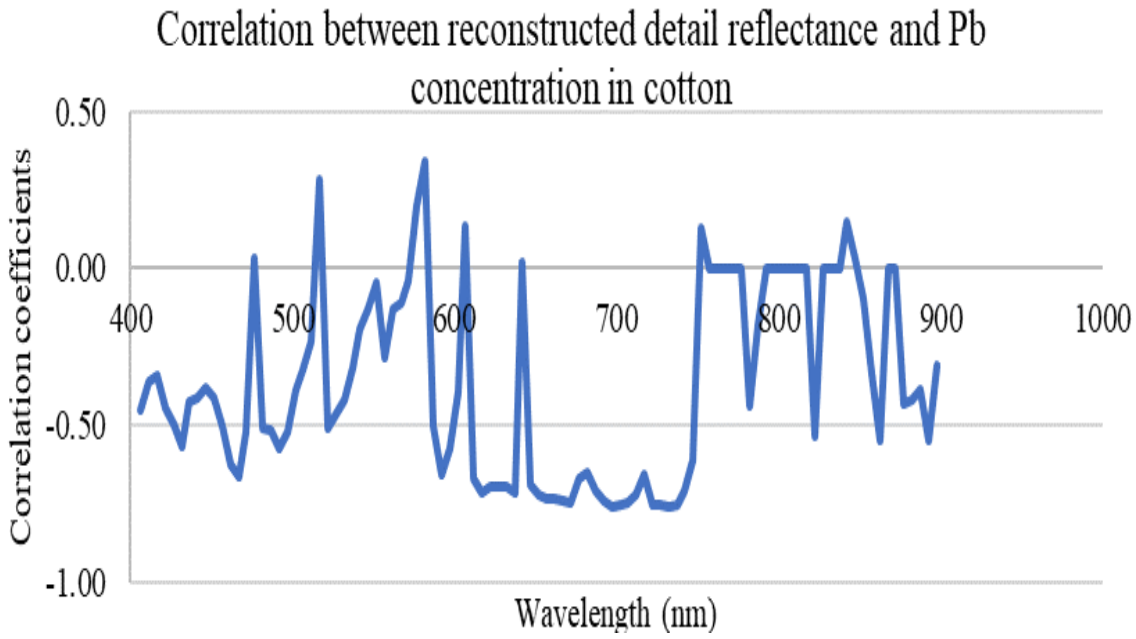

Figure 3.18: Correlation analysis of wavelet coefficient with Pb concentration in cotton leaves

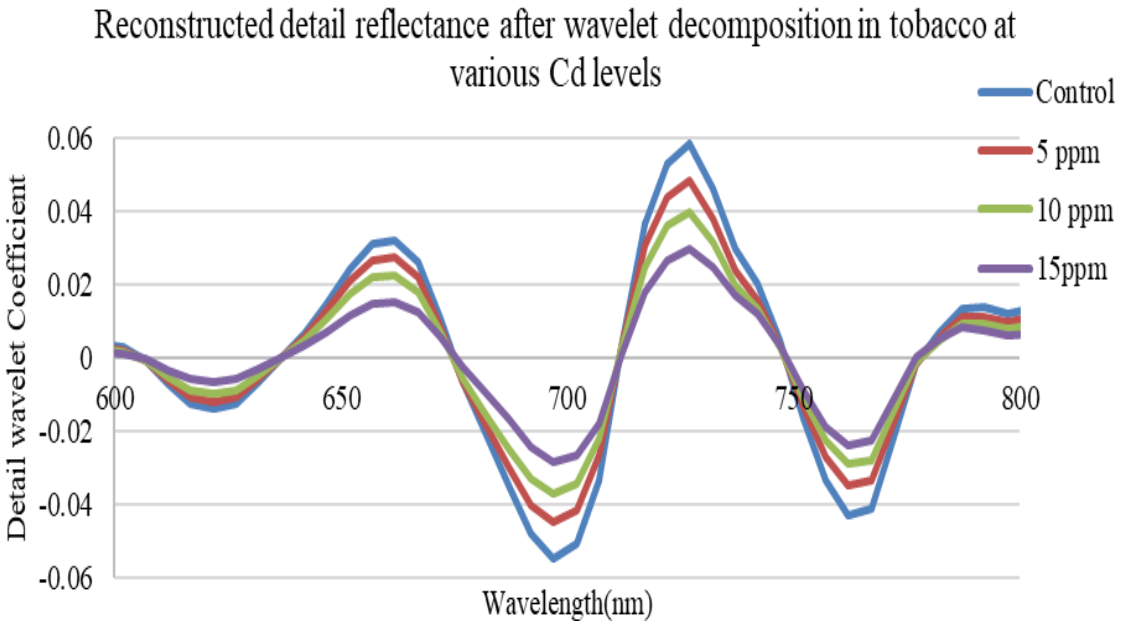

Figure 3.19: Reconstructed detail wavelet coefficients of tobacco reflectance spectra at various levels of Cd

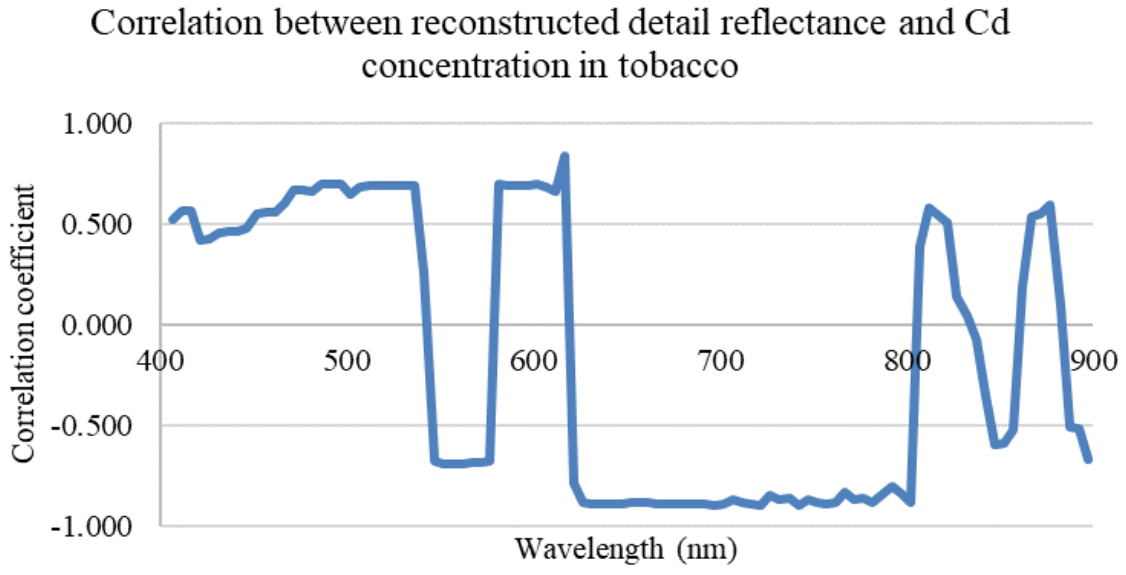

Figure 3.20: Correlation analysis of wavelet coefficient with Cd concentration in tobacco leaves

stress in cotton (651-742) nm and Cd stress in tobacco (631-802 nm). This region belongs to the visible and infrared regions of the electromagnetic spectrum and is associated with a decrease in chlorophyll concentration with an increase in heavy metal levels resulting in changes in leaf spectral characteristics. The reduction in chlorophyll biosynthesis due to the presence of heavy metals can result in these spectral changes. The studies by different researchers have also established that different heavy metals have their spectral peculiarity at various wavelengths in different species [197][199].

A similar wavelet-based study was conducted by Wang et al., indicating that the wavelength region 605-720 nm is sensitive to Cu stress in Carex leaves at the fourth level of the wavelet decomposition [115]. Gu et al. found that a higher concentration of Cd is associated with a decrease in spectral response at the NIR wavelength region in *Brassica* [200]. Higher heavy metal concentration in different plant species is affected the spectral reflectance in visible and NIR regions [201]. These changes may not be so high to trigger changes in original reflectance, but they can be made prominent through further spectral analysis. Several researchers have regarded the spectra in the range of red and near-infrared regions as an indicator of heavy metal stress as the sensitivity in this wavelength range is due to chlorophyll absorption, indicating a strong influence on photosynthesis [201][202].Toxicology study of Pb and Cd on leaves of metal induced plant shows the spectra in the range of red and NIR regions related to chlorophyll absorption as an indicator of heavy metal toxicity, indicating a strong influence on photosynthesis. The significant correlation ranging from -0.58 to -0.72 was noted by Rathod et al. reflectance ranging from 691-721 nm and Pb concentration in leaves of barley durig ealy growyh stage [96]. Exposure to Cd affected the spectral reflectance in the range of 550nm - 680 nm and 750nm - 1050 nm in Cd stressed castor bean [203].

CHAPTER 4

Hyperspectral Data Classification

4.1 Problem statement

In Chapter 3, the pot experiment was discussed. The experiment was undertaken to characterize the reflectance spectra of crops as affected by different levels of Pb and Cd. The effective wavelength region showing the presence of Pb in cotton and Cd in tobacco was established by wavelet decomposition and correlation analysis, which can be further used to quantify the presence of heavy metals in plants. Pot experiment has a limited scope but is very useful for developing training data under controlled conditions. Such field-level spectral data collected from experimental pots must be transferred to the vast geographical region using air or space-borne data for effective and prompt surveillance of heavy metal pollution. The presence of heavy metal in plants can be characterized using specific responses in the visible, near-infrared, and shortwave infrared spectral domains, making it possible to map heavy metal contamination with remotely sensed data. Recent development in hyperspectral technology has made it possible to differentiate even mild level of heavy metal before the actual damage occurs. The crop classification from hyperspectral data is essential for mapping heavy metal in a particular crop over the study area. So, the primary objective of this chapter is to classify tobacco and cotton crops in the Anand and Surendranagar regions of Gujarat, respectively, using airborne hyperspectral data from AVIRIS-NG.

Hyperspectral data provide detailed and continuous information within the full range of 350–2500 nm wavelengths to systematically determine the small changes in spectral properties of leaves, and studies can be carried out to relate

such changes in leaf spectral signature with heavy metal contamination. Hyperspectral data's spectral and spatial richness makes it better in performance than multispectral datasets for classification [204]. While working with hyperspectral data, a major setback is the high dimensions of this data, making it challenging to handle. So, retaining only necessary information and removing redundant information through different feature extraction methods are required for better crop classification performance. Implementation of linear feature extraction methods like Independent Component Analysis (ICA) [205] and Linear Local Embedding (LLE) [206] cannot model nonlinear properties present in hyperspectral data, and better discrimination cannot be achieved in classification. Using an autoencoder with a nonlinear activation function has good scope in extracting highly informative features [207]. In recent years, the neural network model has been used to classify hyperspectral data[208]. Neural networks can learn the nonlinear features present due to various activation functions. We have utilized a combination of autoencoders for feature extraction followed by the artificial neural network to classify hyperspectral data. Classification of crops is an intermediate step to detect heavy metal over larger areas. The classified tobacco crop in the Anand region and cotton in the Surendranagar region will be used for heavy metal mapping based on the training data from the control pot experiment.

4.2 Methodology

Since hyperspectral data consist of a large number of narrow bands. Most of these continuous spectral bands contain redundant information causing a reduction in classification accuracy and increased computational complexity. Hence, feature extraction is vital in hyperspectral data classification, resulting in more accurate classification. Most feature extraction methods are linear and do not capture the non-linearity in hyperspectral data. However, the autoencoder (AE) neural network also considers the non-linearity present in data. AE network is a feed-forward neural network in which the unsupervised training of the network is done [209]. AE consists of the first input layer, which contains the input data,

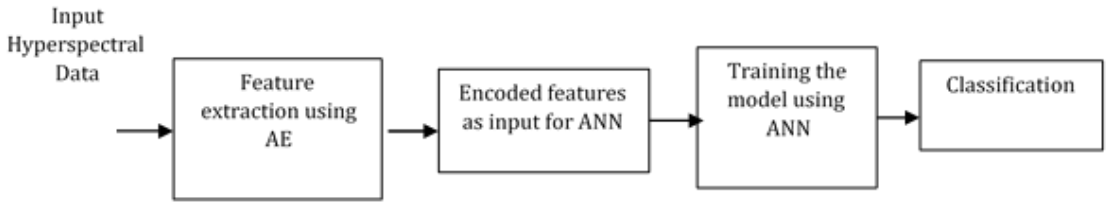

Figure 4.1: An overview of the proposed model

the middle hidden layer, which contains encoded features; and a decoding layer which gives the reconstructed output. The middle layer of the AE network, having encoded features, has been used as input for supervised classification using ANN. The features extracted from the autoencoder network contain maximum information with reduced noise, improving classification accuracy. The ANN for classification consists of an input layer of encoded features, a middle layer containing the ReLu activation function, and the last classification layer using SoftMax to obtain a multiclass classification. The complete overview of the combined model is shown in Figure 4.1.

The training of the network is done by combining two steps:

- Unsupervised feature extraction using Autoencoder (AE) and
- Supervised Artificial Neural Network (ANN)

Layer-wise, training of the AE network is done to learn the critical encoded features. These encoded features are used as inputs for supervised classification using different class labels. This model allows beneficial features to be extracted and used for classification simultaneously.

4.3 Model architecture

4.3.1 Autoencoder (AE) for feature extraction

AE is considered an unsupervised feed-forward neural network that contains three layers: input layer, hidden layer or encoding layer, and output or decoding layer. The first input layer contains the input satellite data X then the middle hidden layer contains encoded features represented by G then a decoding layer

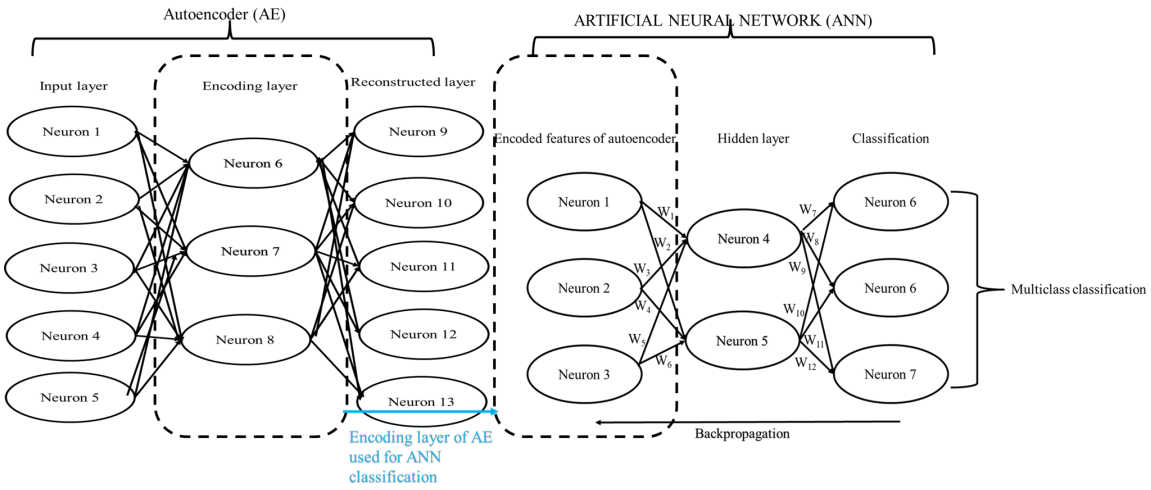

Figure 4.2: The architecture of AE-ANN model

which gives the reconstructed output represented by $G^{|}$. The number of units in the input layer equals the number of bands in the input data X. Figure 4.2 illustrates AE's architecture showing the input, encoding, and reconstruction layers.

The input layer is encoded into the hidden layer by encoding the input layer using the sigmoid activation function as illustrated in equation 4.1.

$$G = f_a(wX + b) \tag{4.1}$$

Where G denotes the hidden or encoded feature layer, w is the encoded weights, $f_a$is the activation function and, b denotes the bias. The sigmoid activation function given in equation 4.2 has been used to accommodate nonlinear features present in the data.

$$f_a = \frac{1}{1 + e^{-x}} \tag{4.2}$$

The sigmoid activation function varies from 0 to 1. These encoded features are then used to reconstruct the original image using a demapping function presented in the equation 4.3.

$$G^{|} = f_a(w^{|}G + b) \tag{4.3}$$

where $G^{|}$ is the reconstruction of original data X and $w^{|}$ is considered as decoding

weights. The output decoding layer has the same number of nodes as the input layer.

4.3.2 ANN for classification

Artificial Neural Networks (ANN) with backpropagation are nowadays popularly used to classify hyperspectral data [210] [208]. ANN framework consists of the input, hidden, and output layers, linked to each other through weights obtained from different activation functions depending on the purpose of its application. In this research, we are using the features extracted from AE as the input layer of the ANN model, not utilizing the reconstructed output of the decoding layer of AE, as depicted in Figure 4.2. Labelled class data is used for fine-tuning of the model. The ReLu activation function is used in the hidden layer as illustrated in equation 4.4.

$$f(x) = max(0, x) \tag{4.4}$$

In the output layer of the network, classification is done using SoftMax to obtain a multiclass crop classification. It determines the maximum probability of the input for being in particular class represented in equation 4.5.

$$\sigma(x)k = \frac{e^{xk}}{\sum_{j=1}^{j} e^{kj}} \tag{4.5}$$

$(k = 1.....j)$, k is the number of classes.

It gives us the probability of finding out the classes to which the input belongs. It is well suited for multiclass classification problems.

4.4 Dataset

Crop classification using the proposed model was done using the hyperspectral dataset collected by AVIRIS- NG sensor over Anand and Surendranagar, in Gujarat, collected during February 2016 [204]. The dataset contains 425 spectral bands in the wavelength range of 380-2500 nm with 5nm spectral resolution. The

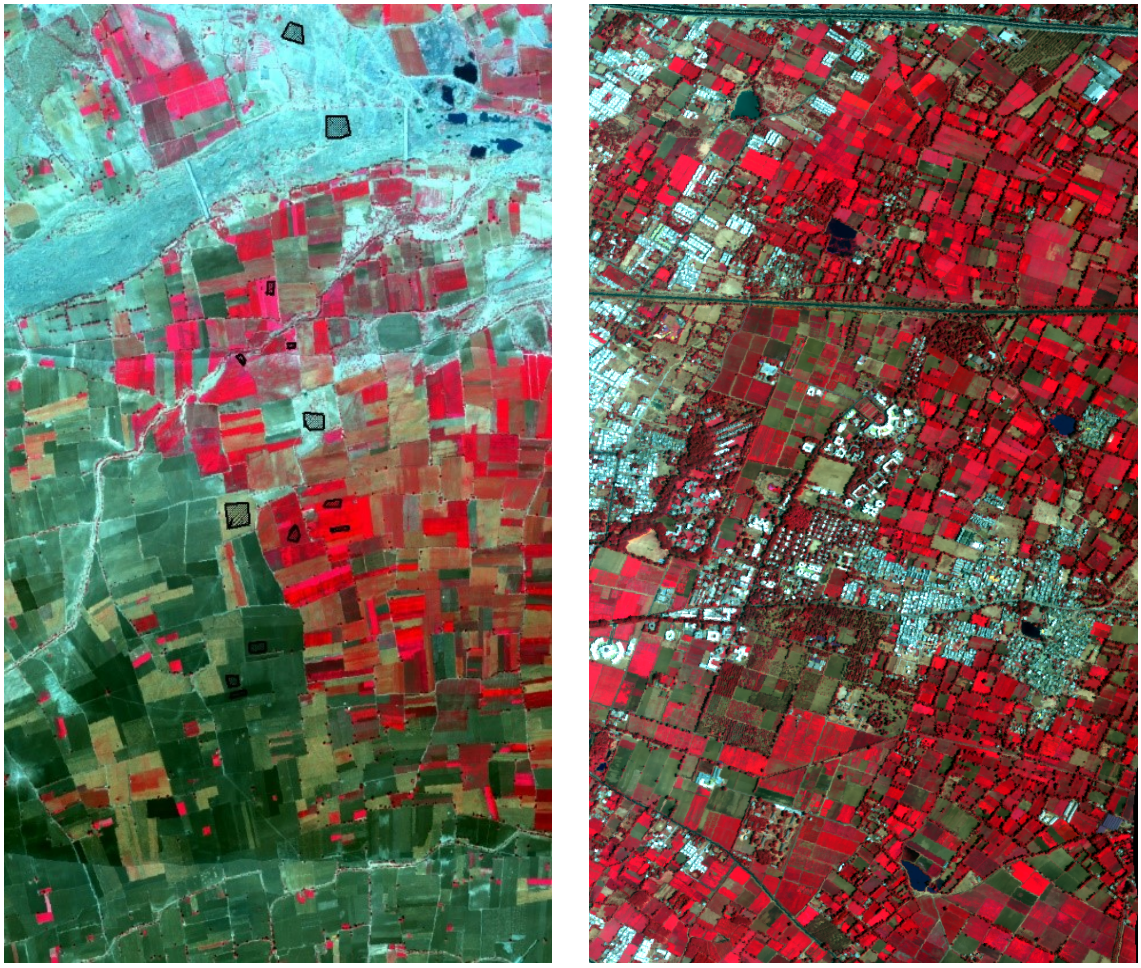

(a) Surendranagar region (b) Anand region

Figure 4.3: FCC of AVIRIS-NG showing polygons of the labeled crop

radiometrically and geometrically corrected L2 data with 368 bands after removing the water absorption and noise-containing bands was used for further classification study. Figure 4.3 represents the False Color Composite (FCC) of the hyperspectral dataset for the Surendranagar and Anand region by taking the infrared band in the red channel, the red region in the green channel, and the green region in the blue channel.

The labelled data was obtained during field study at the time of AVIRIS-NG flight. The polygons were drawn to different classes of labelled data. Various steps performed while testing the model over the given hyperspectral dataset is given below:

- hyperspectral dataset is normalized and used as input for the autoencoder network

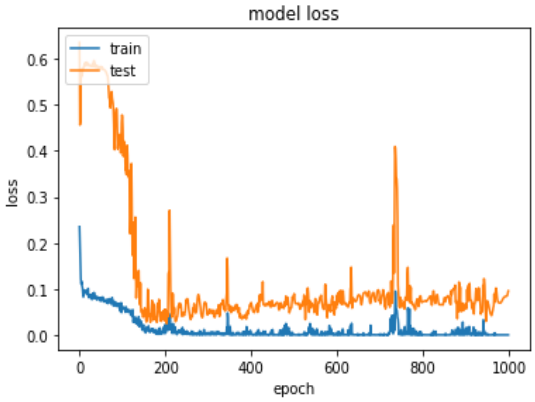

(a) Model loss for Anand

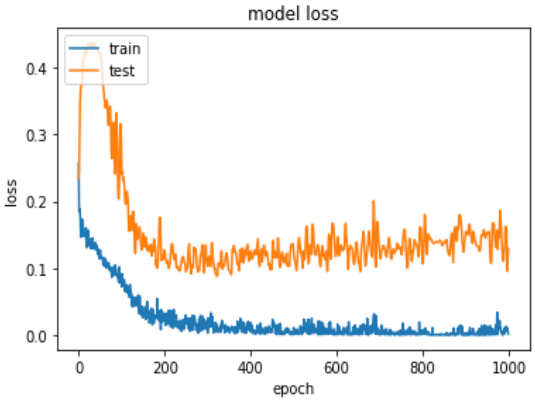

(b) Model Loss for Surendranagar

Figure 4.4: Model loss

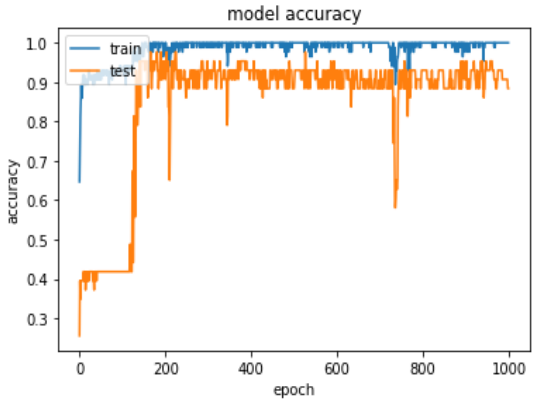

(a) Model accuracy for Anand

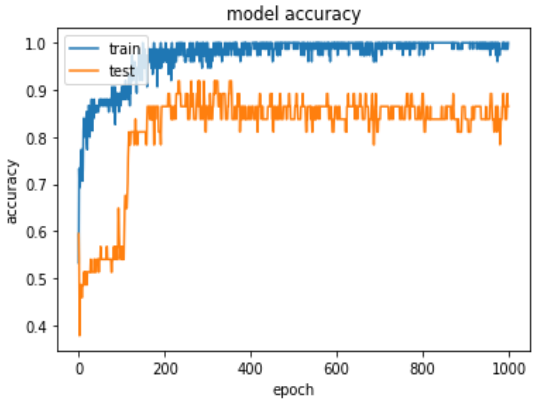

(b) Model accuracy for Surendranagar

Figure 4.5: Model accuracy

- random splitting of the dataset into training and testing set
- the autoencoder training is done using the sigmoid activation function
- the features are encoded in encoding layers
- these encoded features are used as input for classification using ANN
- labelled dataset is used for fine-tuning the model.
- the output classified image after applying ReLu and SoftMax function

The loss function used in ANN is binary cross entropy. The model's performance was evaluated in terms of model loss and model accuracy.

Figure 4.4a and Figure 4.5a indicate the training and validation loss and the training and testing accuracy of the proposed model while training the model for classification in 1000 epochs for Anand region. Figure 4.4b and Figure 4.5b indicate the training and testing accuracy of the proposed model while training the model for classification in 1000 epochs for Surendranagar regions. The proposed model gives an accuracy of up to 87% when used for classification in the Surendranagar region and up to 89% for the Anand region.

4.5 Results and discussion

A neural network combining unsupervised and supervised training is proposed for hyperspectral feature extraction and classification. AE trains the network in an unsupervised manner and performs classification in a supervised manner. The features learned by AE are used for further supervised classification to achieve better discriminations of classes by achieving sparsity in features.

The classification model performed best when 20 encoded AE features were used as input for ANN classification. After that, increasing the encoded features did not improve its accuracy. The classification results of the proposed model using 20 encoded features as an input for ANN in Surendranagar and Anand, respectively, are depicted in Figure 4.6a and Figure 4.6b. Figure 4.6a shows the overall classification of the Surendranagar region with different crops, and Figure 4.7a represents only cotton pixels in Surendranagar after masking all other crops. Similarly, Figure 4.6b shows the classification of the Anand region with different crops, and Figure 4.7b represents only tobacco pixels in Anand. After classification, we need to judge the quality of the classification results and evaluate the performance to show the feasibility of the proposed algorithm and further improvements based on their shortcomings. Commonly used evaluation indicators are the confusion matrix, *Kappa* coefficient, and overall classification accuracy [211].

The classification report regarding the overall accuracy and kappa coefficient for Anand and Surendranagar area is given in Table 4.1. Figure 4.8a and 4.8b

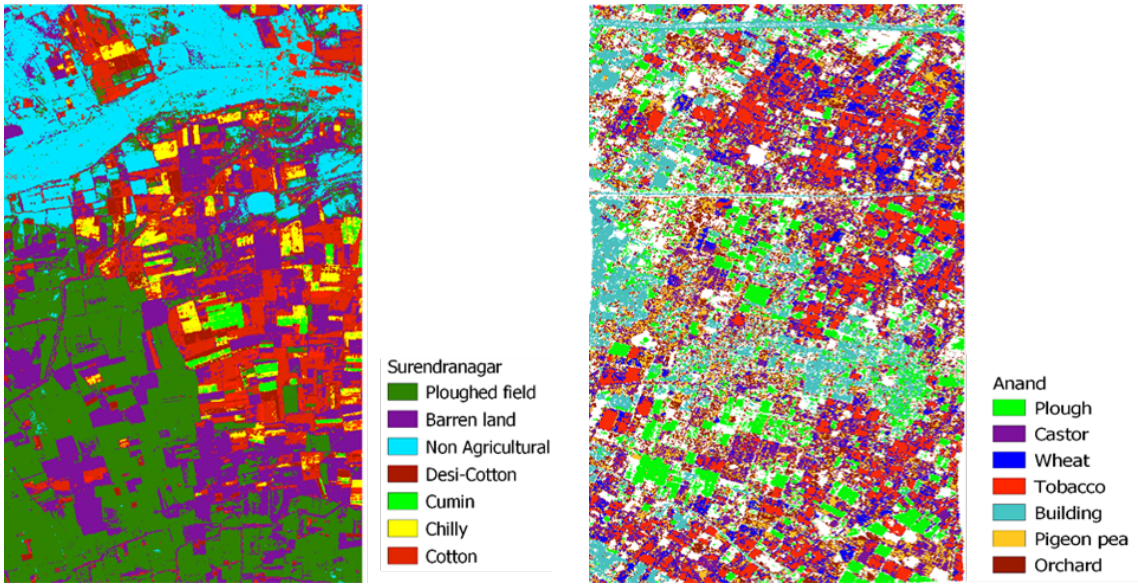

(a) Classified image at Surendranagar (b) Classified image at Anand

Figure 4.6: Classified image showing different classes of crops

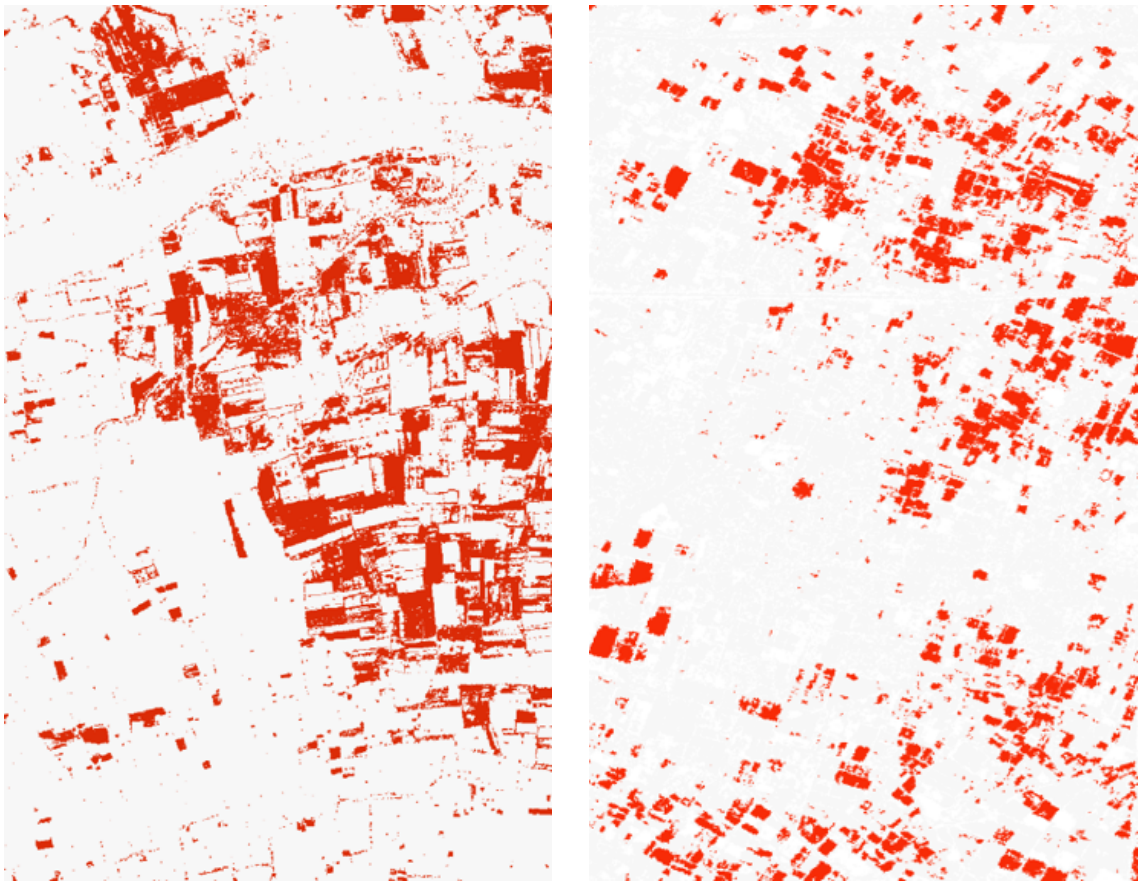

(a) Classified image showing cotton pixels at Surendranagar (b) Classified image showing tobacco pixels at Anand

Figure 4.7: Classified image showing cotton and tobacco pixels

Table 4.1: Overall Accuracy and *Kappa* coefficient for different regions

Study region	**Overall accuracy (%)**	***Kappa* coefficient**
Anand Region	89.68	0.86
Surendranagar Region	86.87	0.83

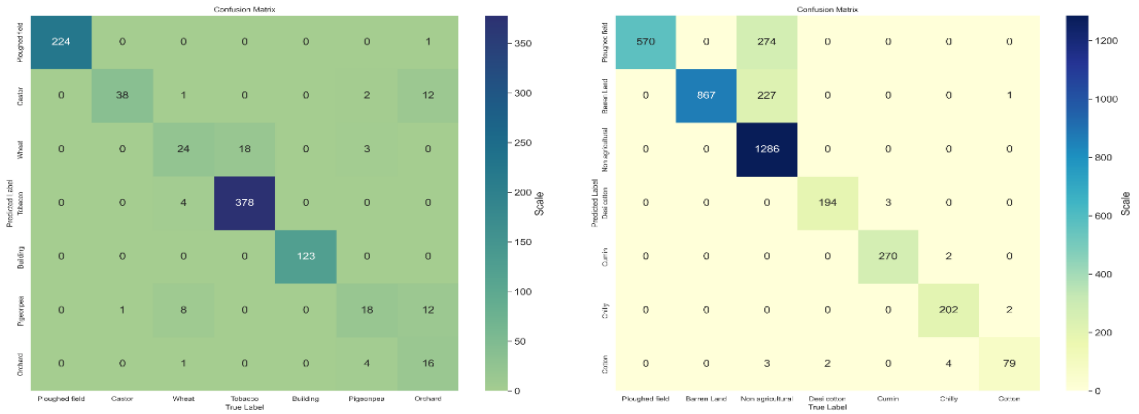

(a) Confusion matrix for Anand

(b) Confusion matrix for Surendranagar

Figure 4.8: Confusion matrix for crop classification

depict the confusion matrix for Anand and Surendranagar, respectively.

The proposed model of a combination of AE and ANN provides good crop discrimination in classification. It has been observed that only 20 spectral features are sufficient for classifying hyperspectral data instead of all 368 spectral bands. The accuracy decreased when 10 encoded features were used for classification, and beyond 20, no substantial improvement was achieved [212][213]. Further, these classified tobacco pixels in Anand and cotton pixels in Surendranagar were utilized for mapping heavy metal pollution.

CHAPTER 5

Detection of Heavy Metal

5.1 Problem statement

The traditional strategy of measuring the leave's heavy metal concentration through laboratory-based chemical procedures is time-consuming and expensive [214]. Considering this limitation, remote sensing techniques can be considered alternative methods with a strong scientific and practical background in measuring environmental parameters [215]. The heavy metal mapping through remote sensing is complicated due to the less heavy metal in leaves and the lack of reference data for the response of a particular heavy metal in a particular crop. Field experiments determining the spectral wavelengths sensitive to the presence of heavy metal in vegetation can provide reference spectra for heavy metal monitoring from airborne hyperspectral data. Under field conditions, the amount of heavy metal may not be enough to trigger spectral responses, so wavelet decomposition of spectral signals can enhance the spectral changes due to heavy metal. The heavy metal levels in field crops are significantly lower, making it challenging to capture the differences. In the pot experiment explained in Chapter 3, some distinct finding of the affinity of heavy metal towards crops was observed. Pb has more affinity towards cotton, while tobacco showed affinity towards Cd. This relationship is further analyzed for mapping heavy metal pollution through remote sensing data. In this chapter, we present a noble algorithm of spectral matching for heavy metal pollution mapping from the AVIRIS-NG dataset using DSW, based on the Dynamic Time Warping (DTW) algorithm. DTW algorithm has been widely used in speech recognition, anomaly detection, and clustering [216][217].

In this study, we have used detailed reconstructed reflectance generated from the pot experiment as reference spectra. The spectral patterns of each target crop pixel with unknown heavy metal levels were matched with a reference spectrum with known heavy metal concentration using the Dynamic Spectral Warping (DSW) model. This study employs in-field spectroscopy in estimating heavy metal contents in plants and using this model over airborne hyperspectral data. The DSW model is used for classifying tobacco and cotton pixels in Anand and Surendranagar region with unknown heavy metal concentrations using reference data obtained from the control pot experiment to detect Cd in tobacco crop and Pb in cotton crop. Altogether, this chapter is designed with the following goals: (i) the development of a pure profile based on the most appropriate wavelength range to detect heavy metal pollution and (ii) the evaluation of the performance of DSW algorithms in modeling the relationships between the foliar spectral response and heavy metal concentrations.

5.2 Methodology

5.2.1 Generation of reference spectra

The reference spectra with different levels of heavy metal concentration needs to be generated to perform the spectral matching using DSW algorithm. The selected detailed wavelet coefficients for Pb and Cd in cotton and tobacco were further used for mapping heavy metals from hyperspectral data. The available samples were first classified into different pollution levels based on the actual heavy metal concentration. The Pb and Cd concentration were classified into three groups based on the research findings: safe level, medium level and high level [218][219]. The findings of several researcher suggest that the presence of Cd above 3 ppm in plant tissue can generate toxicity symptoms [220]. The presence of Pb upto 12 ppm can be considered under the safe level in plants [221] [222]. The detailed wavelet coefficients for Pb and Cd in cotton and tobacco falling in different groups were averaged according to the different levels of heavy metal contamination and were further used for mapping heavy metals from hyperspectral data. The differ-

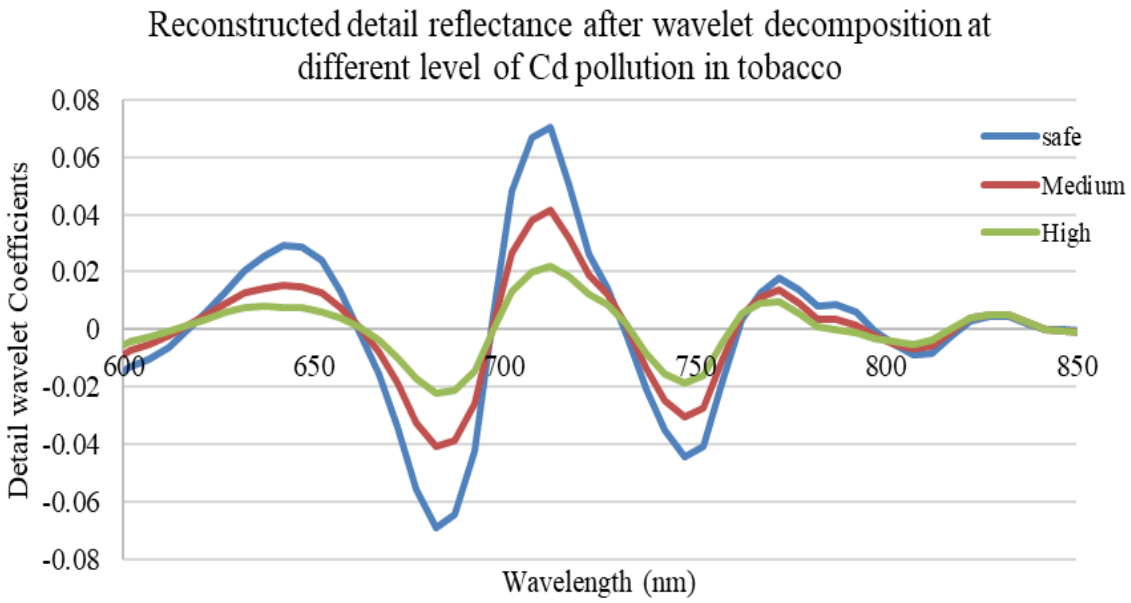

Figure 5.1: Reconstructed detail reflectance of tobacco at different levels of Cd pollution

ent groups based on the amount of heavy metal are given below for both metals.

Cd in Tobacco

- Safe level = 0 ppm to 3 ppm
- Medium level = 3 ppm and seven ppm
- High level = 7 ppm and above

Pb in Cotton

- Safe level = 0 ppm to 12 ppm
- Medium level = 12 ppm and 15 ppm
- High level = 15 ppm and above

The mean reconstructed detail reflectance at the third decomposition level was calculated for Pb in cotton and Cd in tobacco at different levels of heavy metal concentration depicted in Figure 5.1 and Figure 5.2, which served as reference data for mapping heavy metal concentration from hyperspectral data.

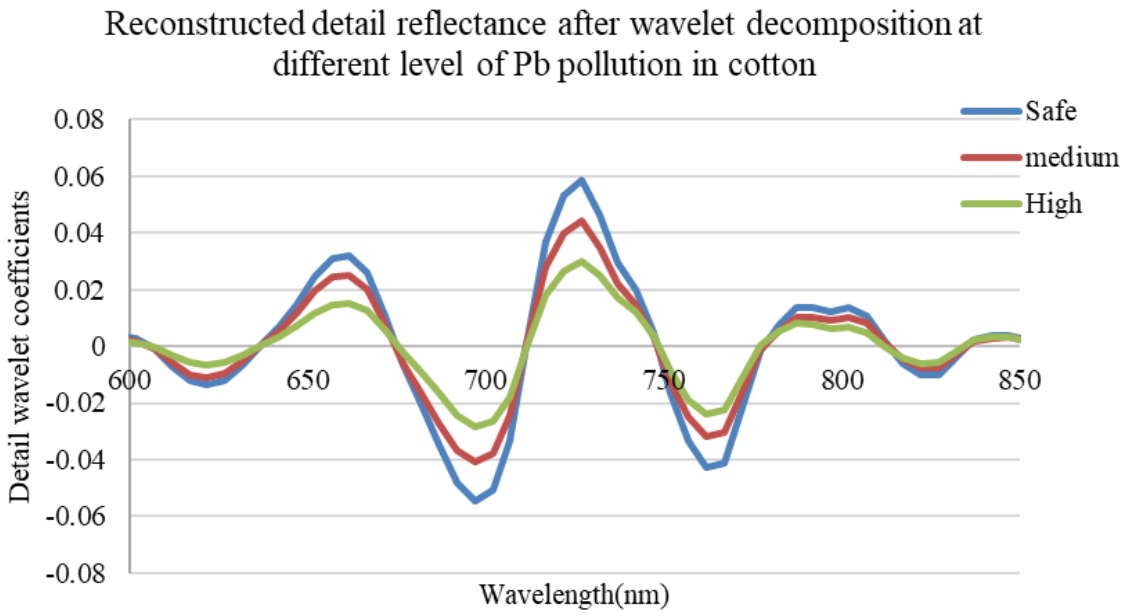

Figure 5.2: Reconstructed detail reflectance of cotton at different levels of Pb pollution

DSW

The correlation analysis of the spectra has revealed that reconstructed detailed wavelet coefficients at the third level of decomposition showed a good correlation with Cd concentration in tobacco leaves and Pb concentration in cotton leaves compared to normal spectra. So, reconstructed detail wavelet coefficients were used to generate reference spectra at three pollution levels. The spectra are categorized into safe, medium, and heavy based on the concentration, divided into three categories, and then averaged. The reference spectra for all three groups were generated from the reconstructed detailed spectra of the control pot experiment.

DSW algorithm determines the extent of Cd in tobacco crops and Pb in cotton crops. It classifies crops with different levels of heavy metal contamination based on the similarity matching with the reference spectra. For this, the reflectance spectra of classified tobacco and cotton pixels from hyperspectral data were also decomposed using wavelet decomposition, and reconstructed detail reflectance was used for matching with reference spectra having known levels of heavy metal pollution. It divides the two series into equal points, and the Euclidean distance

between the first point in the first series and every point in the second series is calculated. The minimum distance is stored through the spectral warp stage for all the data points. All the minimum distances give the measure of similarities between the two series.

DSW is based on DTW to measure the difference between two sequences [223]. Assume we have two spectra; the DSW algorithm is used to compute the similarity between two spectra $X(x_1, x_2, x_3, .., x_j....x_n)$ and $Y(y_1, y_2, y_3, ..., y_j, ..., y_n)$, with lengths m and n, respectively.

The distance matrix (d), i.e., $m \times n$, matrix of the squared distance, $(i, j) = \sqrt{(}xi - yz)^2 (i = 1, ..., m, j = 1, ..., n)$, also known as the "local cost matrix" is calculated to compare the spectra with the equidistant spectral interval [224].

The cumulative cost matrix (D) stores the lowest cumulative cost to reach any element in the $m \times n$ matrix and indicates the direction of search calculated using the given in equation 5.1 [225][226]

$$D(i, j) = d(i, j) + min(D(i-1, j-1), D(i-1, j), D(i, j-1)); i = 1, ..., m; j = 1, ..., n \tag{5.1}$$

The warping path with the lowest cumulative cost with minimum distance between the two sequences is determined to find the similarity between series X and Y. The warping path (W) is determined from (m,n) pointing to the least cumulative cost between adjacent cells showing the direction of alignment and extent of match between X and Y is represented by equation 5.2,

$$W = \langle w_1, w_2, w_3..., \rangle max\ (m,n) \leq K \leq (m + n) - 1 \tag{5.2}$$

where $w_k = (i, j)$ indicates the alignment between X and Y [227].

The illustration of the warping path from DSW and the corresponding alignment is presented in Figure 5.3 [228]. If the two sequences are similar, the warping path appears diagonal; otherwise, it diverges from the diagonal [228]. The DSW determines the shortest and quickest path through the cumulative cost matrix showing the best alignment between sequences. If the target pixel matches the reference spectra with different levels of heavy metal pollution, then the pixel

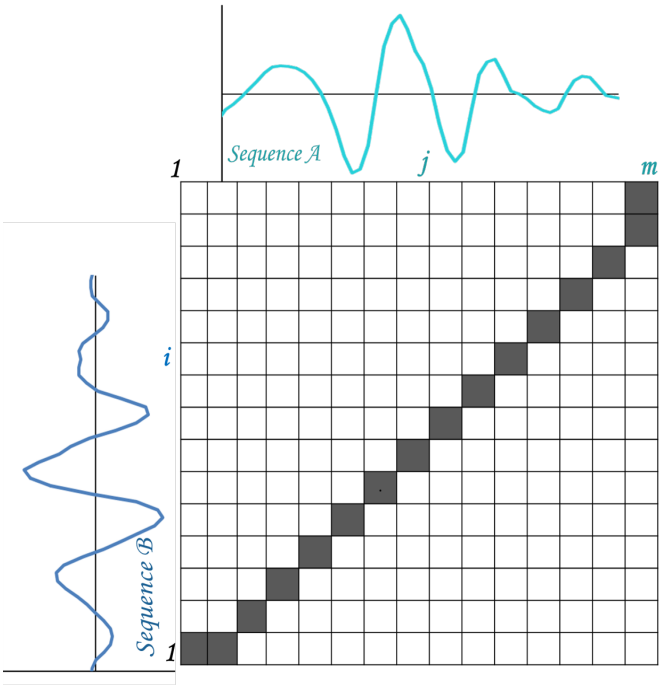

Figure 5.3: Illustration of the warping path of two series

is classified in the same category. However, if the difference between a reference and the target pixel is greater than the standard deviation, the target pixel remains unclassified.

5.3 Results and discussions

The DSW algorithm performed spectral matching for each unknown pixel to identify varying amounts of heavy metal contamination at distinct research locations. the DSW algorithm to detect various levels of heavy metal pollution at different study sites. Medium to low levels of Cd in tobacco was predicted by the DSW model in the Anand region. Figure 5.4 describes the extent of Cd contamination in tobacco crops in the Anand region. Few tobacco pixels show a medium Cd contamination level due to the increased level of Cd in the soils. The presence of a higher amount of Cd in the soils of Anand as a result of increased industrialization has been reported by Jha et al. in their study [229]. In a study, Nirmal Kumar et al. found higher amounts of Cd heavy metal in vegetables in Anand [230]. Such a study gives an insight into the presence of Cd in soils of Anand

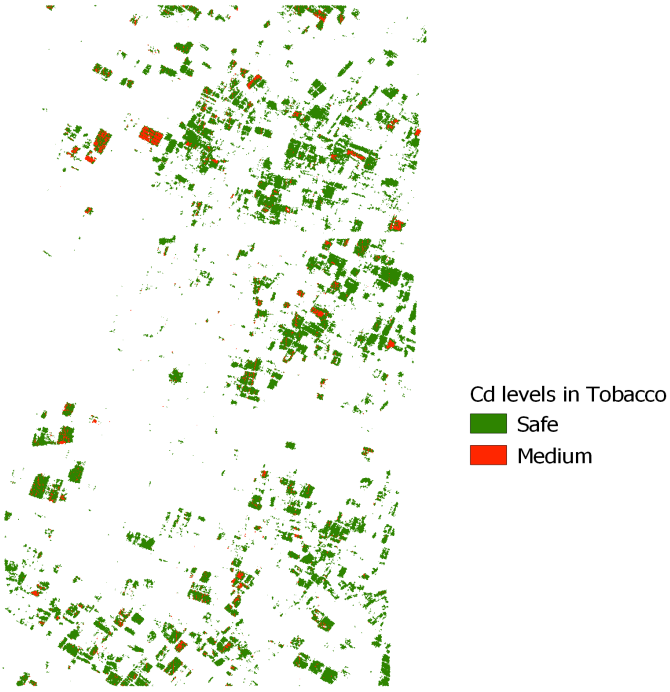

Figure 5.4: Different levels of Cd pollution in tobacco using DSW in Anand

which gets accumulated in tobacco plants due to the high sensitivity towards Cd. However, a high level of Cd contamination is not observed at any sites. The presence of moderate levels of Cd can be reduced using soil amendments and proper planning.

The degree of Pb contamination in cotton in the Surendranagar region can be observed in Figure 5.5. The safe and medium level was observed with none of the sites with high pollution levels. The current study demonstrates the presence of Pb in Surendranagar soils, which may be demonstrated by enhanced Pb absorption in cotton leaves. Various studies have shown an increased Pb metal in the soils of Gujarat and around the Surendranagar region [231][232].

The confusion matrix shows the predictive performance of the proposed algorithm. The points with known level of heavy metal content was compared with predicted values of heavy metal obtained from the DSW algorithm. The validation set was prepared using exact field points from the hyperspectral data. Twenty random field points were taken at Anand and Surendranagar, corresponding to different levels of heavy metal pollution for both the study area. The actual Cd concentration in tobacco leaves and Pb concentration in cotton leaves from the

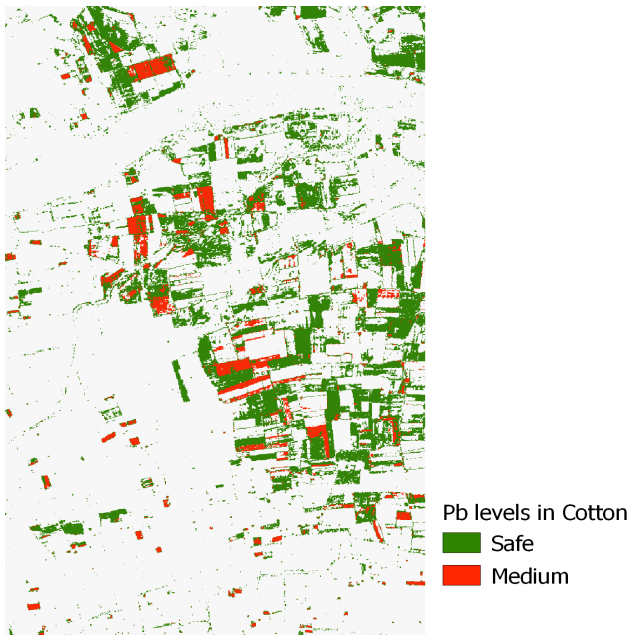

Figure 5.5: Different levels of Pb pollution in cotton using DSW in Surendranagar

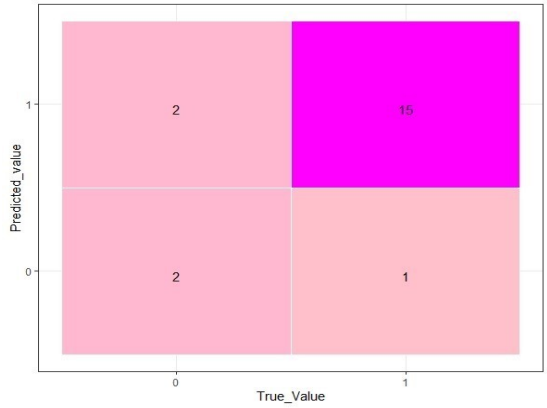

(a) Matrix for validation of Cd pollution in tobacco crop at Anand

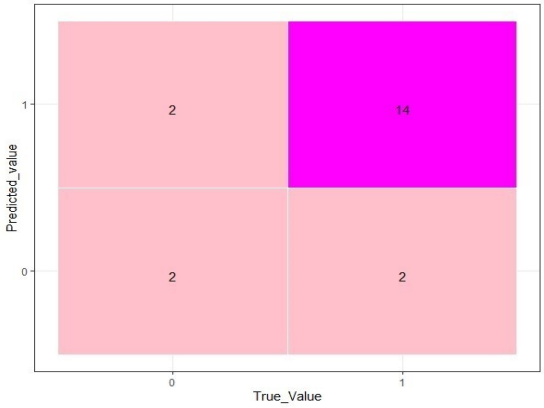

(b) Matrix for validation of Pb pollution in the cotton crop at Surendranagar

Figure 5.6: Confusion matrix for heavy metal pollution

field points were calculated in the lab and compared with the level of heavy metal pollution obtained using the DSW algorithm. The results of field points corresponded well with that obtained with this novel algorithm as shown by the confusion matrix in Figure 5.6, representing the model's predicted value for the validation point and the actual value of heavy metal content. The validation from field survey points with known heavy metal concentrations of Pb and Cd pollution levels using 20 data set points showed 80 % accuracy for Cd pollution in tobacco and 85% accuracy for Pb pollution in cotton. The validation results for Cd pollution in tobacco at Anand are shown in Figure 5.6a and for Pb pollution in cotton at Surendranagar in Figure 5.6b.

Khalili *et al.* also used a combination of biochemical and remote sensing data using standard spectral reflectance for Eucalyptus plants [233]. The wavelet decomposition of standard reflectance provided information through reconstructed detail reflectance about the presence of heavy metal and the wavelength affected by it. The wavelet coefficients are less sensitive to external environments, noise, and leaf structures, thus enhancing their correlation with biochemical and biophysical parameters[116]. Combining control experiments with hyperspectral data using the DSW model for reconstructed detail reflectance showed satisfactory performance in differentiating levels of heavy metal.

CHAPTER 6

Soil Sampling Site Selection[1]

6.1 Problem statement

Clay minerals in the soil are crucial for stability, erodibility, and other soil characteristics. It is vital to map the distribution of clay minerals to conserve and manage soil. Due to challenging topography, increasing lab analysis costs, and being labor-intensive, field sampling in specific locations is not viable. Compared to field-based and lab-based methods, these remote sensing techniques have the distinct advantage of covering vast, unexplored regions for a relatively low cost. Remote sensing works on the principle that everything on Earth reflects or absorbs electromagnetic radiation [234]. The most effective application of remote sensing in geology is identifying and mapping different clay mineral types [235].

Imaging spectroscopy and hyperspectral data from satellite or air-borne platforms have increased importance in mapping features like mineral identification and geological mapping [236]. Hyperspectral data's high spectral and spatial resolution helps to identify and map the soil clay minerals such as kaolinite, montmorillonite, and illite more accurately based on the distinct absorption features in the range of 0.4–2.5 μm. A vast amount of spectral data and noise in these data make it challenging to utilize for various analyses. Therefore, pre-processing and noise removal are required to extract useful information from the hyperspectral data.

In addition, spectral analysis techniques, such as Principle Component Anal-

[1]Parts of this chapter is published in the following paper:
Priya, S. and Ghosh, R., "Soil clay minerals abundance mapping using AVIRIS-NG data". *Advances in Space Research*, 2022.

ysis (PCA) and Mixture Tuned Matched Filtering (MTMF), are used to identify the mineralized zones related to clay minerals more precisely from hyperspectral data [237][236]. It is very difficult to conduct time-consuming field surveys and expensive lab analyses using XRD at all locations to prepare clay mineral abundance maps. So, a few representative sites are selected from hyperspectral data to identify the presence of zones related to different clay minerals and know about their distribution.

The primary goal of this chapter is to use hyperspectral data to determine sampling sites for various clay minerals, which can then be utilized for further regression analysis for mineral abundance mapping in the Ambaji region of Gujarat and the Udaipur region of Rajasthan. Air-borne Visible/Infrared Imaging Spectrometer Next Generation (AVIRIS-NG) data is used to select representative soil sampling sites after Spectral Feature Fitting (SFF) algorithm. The pure pixels of minerals extracted from hyperspectral data were utilized for SFF analysis to have a preliminary idea about the presence of clay minerals in the study area [238].

Various sampling sites for three dominant soil clay minerals, e.g., kaolinite, illite, and montmorillonite, were identified from AVIRIS- NG images at the study sites. Out of them, thirty sites were shortlisted at both the study area using purposive sampling and considering the accessibility of these sites.

6.2 Methodology

The specifications of AVIRIS-NG denote the presence of 425 contiguous bands, which also contain much redundant information. Data preprocessing and several other steps are required for further analysis. All the process was completed in ENVI software. The adopted methodology and processing steps are depicted in Figure 2.2.

6.2.1 Preprocessing of hyperspectral image

Radiometrically and geometrically corrected Level 2 dataset of AVIRIS-NG acquired over Ambaji and Udaipur is used for site selection. The initial step is

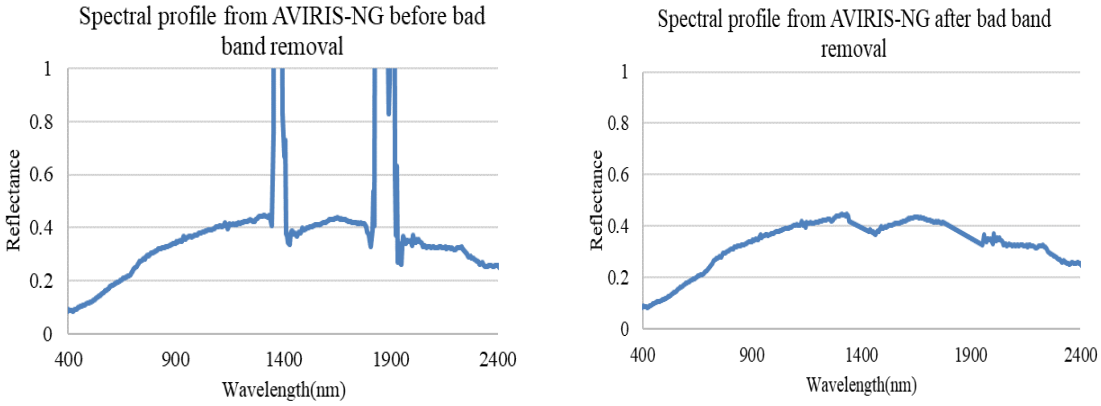

(a) AVIRIS-NG spectra with bad bands

(b) AVIRIS-NG spectra after removal of bad bands

Figure 6.1: AVIRIS-NG spectra with bad bands and after removal of bad bands

preprocessing data by removing the bad bands, i.e., bands containing the noise due to spectral overlap of the sensor and water vapor absorption band. It reduces computation time and avoids image degradation due to such bands. The water vapor absorption bands in the SWIR region 1363 -1403 nm and 1811-1968 nm are removed. After the preprocessing, 363 out of 425 bands are used for further analysis. Figure 6.1a and 6.1b show the reflectance spectra with bad bands and after removal of bad bands.

6.2.2 Minimum Noise Fraction (MNF)

Processing hyperspectral images with such a considerable amount of data increases computational complexity and makes handling difficult. Dimensionality reduction removes redundant information and noise in the data to make further processing faster and more accurate. The Minimum Noise Fraction (MNF) approach given by Green et al. reduces the data's dimensionality without any information loss [239]. MNF transformation divides the data space into two subspaces: (a) components having large eigenvalues (signal subspace) and (b) components having eigenvalues approximately one, containing noise (noise subspace).

The noise is segregated based on noise statistics computed using the nearest neighbor to segregate noise and images are arranged with increasing quality and decreasing noise [240] [241]. The dimensionality reduction of the AVIRIS-NG im-

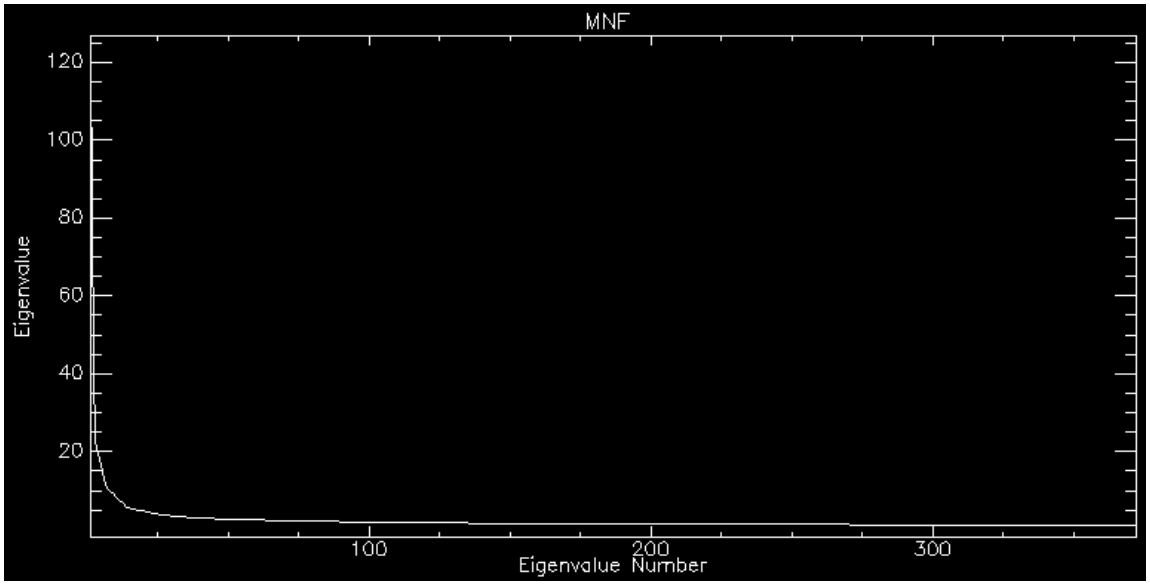

Figure 6.2: MNF eigen value graph

age at both the study area was carried out using the MNF approach before mapping minerals. Figure 6.2 represents the MNF eigenvalue graph showing that the first 20 component contains the most valuable information and are used for further analysis.

6.2.3 Pixel purity Index (PPI)

PPI (pixel purity index) is a statistical technique to identify pure pixels from hyperspectral images. It is performed on MNF components to identify the highly pure spectra of minerals that can be used as a reference for mapping. These pixels have spectrally unique signatures characterizing ground features such as soil minerals in a hyperspectral image can be estimated according to the brightness of the pixels in the PPI image [242][243]. Mostly such spectrally pure pixels occur near the boundaries of the data cloud. They are extracted using numerous, repeated projections of n-d scatter plots (n-D) in an n-D visualizer from the spectral mixing space where n is the number of bands [243]. Relatively pure pixels are separated into different classes. The average spectra of the pure pixel's classes collected are then matched using United States Geological Survey (USGS) mineral spectral library matching to find the mineral spectra for SFF[244][245].

6.2.4 Spectral Feature Fitting (SFF)

After resampling using the USGS mineral library, the pixels extracted using PPI are further utilized for identifying dominant clay minerals. Dominant clay minerals were classified using the SFF technique by comparing the spectra of the unknown pixel with the known spectrum in terms of shape and position of absorption features [241]. Before applying SFF, the spectra are normalized to quantify the absorption features present by a technique known as continuum removal to identify the individual absorption features [242]. The SFF algorithm compares the continuum-removed image spectra with the selected reference using the least-squares technique [246]. The selection of the best fit is based on spectral features, or a group of features is done by least squares fitting [247].

The endmembers extracted using PPI is after resampling using USGS mineral library is further utilized for the identification of dominant clay minerals is done by comparing the spectra of unknown pixel with known spectrum in terms of shape and position of absorption features for different clay minerals [241]. Classification of dominant clay minerals was done using the SFF technique. The continuum removal is done before applying SFF to quantify absorption features. Continuum removal is a technique to normalize the spectra to identify the individual absorption features [242]. The original spectrum is divided by a continuum curve obtained by fitting a straight line that joins the local maxima of spectra. The continuum removed spectra are further utilized for SFF. This technique compares the image spectra with the selected reference spectra from US geological survey mineral spectral library using the least-squares technique [246]. The selection of the best fitting material on the basis of spectral features or group of features is done by comparing the correlation coefficient of fits [247]. Figure 6.3 depicts the procedure of the SFF algorithm[2].

The abundance of spectral features represented by scale factor by calculation of band to band through the computation of the least-square fit process. The SFF gives scale and RMSE images where the scale image indicates the presence of absorption features related to different clay minerals, and the RMSE (Root Mean Square Error) image indicates the RMSE value for each reference mineral spec-

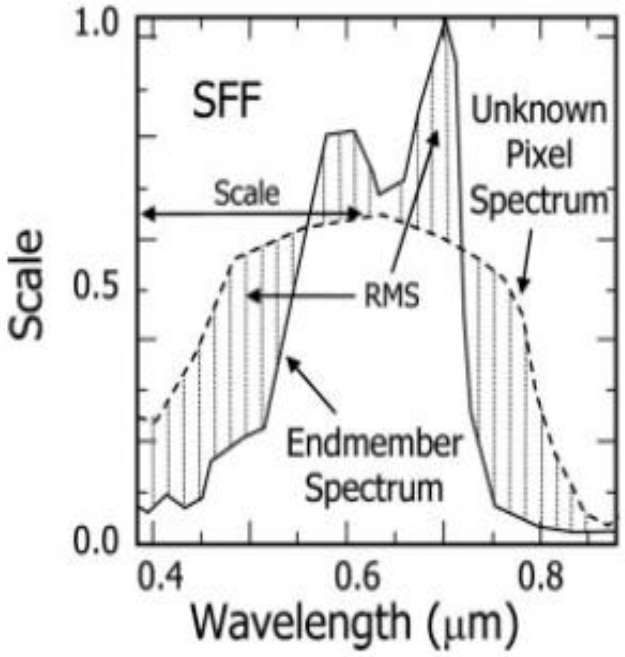

Figure 6.3: Working principle of SFF algorithm [2]

tra. A higher scale value and low RMSE value represent a strong matching with reference spectra of minerals indicating absorption in the mineral's spectral band related to mineral abundance [247] [248]. The fit images are generated by making a ratio between the scale image and the RMS error image to measure the similarities (match) between the unknown spectrum and reference spectrum on a pixel-by-pixel basis [249][240].

6.3 Results and discussions

Soil sample sites were selected using the SFF algorithm for three dominant minerals on the hyperspectral image of the study area. A combined approach of MNF, PPI and n-d visualization followed by SFF algorithm mineral zones can be mapped, providing a precursor knowledge about the presence of different minerals like quartz, talc, goethite, and dolomite and soil clay minerals helpful in selecting sampling sites for laboratory analysis [250][240]. The identified mineral zones for clay minerals like kaolinite, montmorillonite, and illite obtained from SFF are converted into polygons. The polygons are then laid on Google Earth to

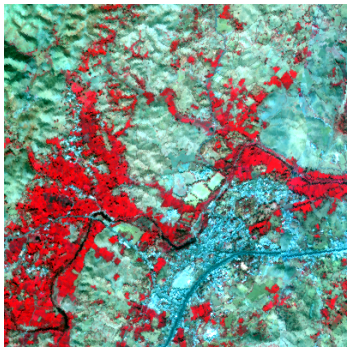

(a) AVIRIS-NG Image

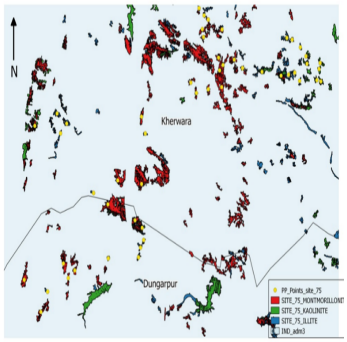

(b) SFF polygons for Montmorillonite, Kaolinite and Illite

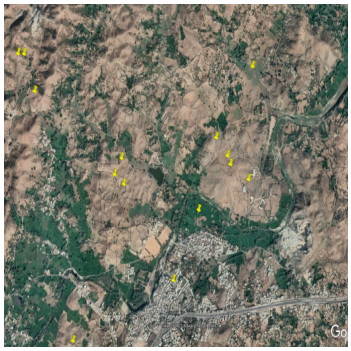

(c) Google Earth image showing markers for selected sites

Figure 6.4: Soil sampling sites for Udaipur region, Rajasthan

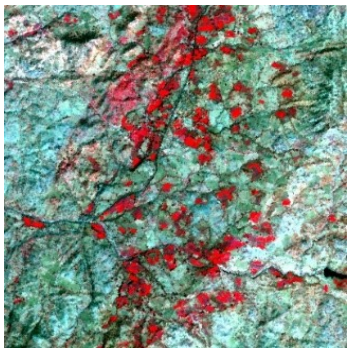

(a) AVIRIS-NG Image

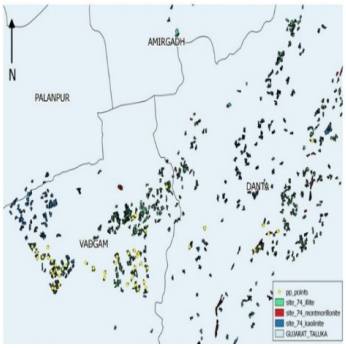

(b) SFF polygons for Montmorillonite, Kaolinite and Illite

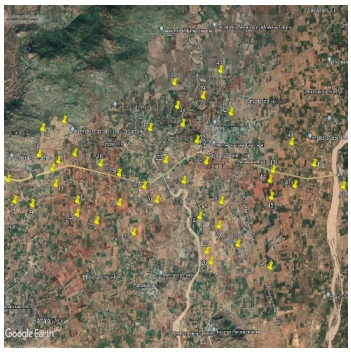

(c) Google Earth image showing markers for selected sites

Figure 6.5: Soil sampling sites for Ambaji region, Gujarat

select representative soil sampling sites corresponding to different soil clay minerals for lab analysis. Figure 6.4a and Figure 6.5a represent FCC of AVIRIS-NG images at Udaipur and Ambaji region. The polygons for different clay minerals obtained after SFF algorithm are shown in Figure 6.4b and Figure 6.5b for both the study area. Figure 6.4c and Figure 6.5c depict the selected soil sampling site as markers on Google Earth in Udaipur and Ambaji regions, respectively. Further validation through XRD analysis of samples is required to know the relative distribution of different clay minerals.

Representative soil sampling sites were selected based on the study of SFF polygons laid on google earth. Purposive sampling was carried out based on the requirement for clay abundance mapping and ease of collection. Mostly barren

(a) Collection of soil samples using Auger

(b) Soil sampled collected

Figure 6.6: Soil sampling and collection

fields with road connectivity to reach there were selected as sampling sites from Google Earth, represented in Figure 6.4 and Figure 6.5. After selecting sampling sites from hyperspectral data, the field survey was done at Udaipur and Ambaji study area to collect soil samples for analysis shown in Figure 6.6a and Figure 6.6b. Around 500 g of soil was collected after removing the dirt and pebbles from the surface at a depth of 0-15 cm for further analysis. Soil analysis and x-ray diffraction were carried out on the sample collected from different sites to study the relationship between the depth of absorption features and different clay minerals.

CHAPTER 7

Soil sample analysis using XRD[1]

7.1 Problem statement

XRD is widely used for characterizing different materials based on atomic positions, size, and the shape of the unit cell. The XRD analysis provides the intensity and position of peaks at different d spacing, which is unique for different crystalline materials and determines the relative percentage of different materials in the sample. The intensity of diffraction peaks obtained from the XRD analysis enables the identification of different minerals in the selected sample.

Several researchers consider XRD a reliable technique for the characteristics and distribution of various minerals and have used it for clay mineral quantification. It is used in remote sensing to validate the presence of minerals obtained through the analysis of satellite images. The dominance of different minerals in the identified samples can be related to absorption features in hyperspectral imagery and quantified over large areas through statistical methods. Satellite data and laboratory-based XRD data can be used to create mineral abundance maps at different geographic locations.

Extraction of clay minerals from a soil sample is required before XRD analysis. This chapter deals with soil sample preparation after different soil treatments and XRD analysis of the samples. The mineralogical analysis provided information about the percentage dominance of different clay minerals, which can be utilized to carry out further analysis to prepare soil mineral maps for the study area.

[1]Parts of this chapter is published in the following paper:
Priya, S. and Ghosh, R., "Soil clay minerals abundance mapping using AVIRIS-NG data". *Advances in Space Research*, 2022.

7.2 Methodology

Collected soil samples contain many impurities and cannot be used directly for XRD. Sample preparation is considered necessary for reliable XRD analysis. The procedure mentioned in the laboratory manual for X-ray diffraction by U. S. Geological Survey was followed to extract and identify clay minerals [251].

7.2.1 Soil treatment

Soil samples are chemically treated to remove dirt and other impurities. Removing carbonates from the soil is required for better identification of clay minerals. Dilute acetic acid was used to remove carbonates from soil samples without affecting the crystallinity of clay. Similarly, soil organic matter interferes with clay minerals' diffraction pattern. So, removing organic matter from soil samples is a prerequisite for the XRD of clay minerals. Organic matter from the soil was removed using laboratory-grade (3%) hydrogen peroxide.

7.2.2 Extraction of clay fraction

After soil treatment, the coarse particles from the soil are removed using a sieve. Silt and clay fractions need to be separated from the soil sample, and clay fractions are used for XRD analysis. The centrifugation method separates clay fraction from clay and silt suspension. The clay portion separated from the suspension is oven dried at 60^{o} Celsius overnight. The samples were treated with ethylene glycol before x-ray diffraction to identify swelling clay montmorillonite from other non-swelling clays. Figure 7.1 shows the laboratory analyses to extract clay fraction from soil samples for the different study areas at Central Instrumentation Laboratory at SDAU, Dantiwada.

7.2.3 XRD analysis of samples

The dried samples are finely powdered and randomly oriented for carrying out X-ray diffraction. The random orientation of the sample helps in determining the

Figure 7.1: Laboratory analysis for separation of clay fraction from soil sample

Table 7.1: D spacing (Å) of Different clay minerals

Clay Minerals	**D spacing (Å)**
Kaolinite	12.3, 24.8, 37.7, 51.0, 65.1
Illite	8.84, 17.7, 26.7, 35.8, 45.3, 55.0, 65.2
Montmorillonite	4.9, 9.82, 14.7, 19.7, 24.7, 29.7, 34.8, 40.04, 45. 3, 50.6

mineralogy of the samples more accurately [153] . The dominant clay minerals present are estimated based on the d spacing. The sample is x rayed between angles of 2° and 70° 2θ using copper K alpha radiation at a scanning rate of 2° per minute. The 2θ angle at which the XRD peak is observed is converted into interplanar spacing using Bragg's Equation 7.1as given below:

$$D = \frac{\gamma_0}{2\sin(0.5x2\theta xR)} \tag{7.1}$$

where d = Inter lattice spacing in angstroms; γ_0 = X-ray wavelength θ = incidence angle of X-ray; R= conversion factor 0.0174532925199433 to change the degree to radian;

Each mineral has a unique XRD pattern showing interplanar spacing and relative intensities, used for their identification from unknown samples [252] . XRD provides peak position with corresponding interplanar spacing (d spacing) calculated using Bragg's law [253]. The minerals were identified based on the location of XRD peaks and corresponding d spacing. Table 7.1 represents the d spacing for XRD peaks for kaolinite, illite, and montmorillonite clay minerals.

XRD analysis after preparation of clay samples was done using the XRD instrument facility at Indian Institute of Technology (IIT), Gandhinagar, shown in Figure 7.2.

After XRD analysis, the constituent minerals are identified by matching the peak intensity from the stored database. The International Centre for Diffraction Data (ICDD) software was used to identify minerals present in the collected sample [254]. The mineral has different peaks, which can be matched with the reference spectra. Figure 7.3 illustrates the working of peak matching software ICDD for the prepared soil sample with montmorillonite. The blue line shows the sample, and the green line is the reference clay minerals. According to scientific

Figure 7.2: XRD instrument used for analysis at IIT Gandhinagar

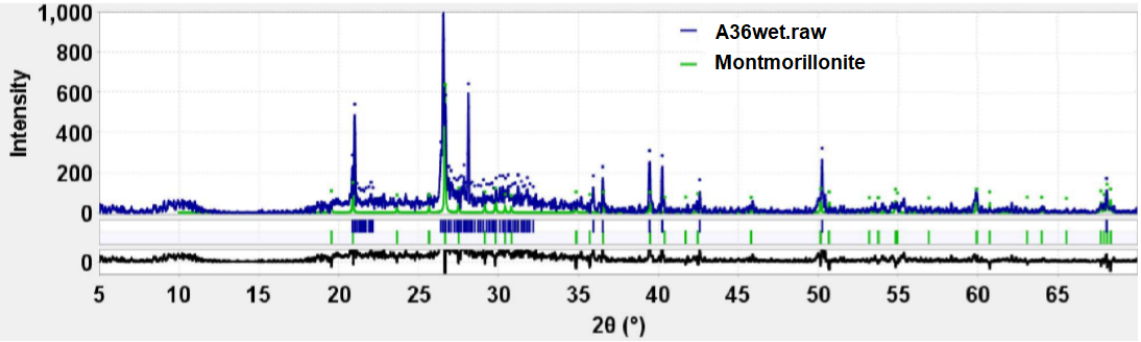

Figure 7.3: Matching of XRD pattern of samples with reference spectra

Table 7.2: Mineralogical analysis of soil samples of Udaipur Region (weight percentage)

Parameter	**Montmorillonite**	**Illite**	**Kaolinite**
Mean	50.9	33.9	15.2
Std. Dev	6.2	6.5	6.6
Maximum	62.0	42.0	36.0
Minimum	39.0	16.0	6.0

studies, XRD analysis is used to know the proportion of minerals in a mixture through the intensity of peaks and interplanar spacings. The quantification of different clay minerals was established by the Rietveld method [255].

7.3 Results and discussions

The mineralogy of the soil samples for both the study area has been assessed through XRD analysis of the soil samples [256]. The dominant clay minerals were identified, and the percentage composition of dominant clay minerals in the soil samples was estimated through the Rietveld refinement [257]. The soil samples were subsequently grouped based on dominant minerals in the soil. The results of the mineralogical analysis for Udaipur and Ambaji are shown in Table 7.2 and Table 7.3.

X-ray diffraction is a powerful technique for providing valuable qualitative, quantitative, and structural information about different minerals. The preliminary analysis shows the dominance of montmorillonite compared to illite and kaolinite in the soil samples collected from the Udaipur region and the dominance

Table 7.3: Mineralogical analysis of soil samples of Ambaji Region (weight percentage))

Parameter	**Montmorillonite**	**Illite**	**Kaolinite**
Mean	17.0	31.9	47.8
Std. Dev	4.2	4.3	4.3
Maximum	23.0	39.0	55.6
Minimum	10	21.0	41.1

of kaolinite in the Ambaji region.

CHAPTER 8

Mineral Abundance Mapping[1]

8.1 Problem statement

Soil clay minerals significantly influence ground stability due to their swelling properties affecting the soil quality and productivity [256]. The study of soil clay mineralogy helps policy-making for effective agricultural management and sustainable land use planning [258]. Conventional laboratory methods for exploring clay properties involve XRD, Scanning Electron Microscopy (SEM) and various chemical analysis methods. Mapping clay minerals through these methods is costly and time-consuming, consisting of laborious field surveys and sophisticated laboratory analysis [259]. Remote sensing techniques, with the advent of the hyperspectral sensor having higher spectral and spatial resolution, play a significant role in soil survey and clay mineral mapping and offers efficient alternatives to conventional methods [260]. For effective soil planning, area-specific high-resolution maps highlighting the prevalence of different soil clay minerals are essential.

A clay mineral abundance map is prepared in three main steps—first, identify dominant clay mineral zones from AVIRIS -NG data: second, ground truth collection and XRD of collected soil samples to identify the proportion of dominant minerals. Third, the statistical analysis relates the absorption peak depth with the dominance of various clay minerals from airborne hyperspectral data. The first two steps are covered in previous chapters. The XRD analysis of the soil samples

[1]Parts of this chapter is published in the following paper:
Priya, S. and Ghosh, R., "Soil clay minerals abundance mapping using AVIRIS-NG data". *Advances in Space Research*, 2022.

depicting the dominance of different clay minerals from selected sampling sites is discussed in Chapter 7.

In this chapter, the airborne AVIRIS-NG dataset was used to calculate the depth of absorption feature around 2200 nm through the APD technique. Linear regression was used to find the relation between the proportion of different clay minerals in XRD samples and the APD corresponding to the soil samples. This technique is based on the fact that the depth of an absorption feature at a specific wavelength is strongly related to the abundance of the absorbing material [261]. The relationship between clay content and APD was further used to predict mineral abundance from AVIRIS-NG data at unknown places. The mineral abundance map representing the distribution of montmorillonite, kaolinite, and illite was prepared for Udaipur and Ambaji region from airborne hyperspectral data for soil monitoring.

8.2 Methodology

8.2.1 Absorption Peak Depth (APD)

Clay minerals show some characteristic absorption features at different wavelengths related to their distribution in the soil samples. At a specific wavelength, the depth of an absorption feature is strongly related to the abundance of the absorbing minerals. Calculating the depth of absorption peak at different wavelengths indicates a correlation between the spectral features and content of absorbing clay minerals. Therefore, this study used the AVIRIS-NG dataset to calculate APD. Before calculating APD, normalization was achieved through the "convex-hull quotients" technique [143], according to equation 8.1

$$R'(\lambda) = \frac{R_b(\lambda)}{R_c(\lambda)} \tag{8.1}$$

where R_b is the reflectance of a specific peak at the wavelength λ, and R_c is the reflectance of the continuum at the same wavelength.

After normalization, the absorption peak depth can be calculated through the

equation 8.2 :

$$APD(\lambda) = 1 - R'(\lambda) \tag{8.2}$$

The presence of clay minerals influences the SWIR portion of the spectrum $(1300nm - 2500nm)$, with the regions $1400nm, 1900nm, and 2200nm$ showing the absorption features characteristic of clay minerals [129]. Soil clay content and mineralogy are related to the depth of the clay absorption peak around $2210nm$, corresponding to the absorption of OH in the clay lattice, a component of clay minerals. Moreover, absorption features at approximately $1400nm$ *and* $1900nm$ are generally present but are not so important due to water absorption bands.

8.2.2 Regression analysis

Linear regression was used to relate the clay content to the corresponding APD. The relationship between the APD derived from airborne hyperspectral data and the clay content values obtained from XRD analysis was established. The relationship was then inversed to prepare mineral abundance maps. The complete procedure is organized in the following steps:

- The APD values were extracted corresponding to each sampling point.
- Calculation of the correlation between the APD values at $2205nm - 2214nm$ and corresponding clay minerals content.
- Linear regression analysis between the APD values calculated from the AVIRIS-NG for each training site and the corresponding clay content value from XRD analysis of clay samples.
- Inversion of APD value map into a predicted clay content map, using the regression lines for clay minerals.

8.3 Results and discussions

The linear regression analysis relates the clay mineral content to corresponding APD values obtained from AVIRIS-NG data at different study areas. At the Udaipur

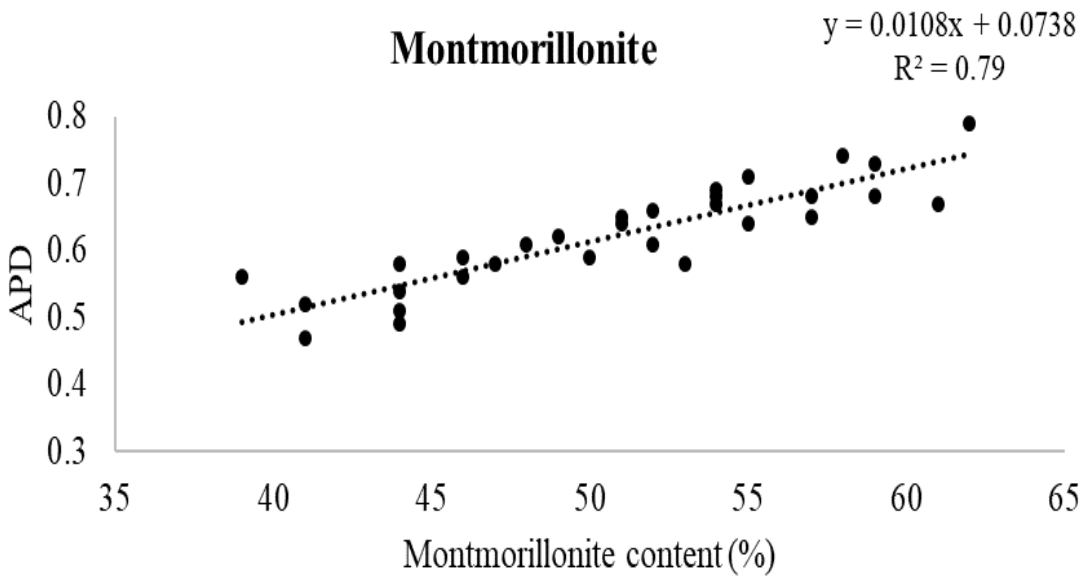

Figure 8.1: Regression lines of montmorillonite and APD for the Udaipur region

region, for all three minerals, the determination coefficient was more than 0.55 showing a good relationship with different minerals. A clear relationship was visible between montmorillonite content ($R^2 = 0.79, n = 30$) and illite content ($R^2 = 0.79, n = 30$), as represented in Figure 8.1, Figure 8.2. At the same time, determination coefficients were less for kaolinite content ($R^2 = 0.63, n = 30$), shown in Figure 8.3 in the Udaipur study area.

As observed in Figure 8.6, Figure 8.4 and Figure 8.5, the soil samples from the Ambaji region demonstrate a favorable relationship between kaolinite ($R^2 = 0.73, n = 30$) and montmorillonite ($R^2 = 0.67, n = 30$) with APD compared to illite ($R^2 = 0.62, n = 30$).

The statistical analysis shows that the depth of absorption peak around $2205nm - 2214nm$ is mainly due to different clay minerals, which can be quantified to predict the clay content [134] [262]. The studies conducted by various researchers on different hyperspectral datasets support this research's findings. R^2 values of 0.68 and 0.60 were observed by Curcio et al. and Garfagnoli et al. using airborne hyperspectral data in Italy, respectively, for predicting soil clay content using the absorption-based approach [142][143]. Gomez et al. (2008) reported R^2 values of 0.58 for soil clay content in France using HYMAP hyperspectral data [263]. The

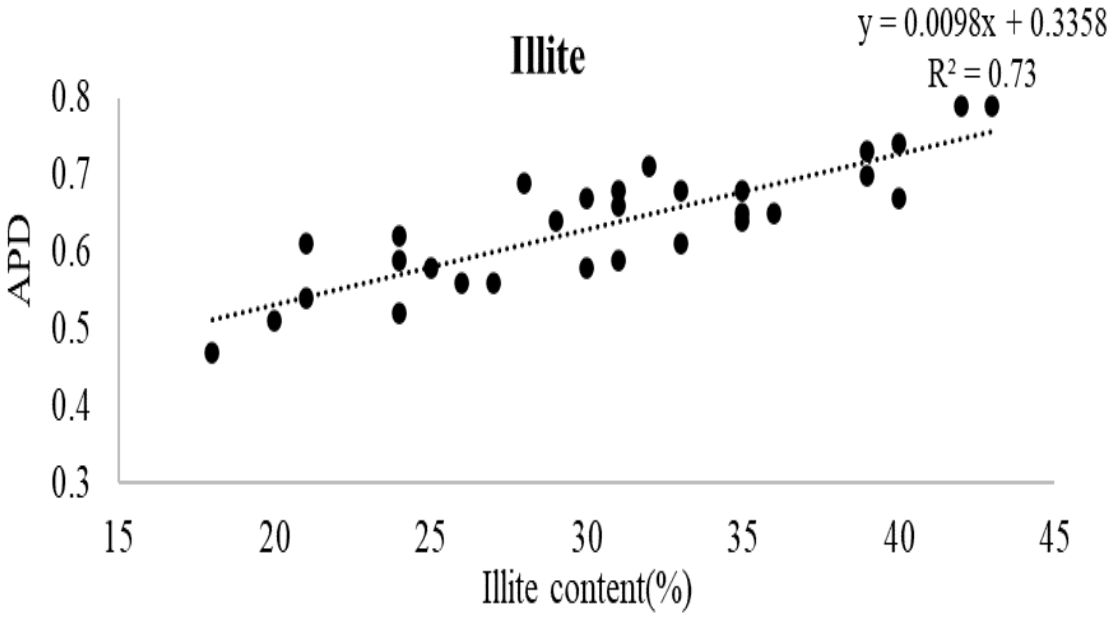

Figure 8.2: Regression lines of illite and APD for the Udaipur region

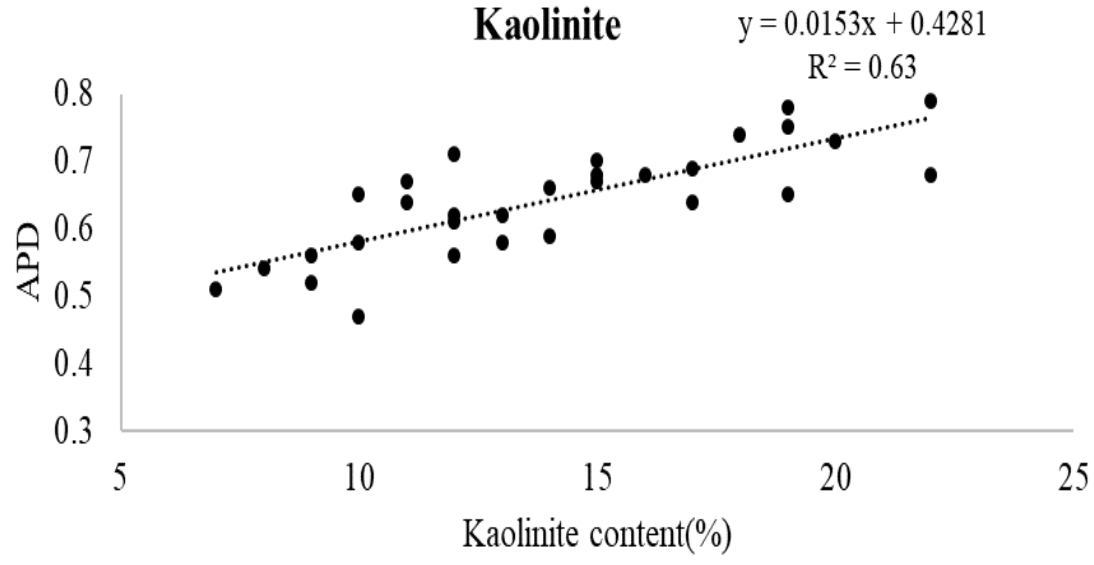

Figure 8.3: Regression lines of kaolinite and APD for the Udaipur region

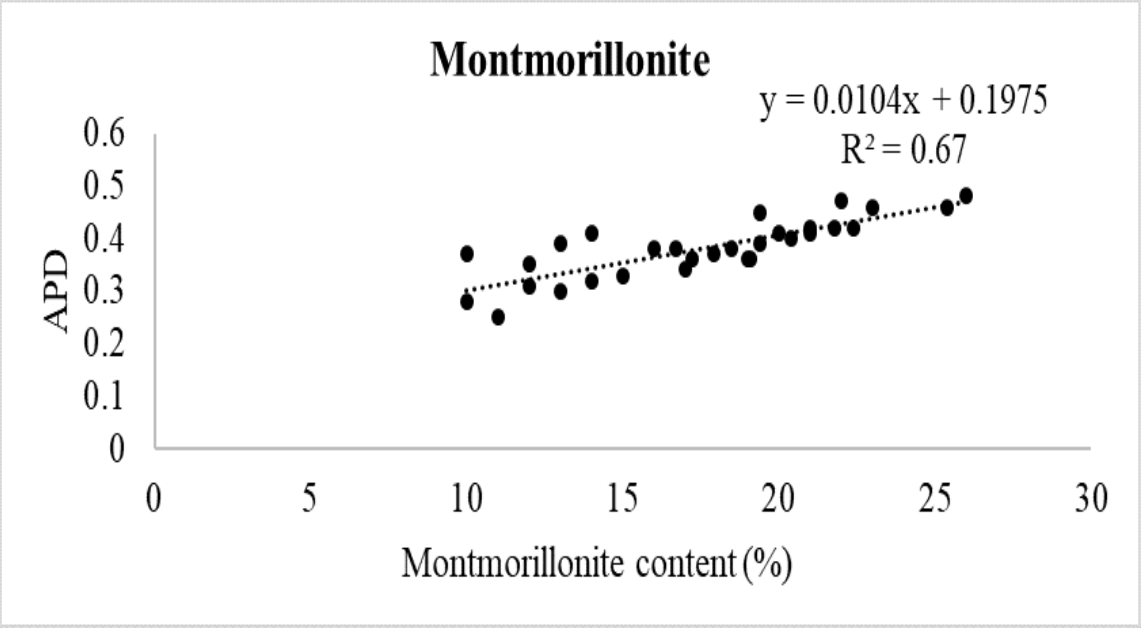

Figure 8.4: Regression lines of montmorillonite and APD for Ambaji region

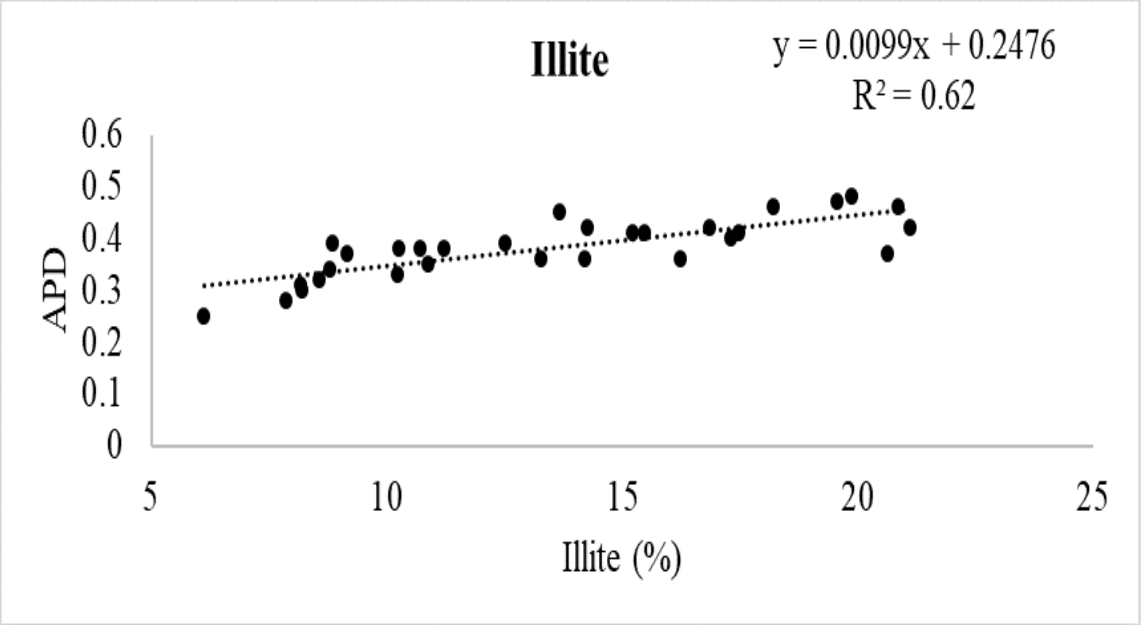

Figure 8.5: Regression lines of illite and APD for Ambaji region

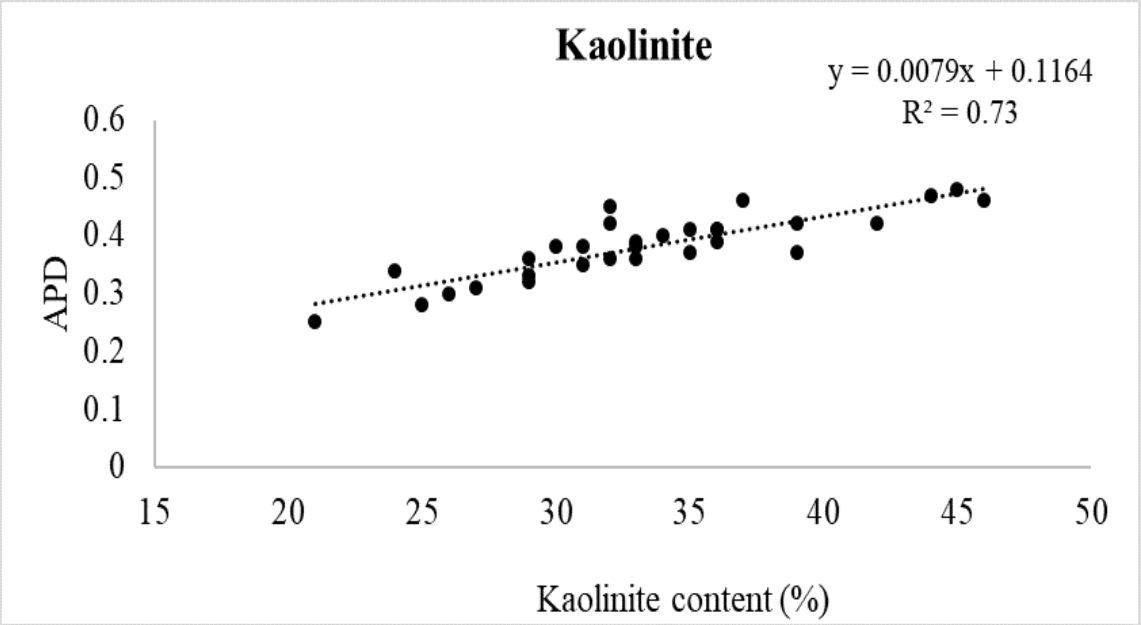

Figure 8.6: Regression lines of kaolinite and APD for Ambaji region

tedious and costly lab analysis and hostile terrain resulted in a small number of samples. For cross-validation, the leave-one-out technique has been utilized in this study by taking all thirty samples, which is more appropriate for a smaller number of samples [264]. Lagacherie et al. also utilized this method for cross-validation, as data collection is challenging in hostile geological terrain [134]. In this process, one sample was used for prediction, all other samples were used to build a regression model, and the Root Mean Square Error (RMSE) was calculated. The process was repeated for all the n samples, and the average of all the RMSE was calculated as Root Mean Square Error of Prediction (RMSEP) was calculated. The descriptive statistics showing the performance of the regression model are provided in Table 8.1 and Table 8.2 for Udaipur and Ambaji regions, respectively. The RMSEP for the three clay minerals, montmorillonite, illite, and kaolinite, at different study areas, are represented in Table 8.1 and Table 8.2.

Based on the model's performance, we calculated the regression line between the APD values obtained from AVIRIS-NG data and the corresponding clay content at each sampling site. The inverse regression line predicts clay mineral content (x) for unknown pixels using the respective APD values (y) for Udaipur and Ambaji study areas respectively as represented in Table 8.3 and Table 8.4 for each

Table 8.1: Descriptive statistics for the regression model for Udaipur[1]

Covariate	Coefficients	Standard Error	t-statistic	P-value	R^2	RMSEP
Montmorillonite						
Intercept APD	5.249485 73.2753	4.47187 7.12612	1.173891 10.28264	0.250327* $5.18E-11$*	0.79	6.20
Illite						
Intercept APD	-16.9837 74.90893	5.46664 8.51964	-3.10678 8.792499	0.004306* $1.52E-09$*	0.73	8.05
Kaolinite						
Intercept APD	-12.4535 41.23527	3.868403 5.977978	-3.21928 6.897863	0.003243* $1.7E-07$*	0.63	12.08

[1] **Statistically significant p-value* $p < 0.05$

Table 8.2: Descriptive statistics for the regression model for Ambaji [1]

Covariate	Coefficients	Standard Error	t-statistic	P-value	R^2	RMSEP
Montmorillonite						
Intercept APD	-7.0395 64.6008	3.2645 8.4791	-2.1564 7.6188	0.0398* $2.67E-08$*	0.67	6.18
Illite						
Intercept APD	-10.9913 64.275	3.8926 10.0295	-2.8235 6.4085	0.0088* $7.26E-07$*	0.60	7.40
Kaolinite						
Intercept APD	1.9695 92.74465	4.04825 10.51477	-0.4864 8.8204	0.6304* $1.42E-09$*	0.73	9.50

[1] **Statistically significant p-value* $p < 0.05$

soil clay mineral.

The clay mineral maps resulting from this procedure for all three clay minerals in the Udaipur region are presented in Figures 8.7a 8.7b 8.7c. Red represents the higher percentage, and blue shows a lower percentage. The maps of illite and montmorillonite minerals show a similar trend and are in agreement with the XRD analysis data of the samples indicated in Figure 8.7. A comparison among the maps shows that the low presence of kaolinite is related to the low kaolinite concentrations in the sampled soil from Udaipur. The RMSEP for kaolinite is also higher at the Udaipur region than montmorillonite and illite, indicating more variations in the model.

The clay content map of the Ambaji region shows the dominance of kaolin-

Table 8.3: Regression lines for target mineral in Udaipur

Target mineral	**Regression line**
Montmorillonite	$x = 73.28y + 5.25$
Illite	$x = 74.90y - 16.98$
Kaolinite	$x = 41.23y - 12.45$

Table 8.4: Regression lines for target mineral in Ambaji region

Target Mineral	**Regression Line**
Montmorillonite	$x = 64.601y - 7.0396$
Illite	$x = 63.327 - 10.601$
Kaolinite	$x = 92.745y - 1.969$

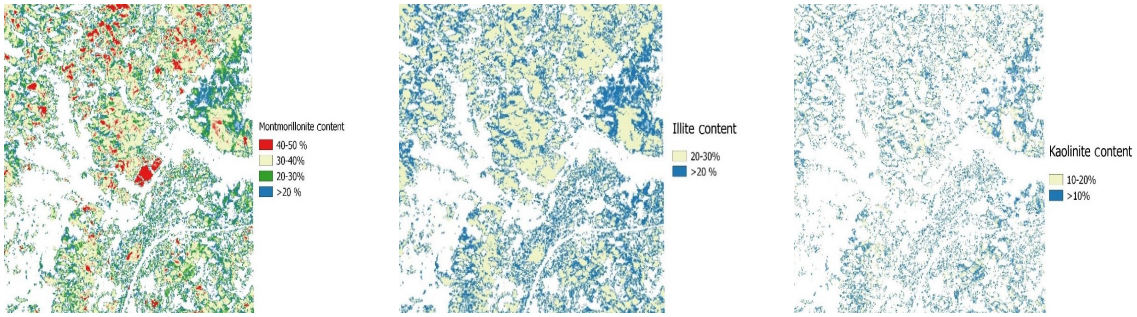

(a) (b) (c)

Figure 8.7: Soil clay mineral abundance map for (a) montmorillonite (b) illite and (c) kaolinite at Udaipur region

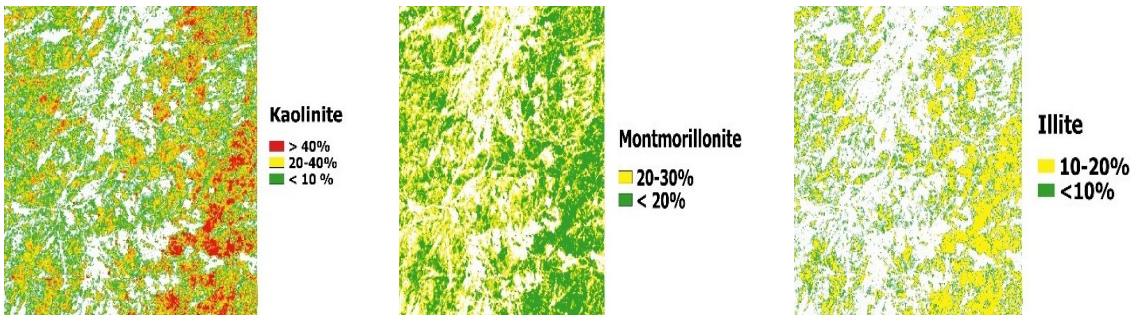

(a) (b) (c)

Figure 8.8: Soil clay mineral abundance map for (a) kaolinite (b) montmorillonite and (c) illite at Ambaji region

ite and montmorillonite compared to illite, as indicated in Figure 8.8. The results are in agreement with XRD-based mineralogical analysis. The findings of this research indicate that regression analysis using APD at $2205nm - 2214nm$ can be a potential technique for mapping the abundance of different soil clay minerals. The mineral abundance map obtained using a regression line shows a striking similarity with the results of the XRD analysis of samples. The abundance of montmorillonite in the Udaipur region has also been reported by Govil et al. [261]. The presence of minerals like kaolinite, as well as halloysite, was reported in preliminary hyperspectral studies of the Ambaji region[265].

The results show that AVIRIS-NG data can be used to prepare reliable clay mineral abundance maps for cultivated soil. This method can be more robust by increasing the number of soil sampling sites from the agricultural and wasteland. Regardless of these limitations, the regression models developed show promising potential in mapping the distribution of clay minerals. However, the performance of this method could further be compared with other machine learning techniques, such as artificial neural networks, random forests, and deep learning, using the AVIRIS-NG dataset.

CHAPTER 9

Conclusion and Future Scope

9.1 First objective

The effects of heavy metal on food chains, human health, and the long-term health of ecosystems make it crucial to focus on them. Pb and Cd in plants induce changes in biochemical parameters, especially chlorophyll resulting in changes in the spectral reflectance pattern in the visible region. Hyperspectral data can effectively detect such changes in the reflectance and correlate with heavy metal content to find the spectral region sensitive to heavy metal.

This thesis integrated biochemical and hyperspectral approaches to indicate the spatial distribution of heavy metal, specifying the extent of contamination at the research site for the target crops. In this regard, biochemical analysis reveals the most sensitive growth stage of the crop, which can be further utilized for spectral analysis for estimation of heavy metal pollution in plants. The obtained results confirm a significant effect of heavy metals on the different biochemical and spectral behavior of cotton and tobacco crops.

Biochemical measurements like chlorophyll estimation and accumulation of heavy metals combined with spectral measurement provide helpful information about plant behavior during stress due to heavy metals like Pb and Cd in crops. The research findings clearly show a distinguished affinity in the accumulation of Pb and Cd in cotton and tobacco. Cotton showed more affinity toward Pb, resulting in a higher accumulation of Pb than Cd, and tobacco crops showed a preferential accumulation of Cd over Pb. The vegetative stage of the cotton tends to accumulate a higher level of Pb, making it the suitable growth stage for study-

ing Pb stress.

In contrast, tobacco accumulates more Cd at later stages of growth. The higher TF represents a higher concentration of Pb and Cd in the soil resulting in an increased presence of heavy metals in plants., The biochemical analysis reveals the decreased level of chlorophyll content with increased levels of heavy metal contamination in both crops. The spectral analysis demonstrates that the reconstructed detailed reflectance obtained using wavelet decomposition is more effective in detection of Pb and Cd pollution than the original reflectance spectra and first derivative. The correlation study reveals that the spectral region $651nm - 742nm$ is sensitive to the presence of Pb in cotton and $631nm - 802nm$ is sensitive to Cd in tobacco. Thus, it can be concluded that cotton and tobacco crops indicate Pb and Cd pollution in a given agricultural ecosystem.

Results of the present study demonstrate that wavelet decomposition of spectral reflectance has the potential for assessing the presence of heavy metal in leaves and determining the wavelength region sensitive to heavy metal stress. The spectral analysis using ground-based sensing in a control experiment with known levels of heavy metal applied is used to generate reference spectra of heavy metal under study (Pb and Cd). The DSW spectral matching approach was utilized to know the level of Pb contamination in cotton and Cd contamination in tobacco from the airborne hyperspectral data. The DSW algorithm showed a good performance in mapping Cd in tobacco in the Anand region and Pb in cotton in the Surendranagar region. DSW approach shows potential for mapping heavy metal contamination for different heavy metals in different crops. Combined field-based studies of hyperspectral data allow accurate and fast detection of heavy metal concentrations in crops over large areas can be achieved. Therefore, developing a method for effectively integrating spectral and environmental parameters is of great future interest and provides a reference for assessing extent of heavy metal contamination in farmland environments. However, this type of estimation is still exploratory and requires more investigation and testing with other heavy metals and plant species.

The study shows potential in detecting heavy metal but has some limitations.

In controlled experiments, however, various factors play essential roles that must be considered. There is a need to develop reference spectra every time, as the interaction of plants varies with the type of heavy metal, environmental conditions, and soil type that can influence the spectral characteristics. A control experiment considering two cycles of plant growth is required to capture all the biochemical and spectral changes due to the presence of heavy metals. The differentiation of heavy metal stress from other stress like environmental factors, pests, and disease is complicated and needs further discussion. However, such factors are time-specific and short-term. Therefore, a long time series of remote sensing data with higher spectral and temporal information can be used to determine the level of heavy metal. More controlled strict experiments can improve the detection of heavy metal pollution in plants.

There is excellent potential to analyze and evaluate the level of different heavy metals using a combination of wavelet and DSW approach to generate an early warning system for different heavy metals. Despite the benefits of such an integrated approach, more studies are required to see if they can be used to estimate the concentrations of heavy metals in other plant species under various biological and environmental situations. In the future, the interaction effect due to the presence of different heavy metals and its effect on spectral properties also need to be considered. Remote sensing with more advanced equipment will eventually grow into a *single window* system, encouraging farmers and policymakers to quickly comprehend the condition of heavy metal-contaminated plants over large areas without extensive sampling and chemical tests.

9.2 Second objective

Hyperspectral remote sensing has emerged as one of the most promising and advanced tools for detecting and identifying minerals. It provides absorption features at adequate spectral resolution related to clay mineral abundance. Analyzing the exact position, strength, and depth of such absorption features provides

insight into the weight or proportion of minerals in the target study area. Present research reveals the potential of hyperspectral data to predict one of the vital soils' properties; soil clay minerals. After reducing spectral and spatial dimensions, the SFF analysis of hyperspectral data gives a rough estimate of soil clay minerals zones, which can be utilized to select sites for XRD analysis. Mineral abundance mapping is further done by relating the proportion of soil clay minerals from XRD analysis with a corresponding depth of absorption feature (APD) between $2205nm - 2214nm$. The research findings represent an excellent agreement between APD, calculated from AVIRIS-NG data, and the percentage of different soil clay mineral content, calculated from XRD analysis.

The abundance of various soil minerals at unknown pixels can be established using the relation between APD and soil clay minerals. An integrated approach using hyperspectral and XRD analysis give a much better result than in the mineral abundance mapping. It can be used to prepare mineral abundance maps for different clay minerals that can be prepared from hyperspectral data for agricultural lands of other areas. Such maps showing the distribution of various clay minerals in cultivable soil can be critical in agricultural planning and soil fertility management. This study can be a basis for quantifying various clay minerals in agricultural land using hyperspectral data and demonstrates its suitability for large-scale mineral mapping using absorption features.

The proposed method was used to assess the dominant soil minerals. In the future, it can be widely used to rapidly predict other soil minerals from complex soil mineral mixtures using the information from hyperspectral data and XRD analysis. The given technique, evaluated for clay minerals, can be extended for many soil properties like organic carbon and calcium carbonate, which influence soil reflectance spectra. Digital mapping of various soil properties and their evaluation can be a future work area with less dependency on lab analysis. The perspective of using soil spectroscopy to study mineral abundance explores the future possibilities of using unmanned aerial vehicles (UAV) and hyperspectral cameras in short-wave infrared regions for more accurate and less expansive soil mapping.

The research showed encouraging and reliable results for mapping clay minerals through regression. Machine learning methods like neural networks, random forests, and regression trees can be applied to produce more accurate and less expansive clay minerals maps of a geographical area. However, some limitations affecting the reflectance characteristics, like the presence of vegetation, variable moisture regime, mixed nature of minerals, and uneven solar radiation influence the spectral reflectance need to be focussed on in the future work.

Publications

[A] Priya, S. and Ghosh, R., "Monitoring effects of heavy metal stress on biochemical and spectral parameters of cotton using hyperspectral reflectance", *Environmental Monitoring and Assessment*, 195(1), p.112, 2023.

[B] Priya, S. and Ghosh, R., "Soil clay minerals abundance mapping using AVIRIS-NG data". *Advances in Space Research*, 2022.

[C] Swati Priya, Ranendu Ghosh, and B.K Bhattacharya, "Non-linear autoencoder based algorithm for dimensionality reduction of airborne hyperspectral data", *International Archives of the Photogrammetry, Remote Sensing and Spatial Information Sciences*, Volume XLII-3/W6, pp.593-598, 2019.

[D] Swati Priya, Ranendu Ghosh, and B.T Patel, "Pot Experiment to study the effect of various levels of Lead (Pb) and Cadmium (Cd) on Cotton and tobacco plants". *Technical Report of MoU between DAIICT and SDAU* 2018.

[E] Swati Priya, and Ranendu Ghosh, "Neural Network-based Feature Extraction and Classification Model for Hyperspectral Data". *International Conference on Advances in System, Control, and Computing*, *27th - 28th February*, 2020.

[F] Swati Priya, and Ranendu Ghosh, "Novel Approach for heavy metal pollution Detection in tobacco crop through Dynamic Spectral Warping using hyperspectral Data". *Under Review*

References

[1] M. F. Buitrago, T. A. Groen, C. A. Hecker, and A. K. Skidmore, "Changes in thermal infrared spectra of plants caused by temperature and water stress," *ISPRS journal of photogrammetry and remote sensing*, vol. 111, pp. 22–31, 2016.

[2] A. T. Harris, "Spectral mapping tools from the earth sciences applied to spectral microscopy data," *Cytometry Part A: The Journal of the International Society for Analytical Cytology*, vol. 69, no. 8, pp. 872–879, 2006.

[3] I. A. Mirsal, *Soil pollution*. Springer, 2008.

[4] H. Ali, E. Khan, and I. Ilahi, "Environmental chemistry and ecotoxicology of hazardous heavy metals: environmental persistence, toxicity, and bioaccumulation," *Journal of chemistry*, vol. 2019, 2019.

[5] Z. L. He, X. E. Yang, and P. J. Stoffella, "Trace elements in agroecosystems and impacts on the environment," *Journal of Trace elements in Medicine and Biology*, vol. 19, no. 2-3, pp. 125–140, 2005.

[6] H. Bradl, *Heavy metals in the environment: origin, interaction and remediation*. Elsevier, 2005.

[7] M. Csuros and C. Csuros, *Environmental sampling and analysis for metals*. CRC Press, 2016.

[8] L. Järup, "Hazards of heavy metal contamination," *British medical bulletin*, vol. 68, no. 1, pp. 167–182, 2003.

[9] Y. Lou, H. Luo, T. Hu, H. Li, and J. Fu, "Toxic effects, uptake, and translocation of cd and pb in perennial ryegrass," *Ecotoxicology*, vol. 22, pp. 207–214, 2013.

[10] V. Srivastava, A. Sarkar, S. Singh, P. Singh, A. S. De Araujo, and R. P. Singh, "Agroecological responses of heavy metal pollution with special emphasis on soil health and plant performances," *Frontiers in Environmental Science*, vol. 5, p. 64, 2017.

[11] B. J. Alloway, *Heavy metals in soils: trace metals and metalloids in soils and their bioavailability*. Springer Science & Business Media, 2012, vol. 22.

[12] R. Athar and M. Ahmad, "Heavy metal toxicity: effect on plant growth and metal uptake by wheat, and on free living azotobacter," *Water, Air, and Soil Pollution*, vol. 138, pp. 165–180, 2002.

[13] P. Sharma and R. S. Dubey, "Lead toxicity in plants," *Brazilian journal of plant physiology*, vol. 17, pp. 35–52, 2005.

[14] S. J. Flora, G. Flora, and G. Saxena, "Environmental occurrence, health effects and management of lead poisoning," in *Lead*. Elsevier, 2006, pp. 158–228.

[15] W. H. Organization *et al.*, "Coastal modelling/imo/fao/unesco/wmo/who/iaea/un/unep joint group of experts on the scientific aspects of marine pollution," in *Coastal modelling/IMO/FAO/UNESCO/WMO/WHO/IAEA/UN/UNEP Joint Group of Experts on the Scientific Aspects of Marine Pollution*, 1991.

[16] C. Grant and S. Sheppard, "Fertilizer impacts on cadmium availability in agricultural soils and crops," *Human and Ecological Risk Assessment*, vol. 14, no. 2, pp. 210–228, 2008.

[17] X. Zhang, L. Yan, J. Liu, Z. Zhang, and C. Tan, "Removal of different kinds of heavy metals by novel ppg-nzvi beads and their application in simulated stormwater infiltration facility," *Applied Sciences*, vol. 9, no. 20, p. 4213, 2019.

[18] H. Liu, A. Probst, and B. Liao, "Metal contamination of soils and crops affected by the chenzhou lead/zinc mine spill (hunan, china)," *Science of the total environment*, vol. 339, no. 1-3, pp. 153–166, 2005.

[19] S. Murzaeva, "Effect of heavy metals on wheat seedlings: activation of antioxidant enzymes," *Applied Biochemistry and Microbiology*, vol. 40, pp. 98–103, 2004.

[20] T. Shi, H. Liu, Y. Chen, J. Wang, and G. Wu, "Estimation of arsenic in agricultural soils using hyperspectral vegetation indices of rice," *Journal of hazardous materials*, vol. 308, pp. 243–252, 2016.

[21] E. Choe, F. van der Meer, F. van Ruitenbeek, H. van der Werff, B. de Smeth, and K.-W. Kim, "Mapping of heavy metal pollution in stream sediments using combined geochemistry, field spectroscopy, and hyperspectral remote sensing: A case study of the rodalquilar mining area, se spain," *Remote sensing of environment*, vol. 112, no. 7, pp. 3222–3233, 2008.

[22] Y. Z. Wu, J. Chen, J. F. Ji, Q. J. Tian, and X. M. Wu, "Feasibility of reflectance spectroscopy for the assessment of soil mercury contamination," *Environmental science & technology*, vol. 39, no. 3, pp. 873–878, 2005.

[23] T. Lillesand, R. W. Kiefer, and J. Chipman, *Remote sensing and image interpretation*. John Wiley & Sons, 2015.

[24] E. T. Slonecker and G. B. Fisher, *An evaluation of remote sensing technologies for the detection of fugitive contamination at selected Superfund hazardous waste sites in Pennsylvania*. US Department of the Interior, US Geological Survey, 2014.

[25] C. Ryu, M. Suguri, M. Umeda *et al.*, "Estimation of the quantity and quality of green tea using hyperspectral sensing." *Journal of the Japanese Society of Agricultural Machinery*, vol. 72, no. 1, pp. 46–53, 2010.

[26] C. Bock, G. Poole, P. Parker, and T. Gottwald, "Plant disease severity estimated visually, by digital photography and image analysis, and by hyperspectral imaging," *Critical reviews in plant sciences*, vol. 29, no. 2, pp. 59–107, 2010.

[27] J. G. Clevers, L. Kooistra, and M. E. Schaepman, "Estimating canopy water content using hyperspectral remote sensing data," *International Journal of Applied Earth Observation and Geoinformation*, vol. 12, no. 2, pp. 119–125, 2010.

[28] X. Li, X. Liu, M. Liu, C. Wang, and X. Xia, "A hyperspectral index sensitive to subtle changes in the canopy chlorophyll content under arsenic stress," *International Journal of Applied Earth Observation and Geoinformation*, vol. 36, pp. 41–53, 2015.

[29] P. Wang, F. Huang, and X. Liu, "Assessment of heavy metal stress using hyperspectral data," in *2017 IEEE International Geoscience and Remote Sensing Symposium (IGARSS)*. IEEE, 2017, pp. 6178–6181.

[30] B. M. Sridhar, F. Han, S. Diehl, D. Monts, and Y. Su, "Spectral reflectance and leaf internal structure changes of barley plants due to phytoextraction of zinc and cadmium," *International journal of remote sensing*, vol. 28, no. 5, pp. 1041–1054, 2007.

[31] G. P. Asner, "Biophysical and biochemical sources of variability in canopy reflectance," *Remote sensing of Environment*, vol. 64, no. 3, pp. 234–253, 1998.

[32] G. Masaitis, G. Mozgeris, and A. Augustaitis, "Spectral reflectance properties of healthy and stressed coniferous trees," *Iforest-biogeosciences and Forestry*, vol. 6, no. 1, p. 30, 2013.

[33] A. A. Gitelson, Y. Zur, O. B. Chivkunova, and M. N. Merzlyak, "Assessing carotenoid content in plant leaves with reflectance spectroscopy," *Photochemistry and photobiology*, vol. 75, no. 3, pp. 272–281, 2002.

[34] I. Sanches, C. Souza Filho, L. Magalhães, G. Quitério, M. Alves, and W. Oliveira, "Unravelling remote sensing signatures of plants contaminated with gasoline and diesel: an approach using the red edge spectral feature," *Environmental pollution*, vol. 174, pp. 16–27, 2013.

[35] L. Kooistra, E. Salas, J. Clevers, R. Wehrens, R. Leuven, P. H. Nienhuis, and L. Buydens, "Exploring feld vegetation refectance as an indicator of soil contamination in river foodplains," *Environ Pollut*, vol. 127, pp. 281–290, 2004.

[36] J. G. P. W. Clevers, Correspond, L. Kooistra, and E. A. L. Salas, "Study of heavy metal contamination in river floodplains using the red-edge position in spectroscopic data," *Int. J. Remote Sens.*, vol. 25, no. 19, pp. 3883–3895, Oct. 2004.

[37] H.-Y. Ren, D.-F. Zhuang, J.-J. Pan, X.-Z. Shi, R.-H. Shi, and H.-J. Wang, "Study on canopy spectral characteristics of paddy polluted by heavy metals," *Guang Pu Xue Yu Guang Pu Fen Xi*, vol. 30, no. 2, pp. 430–434, Feb. 2010.

[38] G. A. Carter and A. K. Knapp, "Leaf optical properties in higher plants: linking spectral characteristics to stress and chlorophyll concentration," *Am. J. Bot.*, vol. 88, no. 4, pp. 677–684, Apr. 2001.

[39] A. Giannakoula, I. Therios, and C. Chatzissavvidis, "Effect of lead and copper on photosynthetic apparatus in citrus (citrus aurantium l.) plants. the role of antioxidants in oxidative damage as a response to heavy metal stress," *Plants*, vol. 10, no. 1, p. 155, Jan. 2021.

[40] A. Kumar, M. N. V. Prasad, and O. Sytar, "Lead toxicity, defense strategies and associated indicative biomarkers in talinum triangulare grown hydroponically," *Chemosphere*, vol. 89, no. 9, pp. 1056–1065, Nov. 2012.

[41] M. Yusuf, Q. Fariduddin, P. Varshney, and A. Ahmad, "Salicylic acid minimizes nickel and/or salinity-induced toxici-ty in indian mustard (brassica juncea) through an improved antioxidant system," *Environ. Sci. Pollut. Res*, vol. 19, pp. 8–18, 2012.

[42] X. Shu, L. Yin, Q. Zhang, and W. Wang, "Effect of pb toxicity on leaf growth, antioxidant enzyme activities, and photosynthesis in cuttings and seedlings of jatropha curcas L," *Environ. Sci. Pollut. Res. Int.*, vol. 19, no. 3, pp. 893–902, Mar. 2012.

[43] H. Kupper, I. Setlik, M. Spiller, F. C. Kupper, and O. Prasil, "Heavy metal-induced inhibition of photosynthesis: Targets of in vivo heavy metal chlorophyll formation1," *J. Phycol.*, vol. 38, no. 3, pp. 429–441, Jun. 2002.

[44] P. Sharma and R. S. Dubey, "Lead toxicity in plants," *Braz. J. Plant Physiol.*, vol. 17, no. 1, pp. 35–52, Mar. 2005.

[45] E. Maestri, M. Marmiroli, G. Visioli, and N. Marmiroli, "Metal tolerance and hyperaccumulation: Costs and trade-offs between traits and environment," *Environ. Exp. Bot.*, vol. 68, no. 1, pp. 1–13, Mar. 2010.

[46] D. K. Gupta, F. T. Nicoloso, M. R. C. Schetinger, L. V. Rossato, L. B. Pereira, G. Y. Castro, S. Srivastava, and R. D. Tripathi, "Antioxidant defense mechanism in hydroponically grown zea mays seedlings under moderate lead stress," *J. Hazard. Mater.*, vol. 172, no. 1, pp. 479–484, Dec. 2009.

[47] A. H. Afaj, A. J. Jassim, M. M. Noori, and C. Schüth, "Effects of lead toxicity on the total chlorophyll content and growth changes of the aquatic plant ceratophyllum demersum L," *Int. J. Environ. Stud.*, vol. 74, no. 1, pp. 119–128, Jan. 2017.

[48] S. A. Bharwana, S. Ali, M. A. Farooq, B. Ali, N. Iqbal, F. Abbas, and M. S. A. Ahmad, "Hydrogen sulfide ameliorates lead-induced morphological, photosynthetic,

oxidative damages and biochemical changes in cotton," *Environ. Sci. Pollut. Res. Int.*, vol. 21, no. 1, pp. 717–731, Jan. 2014.

[49] H. B. Paliwal, N. Gupta, and A. James, "Study on accumulation of lead in sunflower (helianthus annus)," *I Control Pollution*, vol. 8, 2014.

[50] M. Lamhamdi, O. El Galiou, A. Bakrim, J. C. Nóvoa-Muñoz, M. Arias-Estévez, A. Aarab, and R. Lafont, "Effect of lead stress on mineral content and growth of wheat (triticum aestivum) and spinach (spinacia oleracea) seedlings," *Saudi J. Biol. Sci.*, vol. 20, no. 1, pp. 29–36, Jan. 2013.

[51] K. Yilmaz, İ. E. Akinci, and S. Akinci, "Effect of lead accumulation on growth and mineral composition of eggplant seedlings (solarium melongena)," *N. Z. J. Crop Hortic. Sci.*, vol. 37, no. 3, pp. 189–199, Sep. 2009.

[52] M. Saleem, H. N. Asghar, Z. A. Zahir, and M. Shahid, "Impact of lead tolerant plant growth promoting rhizobacteria on growth, physiology, antioxidant activities, yield and lead content in sunflower in lead contaminated soil," *Chemosphere*, vol. 195, pp. 606–614, Mar. 2018.

[53] S. K. Kohli, N. Handa, S. Bali, S. Arora, A. Sharma, R. Kaur, and R. Bhardwaj, "Modulation of antioxidative defense expression and osmolyte content by co-application of 24-epibrassinolide and salicylic acid in pb exposed indian mustard plants," *Ecotoxicol Environ Saf*, vol. 147, pp. 382–393, 2018.

[54] S. K. Kohli, N. Handa, A. Sharma, V. Gautam, S. Arora, R. Bhardwaj, L. Wijaya, M. N. Alyemeni, and P. Ahmad, "Interaction of 24-epibrassinolide and salicylic acid regulates pigment contents, antioxidative defense responses, and gene expression in brassica juncea l. seedlings under pb stress," *Environ. Sci. Pollut. Res. Int.*, vol. 25, no. 15, pp. 15 159–15 173, May 2018.

[55] A. Maodzeka, N. Hussain, L. Wei, G. Zvobgo, J. M. Mapodzeke, M. F. Adil, S. Jabeen, F. Wang, L. Jiang, and I. H. Shamsi, "Elucidating the physiological and biochemical responses of different tobacco (nicotiana tabacum) genotypes to lead toxicity," *Environ. Toxicol. Chem.*, vol. 36, no. 1, pp. 175–181, Jan. 2017.

[56] M. Lal and Department of Botany and Plant Physiology, CCS HAU, Hisar (India) - 125004, "Effects of different heavy metals and mycorrhizal treatments on various

physiological processes in cotton genotypes," *Int. J. Pure Appl. Biosci.*, vol. 6, no. 3, pp. 146–153, Jun. 2018.

[57] G. Uzu, S. Sobanska, Y. Aliouane, P. Pradere, and C. Dumat, "Study of lead phytoavailability for atmospheric industrial micronic and sub-micronic particles in relation with lead speciation," *Environ. Pollut.*, vol. 157, no. 4, pp. 1178–1185, Apr. 2009.

[58] V. Angelova, R. Ivanova, V. Delibaltova, and K. Ivanov, "Bio-accumulation and distribution of heavy metals in fibre crops (flax, cotton and hemp)," *Industrial crops and products*, vol. 19, no. 3, pp. 197–205, 2004.

[59] X. Wang, X. Wu, L. Ma, D. Zhao, and Y. E. Li, "Antioxidase reaction of cotton seeding by lead and cadmium stress," *Jiangsu Agric Sci*, vol. 40, pp. 105–107, 2012.

[60] B. Pourrut, M. Shahid, C. Dumat, P. Winterton, and E. Pinelli, "Lead uptake, toxicity, and detoxification in plants," in *Reviews of Environmental Contamination and Toxicology*, ser. Reviews of environmental contamination and toxicology. New York, NY: Springer New York, 2011, pp. 113–136.

[61] M. Ali and F. S. Nas, "The effect of lead on plants in terms of growing and biochemical parameters: a review," *MOJ Ecol. Environ. Sci.*, vol. 3, no. 4, Aug. 2018.

[62] N. A. Anjum, S. Umar, and M. Iqbal, "Assessment of cadmium accumulation, toxicity, and tolerance in brassicaceae and fabaceae plants–implications for phytoremediation," *Environ. Sci. Pollut. Res. Int.*, vol. 21, no. 17, pp. 10 286–10 293, Sep. 2014.

[63] R. Bahmani, M. Modareszadeh, and M. R. Bihamta, "Genotypic variation for cadmium tolerance in common bean (phaseolus vulgaris l.)," *Ecotoxicol. Environ. Saf.*, vol. 190, no. 110178, p. 110178, Mar. 2020.

[64] Y. T. Hsu and C. H. Kao, "Role of abscisic acid in cadmium tolerance of rice (oryza sativa l.) seedlings," *Plant Cell Environ.*, vol. 26, no. 6, pp. 867–874, Jun. 2003.

[65] Á. González, V. Chumillas, and M. d. C. Lobo, "Effect of zn, cd and cr on growth, water status and chlorophyll content of barley plants (*H. vulgare L.*)," *Agric. Sci.*, vol. 03, no. 04, pp. 572–581, 2012.

[66] R. K. Sharma, M. Agrawal, and S. B. Agrawal, "Physiological, biochemical and growth responses of lady's finger (abelmoschus esculentus l.) plants as affected by cd contaminated soil," *Bull. Environ. Contam. Toxicol.*, vol. 84, no. 6, pp. 765–770, Jun. 2010.

[67] Á. González, V. Chumillas, and M. d. C. Lobo, "Effect of zn, cd and cr on growth, water status and chlorophyll content of barley plants (*H. vulgare L.*)," *Agric. Sci.*, vol. 03, no. 04, pp. 572–581, 2012.

[68] D. Kapoor, S. Kaur, and R. Bhardwaj, "Physiological and biochemical changes in brassica juncea plants under cd-induced stress," *Biomed Res. Int.*, vol. 2014, p. 726070, Jul. 2014.

[69] C. Zayneb, K. Bassem, K. Zeineb, C. D. Grubb, D. Noureddine, M. Hafedh, and E. Amine, "Physiological responses of fenugreek seedlings and plants treated with cadmium," *Environ. Sci. Pollut. Res. Int.*, vol. 22, no. 14, pp. 10 679–10 689, Jul. 2015.

[70] T. Ling, Q. Gao, H. Du, Q. Zhao, and J. Ren, "Growing, physiological responses and cd uptake of corn (zea mays l.) under different cd supply," *Chem. Spec. Bioavail.*, vol. 29, no. 1, pp. 216–221, Jan. 2017.

[71] R. Zheng, H. Li, R. Jiang, V. Römheld, F. Zhang, and F.-J. Zhao, "The role of root hairs in cadmium acquisition by barley," *Environ. Pollut.*, vol. 159, no. 2, pp. 408–415, Feb. 2011.

[72] Y. Huang, Z. Zhu, X. Wu, Z. Liu, J. Zou, Y. Chen, N. Su, and J. Cui, "Lower cadmium accumulation and higher antioxidative capacity in edible parts of brassica campestris l. seedlings applied with glutathione under cadmium toxicity," *Environ. Sci. Pollut. Res. Int.*, vol. 26, no. 13, pp. 13 235–13 245, May 2019.

[73] G. Zhang, M. Fukami, and H. Sekimoto, "Influence of cadmium on mineral concentrations and yield components in wheat genotypes differing in cd tolerance at seedling stage," *Field Crops Res.*, vol. 77, no. 2-3, pp. 93–98, Sep. 2002.

[74] J. F. Gonçalves, F. G. Antes, J. Maldaner, L. B. Pereira, L. A. Tabaldi, R. Rauber, L. V. Rossato, D. A. Bisognin, V. L. Dressler, E. M. d. M. Flores, and F. T. Nicoloso, "Cadmium and mineral nutrient accumulation in potato plantlets grown under

cadmium stress in two different experimental culture conditions," *Plant Physiol. Biochem.*, vol. 47, no. 9, pp. 814–821, Sep. 2009.

[75] T. Yoshihara, N. Suzui, S. Ishii, M. Kitazaki, H. Yamazaki, K. Kitazaki, N. Kawachi, Y.-G. YIN, S. ITO-TANABATA, S.-N. HASHIDA *et al.*, "A kinetic analysis of cadmium accumulation in a cd hyper-accumulator fern, a thyrium yokoscense and tobacco plants," *Plant, cell & environment*, vol. 37, no. 5, pp. 1086–1096, 2014.

[76] K. Patel, V. Ramani, and J. Patel, "Trace and heavy metals composition in crops grown in sewage irrigated peri urban area of vadodara, india," *Asian Journal of Environmental Science*, vol. 3, no. 1, pp. 39–44, 2008.

[77] C. Dordas, "İncreased concentration of soil cadmium affects on plant growth, dry matter accumulation, cd, and zn uptake of different tobacco cultivars (nicotiana tabacum l)," *İnt. Journal of Phytoremediation*, vol. 11, pp. 115–130, 2009.

[78] Y. Yang, Y. Ge, H. Zeng, X. Zhou, L. Peng, and Q. Zeng, "Phytoextraction of cadmium contaminated soil and potential of regenerated tobacco biomass for recovery of cadmium," *Scientific reports*, vol. 7, no. 1, pp. 1–10, 2017.

[79] P. Yao, H. Zhou, X. Li, L. Wei, J. Wang, S. Zhang, and X. Ye, "Effect of biochar on the accumulation and distribution of cadmium in tobacco (yunyan 87) at different developmental stages," *Ecotoxicol. Environ. Saf.*, vol. 207, no. 111295, p. 111295, Jan. 2021.

[80] H. Erdem, A. Kınay, M. Ozturk, and Y. Tutus, "Effect of cadmium stress on growth and mineral composition of two tobacco cultivars," *Journal of Food, Agriculture & Environment*, vol. 10, no. 1, pp. 965–969, 2012.

[81] G. J. Mistry and K. P. Patel, "Relative efficiency of different crops for their phytoextraction capacity in managing heavy metals stress," *International journal of Bioresource and Stress Management*, vol. 4, no. 2s, pp. 304–308, 2013.

[82] J. C. Zinnert, S. M. Via, and D. R. Young, "Distinguishing natural from anthropogenic stress in plants: physiology, fluorescence and hyperspectral reflectance," *Plant and Soil*, vol. 366, pp. 133–141, 2013.

[83] P. S. Thenkabail, R. B. Smith, and E. De Pauw, "Hyperspectral vegetation indices and their relationships with agricultural crop characteristics," *Remote Sens. Environ.*, vol. 71, no. 2, pp. 158–182, Feb. 2000.

[84] C. H. Bock, G. H. Poole, P. E. Parker, and T. R. Gottwald, "Plant disease severity estimated visually, by digital photography and image analysis, and by hyperspectral imaging," *CRC Crit. Rev. Plant Sci.*, vol. 29, no. 2, pp. 59–107, Mar. 2010.

[85] J. G. P. W. Clevers, L. Kooistra, and M. E. Schaepman, "Estimating canopy water content using hyperspectral remote sensing data," *Int. J. Appl. Earth Obs. Geoinf.*, vol. 12, no. 2, pp. 119–125, Apr. 2010.

[86] X. Li, X. Liu, M. Liu, C. Wang, and X. Xia, "A hyperspectral index sensitive to subtle changes in the canopy chloro- phyll content under arsenic stress," *International Journal of Applied Earth Observation and Geoinformation*, vol. 36, pp. 41–53, 2015.

[87] P. Wang, F. Huang, and X. Liu, "Assessment of heavy metal stress using hyperspectral data," in *2017 IEEE International Geoscience and Remote Sensing Symposium (IGARSS)*. IEEE, Jul. 2017.

[88] O. Beeri, R. Phillips, J. Hendrickson, A. B. Frank, and S. Kronberg, "Estimating forage quantity and quality using aerial hyperspectral imagery for northern mixed-grass prairie," *Remote Sens. Environ.*, vol. 110, no. 2, pp. 216–225, Sep. 2007.

[89] C. Ryu, M. Suguri, and M. Umeda, "Estimation of the quantity and quality of green tea using hyperspectral sensing," *Journal of the Japanese Society of Agricultural Machinery*, vol. 72, no. 1, pp. 46–53, 2010.

[90] G. Wang, Q. Wang, Z. Su, and J. Zhang, "Predicting copper contamination in wheat canopy during the full growth period using hyperspectral data," *Environ. Sci. Pollut. Res. Int.*, vol. 27, no. 31, pp. 39 029–39 040, Nov. 2020.

[91] S. Cui, R. Ding, and K. Zhou, "A new hyperspectral index for estimating copper content in an indicative plant for the exploration of copper deposit," *J. Plant Growth Regul.*, vol. 38, no. 3, pp. 956–965, Sep. 2019.

[92] C. Ni, D. Zhang, P. Song, S. Zhao, and W. Yang, "Hyperspectral response of dominant plants in the poyang lake wetlands to heavy metal pollution," in *Terrestrial*

Environmental Sciences. Cham: Springer International Publishing, 2019, pp. 99–112.

[93] P. H. Rosso, J. C. Pushnik, M. Lay, and S. L. Ustin, "Reflectance properties and physiological responses of salicornia virginica to heavy metal and petroleum contamination," *Environ. Pollut.*, vol. 137, no. 2, pp. 241–252, Sep. 2005.

[94] H.-Y. Ren, D.-F. Zhuang, J.-J. Pan, X.-Z. Shi, R.-H. Shi, and H.-J. Wang, "Study on canopy spectral characteristics of paddy polluted by heavy metals," *Guang Pu Xue Yu Guang Pu Fen Xi*, vol. 30, no. 2, pp. 430–434, Feb. 2010.

[95] Z. Yang and B. Li, "Effects of cd contamination and physiological and biochemical characteristics on brassica juncea," in *2011 International Conference on Remote Sensing, Environment and Transportation Engineering*. IEEE, Jun. 2011.

[96] P. H. Rathod, C. Brackhage, F. D. Van der Meer, I. Müller, M. F. Noomen, D. G. Rossiter, and G. E. Dudel, "Spectral changes in the leaves of barley plant due to phytoremediation of metals—results from a pot study," *Eur. J. Remote Sens.*, vol. 48, no. 1, pp. 283–302, Jan. 2015.

[97] B. P. Banerjee, S. Raval, H. Zhai, and P. J. Cullen, "Health condition assessment for vegetation exposed to heavy metal pollution through airborne hyperspectral data," *Environ. Monit. Assess.*, vol. 189, no. 12, p. 604, Nov. 2017.

[98] Y. W. Gu, S. Li, W. Gao, and H. Wei, "Hyperspectral estimation of the cadmium content in leaves of brassica rapa chinesis based on the spectral parameters," *Acta Ecologica Sinica*, vol. 35, no. 13, pp. 4445–4453, 2015.

[99] L. Wu, X. Liu, P. Wang, B. Zhou, M. Liu, and X. Li, "The assimilation of spectral sensing and the WOFOST model for the dynamic simulation of cadmium accumulation in rice tissues," *Int. J. Appl. Earth Obs. Geoinf.*, vol. 25, pp. 66–75, Dec. 2013.

[100] M. Liu, X. Liu, W. Ding, and L. Wu, "Monitoring stress levels on rice with heavy metal pollution from hyperspectral reflectance data using wavelet-fractal analysis," *Int. J. Appl. Earth Obs. Geoinf.*, vol. 13, no. 2, pp. 246–255, Apr. 2011.

[101] B. B. M. Sridhar, F. X. Han, S. V. Diehl, D. L. Monts, and Y. Su, "Spectral reflectance and leaf internal structure changes of barley plants due to phytoextraction of zinc and cadmium," *Int. J. Remote Sens.*, vol. 28, no. 5, pp. 1041–1054, Mar. 2007.

[102] S. C. Dunagan, M. S. Gilmore, and J. C. Varekamp, "Effects of mercury on visible/near-infrared reflectance spectra of mustard spinach plants (brassica rapa p.)," *Environ. Pollut.*, vol. 148, no. 1, pp. 301–311, Jul. 2007.

[103] Y. Wu, J. Chen, X. Wu, Q. Tian, J. Ji, and Z. Qin, "Possibilities of reflectance spectroscopy for the assessment of contaminant elements in suburban soils," *Appl. Geochem.*, vol. 20, no. 6, pp. 1051–1059, Jun. 2005.

[104] S. Song, W. Gong, B. Zhu, and X. Huang, "Wavelength selection and spectral discrimination for paddy rice, with laboratory measurements of hyperspectral leaf reflectance," *ISPRS J. Photogramm. Remote Sens.*, vol. 66, no. 5, pp. 672–682, Sep. 2011.

[105] J. Verrelst, G. Camps-Valls, J. Muñoz-Marí, J. P. Rivera, F. Veroustraete, J. G. P. W. Clevers, and J. Moreno, "Optical remote sensing and the retrieval of terrestrial vegetation bio-geophysical properties-a review," *ISPRS J. Photogramm. Remote Sens*, vol. 108, pp. 273–290, 2015.

[106] M. Liu, X. Liu, M. Wu, L. Li, and L. Xiu, "Integrating spectral indices with environmental parameters for estimating heavy metal concentrations in rice using a dynamic fuzzy neural-network model," *Comput. Geosci.*, vol. 37, no. 10, pp. 1642–1652, Oct. 2011.

[107] L. Rossi, M. Bagheri, W. Zhang, Z. Chen, J. G. Burken, and X. Ma, "Using artificial neural network to investigate physiological changes and cerium oxide nanoparticles and cadmium uptake by brassica napus plants," *Environ. Pollut.*, vol. 246, pp. 381–389, Mar. 2019.

[108] M. Liu, X. Liu, M. Li, M. Fang, and W. Chi, "Neural-network model for estimating leaf chlorophyll concentration in rice under stress from heavy metals using four spectral indices," *Biosystems engineering*, vol. 106, no. 3, pp. 223–233, 2010.

[109] M. Misiti, Y. Misiti, G. Oppenheim, and J. Poggi, *Wavelet toolbox for use with matlab, user 's guide, ver. 3., the mathworks*. " Inc. Users Guide, 2004.

[110] M. Liu, X. Liu, L. Wu, L. Duan, and B. Zhong, "Wavelet-based detection of crop zinc stress assessment using hyperspectral reflectance," *Computers & geosciences*, vol. 37, no. 9, pp. 1254–1263, 2011.

[111] S. Kaewpijit, J. Le Moigne, and T. El-Ghazawi, "Automatic reduction of hyperspectral imagery using wavelet spectral analysis," *IEEE Trans. Geosci. Remote Sens.*, vol. 41, no. 4, pp. 863–871, Apr. 2003.

[112] G. Blackburn and J. Ferwerda, "Retrieval of chlorophyll concentration from leaf reflectance spectra using wavelet analysis," *Remote Sens. Environ.*, vol. 112, no. 4, pp. 1614–1632, Apr. 2008.

[113] T. Cheng, B. Rivard, and A. Sánchez-Azofeifa, "Spectroscopic determination of leaf water content using continuous wavelet analysis," *Remote Sens. Environ.*, vol. 115, no. 2, pp. 659–670, Feb. 2011.

[114] M. Liu, X. Liu, W. Ding, and L. Wu, "Monitoring stress levels on rice with heavy metal pollution from hyperspectral reflectance data using wavelet-fractal analysis," *Int. J. Appl. Earth Obs. Geoinf.*, vol. 13, no. 2, pp. 246–255, Apr. 2011.

[115] J. Wang, T. Wang, T. Shi, G. Wu, and A. Skidmore, "A wavelet-based area parameter for indirectly estimating copper concentration in carex leaves from canopy reflectance," *Remote Sens. (Basel)*, vol. 7, no. 11, pp. 15 340–15 360, Nov. 2015.

[116] X. Zhou, J. Sun, Y. Tian, B. Lu, Y. Hang, and Q. Chen, "Hyperspectral technique combined with deep learning algorithm for detection of compound heavy metals in lettuce," *Food Chem.*, vol. 321, no. 126503, p. 126503, Aug. 2020.

[117] Y. Jiang, Y. Qi, W. K. Wang, B. Bent, R. Avram, J. Olgin, and J. Dunn, "Eventdtw: An improved dynamic time warping algorithm for aligning biomedical signals of nonuniform sampling frequencies," *Sensors*, vol. 20, no. 9, p. 2700, 2020.

[118] Y. Permanasari, E. H. Harahap, and E. P. Ali, "Speech recognition using dynamic time warping (DTW)," *J. Phys. Conf. Ser.*, vol. 1366, no. 1, p. 012091, Nov. 2019.

[119] V. Maus, G. Camara, R. Cartaxo, A. Sanchez, F. M. Ramos, and G. R. de Queiroz, "A time-weighted dynamic time warping method for land-use and land-cover mapping," *IEEE J. Sel. Top. Appl. Earth Obs. Remote Sens.*, vol. 9, no. 8, pp. 3729–3739, Aug. 2016.

[120] F. Petitjean, J. Inglada, and P. Gançarski, "Satellite image time series analysis under time warping," *IEEE transactions on geoscience and remote sensing*, vol. 50, no. 8, pp. 3081–3095, 2012.

[121] W. S. Moola, W. Bijker, M. Belgiu, and M. Li, "Vegetable mapping using fuzzy classification of dynamic time warping distances from time series of Sentinel-1A images," *Int. J. Appl. Earth Obs. Geoinf.*, vol. 102, no. 102405, p. 102405, Oct. 2021.

[122] N. Kumari and C. Mohan, "Basics of clay minerals and their characteristic properties," in *Clay and Clay Minerals*. IntechOpen, Dec. 2021.

[123] G. Sposito, N. T. Skipper, R. Sutton, S. Park, A. K. Soper, and J. A. Greathouse, "Surface geochemistry of the clay minerals," *Proc. Natl. Acad. Sci. U. S. A.*, vol. 96, no. 7, pp. 3358–3364, Mar. 1999.

[124] H. H. Murray, "Chapter 2 structure and composition of the clay minerals and their physical and chemical properties," in *Developments in Clay Science*, ser. Developments in clay science. Elsevier, 2006, pp. 7–31.

[125] Y. Bissonnais, "Aggregate stability and assessment of soil crustability and erodibility: I. theory and methodology," *Eur. J. Soil Sci.*, vol. 47, no. 4, pp. 425–437, Dec. 1996.

[126] J. M. Soriano-Disla, L. J. Janik, R. A. Viscarra Rossel, L. M. Macdonald, and M. J. McLaughlin, "The performance of visible, near-, and mid-infrared reflectance spectroscopy for prediction of soil physical, chemical, and biological properties," *Appl. Spectrosc. Rev.*, vol. 49, no. 2, pp. 139–186, Feb. 2014.

[127] D. Ramakrishnan and R. Bharti, "Hyperspectral remote sensing and geological applications," *Current science*, pp. 879–891, 2015.

[128] T. Magendran and S. Sanjeevi, "Hyperion image analysis and linear spectral unmixing to evaluate the grades of iron ores in parts of noamundi, eastern india," *Int. J. Appl. Earth Obs. Geoinf.*, vol. 26, pp. 413–426, Feb. 2014.

[129] R. V. Rossel, R. McGlynn, and A. McBratney, "Determining the composition of mineral-organic mixes using uv–vis–nir diffuse reflectance spectroscopy," *Geoderma*, vol. 137, no. 1-2, pp. 70–82, 2006.

[130] H. Eichstaedt, T. Tsedenbaljir, R. Kahnt, M. Denk, Y. Ogen, C. Glaesser, R. Loeser, R. Suppes, U. Alyeksandr, T. Oyunbuyan, and J. Michalski, "Quantitative estimation of clay minerals in airborne hyperspectral data using a calibration field," *J. Appl. Remote Sens.*, vol. 14, no. 03, Sep. 2020.

[131] E. Ben-Dor, S. Chabrillat, J. A. M. Demattê, G. R. Taylor, J. Hill, M. L. Whiting, and S. Sommer, "Using imaging spectroscopy to study soil properties," *Remote Sens. Environ.*, vol. 113, pp. S38–S55, Sep. 2009.

[132] A. Steinberg, S. Chabrillat, A. Stevens, K. Segl, and S. Foerster, "Prediction of common surface soil properties based on Vis-NIR airborne and simulated EnMAP imaging spectroscopy data: Prediction accuracy and influence of spatial resolution," *Remote Sens. (Basel)*, vol. 8, no. 7, p. 613, Jul. 2016.

[133] L. K. Sørensen and S. Dalsgaard, "Determination of clay and other soil properties by near infrared spectroscopy," *Soil Sci. Soc. Am. J.*, vol. 69, no. 1, p. 159, 2005.

[134] P. Lagacherie, F. Baret, J.-B. Feret, J. Madeira Netto, and J. M. Robbez-Masson, "Estimation of soil clay and calcium carbonate using laboratory, field and airborne hyperspectral measurements," *Remote Sens. Environ.*, vol. 112, no. 3, pp. 825–835, Mar. 2008.

[135] Z. Shi, Q. Wang, J. Peng, W. Ji, H. Liu, X. Li, and R. A. Viscarra Rossel, "Development of a national VNIR soil-spectral library for soil classification and prediction of organic matter concentrations," *Sci. China Earth Sci.*, vol. 57, no. 7, pp. 1671–1680, Jul. 2014.

[136] E. Ben-Dor, S. Chabrillat, J. A. M. Demattê, G. R. Taylor, J. Hill, M. L. Whiting, and S. Sommer, "Using imaging spectroscopy to study soil properties," *Remote Sens. Environ.*, vol. 113, pp. S38–S55, Sep. 2009.

[137] H. Gerighausen, G. Menz, and H. Kaufmann, "Spatially explicit estimation of clay and organic carbon content in agricultural soils using multi-annual imaging spectroscopy data," *Appl. Environ. Soil Sci.*, vol. 2012, pp. 1–23, 2012.

[138] J. R. Michalski, M. D. Kraft, T. G. Sharp, L. B. Williams, and P. R. Christensen, "Emission spectroscopy of clay minerals and evidence for poorly crystalline aluminosilicates on mars from thermal emission spectrometer data," *J. Geophys. Res.*, vol. 111, no. E3, 2006.

[139] G. Grandjean, X. Briottet, K. Adeline, A. Bourguignon, and A. Hohmann, "Clay minerals mapping from imaging spectroscopy," in *Earth Observation and Geospatial Analyses [Working Title]*. IntechOpen, May 2019.

[140] G. Gilles, B. Xavier, A. Karine, B. Anne, and H. Audrey, "Clay minerals mapping from imaging spectroscopy," *Earth Observation and Geospatial Analyses*, pp. 1–14, 2019.

[141] G. Grandjean, X. Briottet, K. Adeline, A. Bourguignon, and A. Hohmann, "Clay minerals mapping from imaging spectroscopy," in *Earth Observation and Geospatial Analyses [Working Title]*. IntechOpen, May 2019.

[142] D. Curcio, G. Ciraolo, F. D'Asaro, and M. Minacapilli, "Prediction of soil texture distributions using VNIR-SWIR reflectance spectroscopy," *Procedia Environ. Sci.*, vol. 19, pp. 494–503, 2013.

[143] F. Garfagnoli, A. Ciampalini, S. Moretti, L. Chiarantini, and S. Vettori, "Quantitative mapping of clay minerals using airborne imaging spectroscopy: new data on mugello (italy) from SIM-GA prototypal sensor," *Eur. J. Remote Sens.*, vol. 46, no. 1, pp. 1–17, Jan. 2013.

[144] W. B. Cohen, T. K. Maiersperger, S. T. Gower, and D. P. Turner, "An improved strategy for regression of biophysical variables and landsat ETM+ data," *Remote Sens. Environ.*, vol. 84, no. 4, pp. 561–571, Apr. 2003.

[145] V. L. Mulder, S. de Bruin, and M. E. Schaepman, "Representing major soil variability at regional scale by constrained latin hypercube sampling of remote sensing data," *Int. J. Appl. Earth Obs. Geoinf.*, vol. 21, pp. 301–310, Apr. 2013.

[146] G. Lassalle, S. Fabre, A. Credoz, R. Hédacq, D. Dubucq, and A. Elger, "Mapping leaf metal content over industrial brownfields using airborne hyperspectral imaging and optimized vegetation indices," *Sci. Rep.*, vol. 11, no. 1, p. 2, Jan. 2021.

[147] I. Melendez-Pastor, J. Navarro-Pedreño, I. Gómez, and M. Almendro-Candel, "The use of remote sensing to locate heavy metal as source of pollution," *Advances in Environmental Research*, vol. 7, pp. 225–233, 2011.

[148] E. Bedini, F. van der Meer, and F. van Ruitenbeek, "Use of HyMap imaging spectrometer data to map mineralogy in the rodalquilar caldera, southeast spain," *Int. J. Remote Sens.*, vol. 30, no. 2, pp. 327–348, Jan. 2009.

[149] F. A. Kruse, J. W. Boardman, and J. F. Huntington, "Comparison of airborne hyperspectral data and eo-1 hyperion for mineral mapping," *IEEE Trans. Geosci. Remote Sens.*, vol. 41, no. 6, pp. 1388–1400, Jun. 2003.

[150] T. Mitran, K. Sreenivas, K. G. Janakirama Suresh, G. Sujatha, and T. Ravisankar, "Spatial prediction of calcium carbonate and clay content in soils using airborne hyperspectral data," *J. Ind. Soc. Remote Sens.*, vol. 49, no. 11, pp. 2611–2622, Nov. 2021.

[151] M. Deb, "Genesis and metamorphism of two stratiform massive sulfide deposits at ambaji and deri in the precambrian of western india," *Econ. Geol.*, vol. 75, no. 4, pp. 572–591, Jul. 1980.

[152] B. K. Bhattacharya, R. O. Green, S. Rao, M. Saxena, S. Sharma, K. Ajay Kumar, P. Srinivasulu, S. Sharma, D. Dhar, S. Bandyopadhyay, S. Bhatwadekar, and R. Kumar, "An overview of AVIRIS-NG airborne hyperspectral science campaign over india," *Curr. Sci.*, vol. 116, no. 7, p. 1082, Apr. 2019.

[153] L. J. Poppe, V. F. Paskevich, J. C. Hathaway, and D. S. Blackwood, "A laboratory manual for x-ray powder diffraction," *US Geological Survey open-file report*, vol. 1, no. 041, pp. 1–88, 2001.

[154] Y. Gu, S. Li, W. Gao, and H. Wei, "Hyperspectral estimation of the cadmium content in leaves of brassica rapa chinesis based on the spectral parameters," *Acta Ecologica Sinica*, vol. 35, no. 13, pp. 4445–4453, 2015.

[155] R. Moran, "Formulae for determination of chlorophyllous pigments extracted with n,n-dimethylformamide," *Plant Physiol.*, vol. 69, no. 6, pp. 1376–1381, Jun. 1982.

[156] M. Arshad, J. Silvestre, E. Pinelli, J. Kallerhoff, M. Kaemmerer, A. Tarigo, M. Shahid, M. Guiresse, P. Pradere, and C. Dumat, "A field study of lead phytoextraction by various scented pelargonium cultivars," *Chemosphere*, vol. 71, no. 11, pp. 2187–2192, May 2008.

[157] Y. Li, K. Yang, F. Cheng, and C. Zhang, "Development of a new heavy metal vegetation index for improving monitoring of copper and lead concentration in corn," *Eur. J. Remote Sens.*, vol. 52, no. 1, pp. 632–639, Jan. 2019.

[158] L. Han, "Estimating chlorophyll-aconcentration using first-derivative spectra in coastal water," *Int. J. Remote Sens.*, vol. 26, no. 23, pp. 5235–5244, Dec. 2005.

[159] M. Misiti, Y. Misiti, G. Oppenheim, and J. M. Poggi, "Matlab wavelet toolbox user's guide," *The MathWorks Inc*, 1996.

[160] E. I. Rabinowitch and Govindjee, "The role of chlorophyll in photosynthesis," *Sci. Am.*, vol. 213, no. 1, pp. 74–83, Jul. 1965.

[161] R. S. Sengar, M. Gautam, R. S. Sengar, R. S. Sengar, S. K. Garg, K. Sengar, and R. Chaudhary, "Lead stress effects on physiobiochemical activities of higher plants," in *Reviews of Environmental Contamination and Toxicology*, ser. Reviews of environmental contamination and toxicology. New York, NY: Springer US, 2008, pp. 73–93.

[162] I. V. Seregin and V. B. Ivanov, "Physiological aspects of cadmium and lead toxic effects on higher plants," *Russian journal of plant physiology*, vol. 48, pp. 523–544, 2001.

[163] A. Piotrowska, A. Bajguz, B. Godlewska-Żyłkiewicz, R. Czerpak, and M. Kamińska, "Jasmonic acid as modulator of lead toxicity in aquatic plant wolffia arrhiza (lemnaceae)," *Environ. Exp. Bot.*, vol. 66, no. 3, pp. 507–513, Sep. 2009.

[164] J. Barceló and C. Poschenrieder, "Structural and ultrastructural changes in heavy metal exposed plants," in *Heavy Metal Stress in Plants*. Berlin, Heidelberg: Springer Berlin Heidelberg, 2004, pp. 223–248.

[165] M. A. Davis, S. G. Pritchard, R. S. Boyd, and S. A. Prior, "Developmental and induced responses of nickel-based and organic defences of the nickel-hyperaccumulating shrub, psychotria douarrei," *New Phytol.*, vol. 150, no. 1, pp. 49–58, Apr. 2001.

[166] B. He, M. Gu, X. Wang, and X. He, "The effects of lead on photosynthetic performance of waxberry seedlings (myrica rubra)," *Photosynthetica*, vol. 56, no. 4, pp. 1147–1153, Nov. 2018.

[167] M. Lal and Department of Botany and Plant Physiology, CCS HAU, Hisar (India) - 125004, "Effects of different heavy metals and mycorrhizal treatments on various

physiological processes in cotton genotypes," *Int. J. Pure Appl. Biosci.*, vol. 6, no. 3, pp. 146–153, Jun. 2018.

[168] S. Malar, S. Shivendra Vikram, P. Jc Favas, and V. Perumal, "Lead heavy metal toxicity induced changes on growth and antioxidative enzymes level in water hyacinths [eichhornia crassipes (mart.)]," *Bot. Stud.*, vol. 55, no. 1, p. 54, Dec. 2016.

[169] G. N. OROPEZA, R. Hausler, M. Glaus, A. R. VEGA, and L. R. ROMERO, "Transport of heavy metals in materials with diameter analogous to xylem vessels," 2014.

[170] M. Ali and F. S. Nas, "The effect of lead on plants in terms of growing and biochemical parameters: a review," *MOJ Ecol. Environ. Sci.*, vol. 3, no. 4, Aug. 2018.

[171] P. K. Padmavathiamma and L. Y. Li, "Phytoremediation technology: Hyper-accumulation metals in plants," *Water Air Soil Pollut.*, vol. 184, no. 1-4, pp. 105–126, Aug. 2007.

[172] H. Qian, J. Li, L. Sun, W. Chen, G. D. Sheng, W. Liu, and Z. Fu, "Combined effect of copper and cadmium on chlorella vulgaris growth and photosynthesis-related gene transcription," *Aquat. Toxicol.*, vol. 94, no. 1, pp. 56–61, Aug. 2009.

[173] H. Y. Yang, G. X. Shi, Q. S. Xu, and H. X. Wang, "Cadmium effects on mineral nutrition and stress in potamogeton crispus," *Russ. J. Plant Physiol.*, vol. 58, no. 2, pp. 253–260, Mar. 2011.

[174] Z. Fang, "Chlorophyllase activities and chlorophyll degradation during leaf senescence in non-yellowing mutant and wild type of phaseolus vulgaris L," *J. Exp. Bot.*, vol. 49, no. 320, pp. 503–510, Mar. 1998.

[175] A. Waheed, Y. Haxim, W. Islam, M. Ahmad, S. Ali, X. Wen, K. A. Khan, H. A. Ghramh, Z. Zhang, and D. Zhang, "Impact of cadmium stress on growth and physio-biochemical attributes of eruca sativa mill," *Plants*, vol. 11, no. 21, p. 2981, Nov. 2022.

[176] H. Kupper, I. Setlik, M. Spiller, F. C. Kupper, and O. Prasil, "Heavy metal-induced inhibition of photosynthesis: Targets of in vivo heavy metal chlorophyll formation1," *J. Phycol.*, vol. 38, no. 3, pp. 429–441, Jun. 2002.

[177] S. S. Gill, N. A. Khan, and N. Tuteja, "Cadmium at high dose perturbs growth, photosynthesis and nitrogen metabolism while at low dose it up regulates sulfur assimilation and antioxidant machinery in garden cress (lepidium sativum l.)," *Plant Sci.*, vol. 182, pp. 112–120, Jan. 2012.

[178] A. Cuypers, T. Remans, N. Weyens, J. Colpaert, A. Vassilev, and J. Vangronsveld, "Soil-plant relationships of heavy metals and metalloids," in *Environmental Pollution*. Dordrecht: Springer Netherlands, 2013, pp. 161–193.

[179] B. Pourrut, M. Shahid, C. Dumat, P. Winterton, and E. Pinelli, "Lead uptake, toxicity, and detoxification in plants," in *Reviews of Environmental Contamination and Toxicology*, ser. Reviews of environmental contamination and toxicology. New York, NY: Springer New York, 2011, pp. 113–136.

[180] S. Ramana, A. K. Tripathi, K. Bharati, A. B. Singh, A. Kumar, A. Sahu, P. S. Rajput, P. Dey, J. K. Saha, and A. K. Patra, "Tolerance of cotton to elevated levels of pb and its potential for phytoremediation," *Environ. Sci. Pollut. Res. Int.*, vol. 28, no. 25, pp. 32 299–32 309, Feb. 2021.

[181] L. Li, X. Yan, J. Li, Y. Tian, P. Ren *et al.*, "Advances in cotton tolerance to heavy metal stress and applications to remediate heavy metal-contaminated farmland soil," *Phyton*, vol. 90, no. 1, p. 35, 2021.

[182] H. Dahmani-Muller, F. van Oort, B. Gélie, and M. Balabane, "Strategies of heavy metal uptake by three plant species growing near a metal smelter," *Environ. Pollut.*, vol. 109, no. 2, pp. 231–238, Aug. 2000.

[183] S. Rangnekar, S. Sahu, G. Pandit, and V. Gaikwad, "Accumulation and translocation of nickel and cobalt in nutritionally important indian vegetables grown in artificially contaminated soil of mumbai, india," *Research Journal of Agriculture and Forestry Sciences*, p. 6063, 2013.

[184] N. Mirecki, R. Agic, L. Sunic, L. Milenkovic, and Z. S. Ilic, "Transfer factor as indicator of heavy metals content in plants," *Fresenius Environmental Bulletin*, vol. 24, no. 11c, pp. 4212–4219, 2015.

[185] P. Sharma and R. S. Dubey, "Lead toxicity in plants," *Braz. J. Plant Physiol.*, vol. 17, no. 1, pp. 35–52, Mar. 2005.

[186] G. J. Mistry and K. P. Patel, "Relative efficiency of different crops for their phyto-extraction capacity in managing heavy metals stress," *International journal of Bio-resource and Stress Management*, vol. 4, no. 2s, pp. 304–308, 2013.

[187] Y. Yang, Y. Ge, H. Zeng, X. Zhou, L. Peng, and Q. Zeng, "Phytoextraction of cadmium-contaminated soil and potential of regenerated tobacco biomass for recovery of cadmium," *Sci. Rep.*, vol. 7, no. 1, p. 7210, Aug. 2017.

[188] Z.-L. Yuan, S.-P. Xiong, C.-M. Li, and X.-M. Ma, "Effects of chronic stress of cadmium and lead on anatomical structure of tobacco roots," *Agric. Sci. China*, vol. 10, no. 12, pp. 1941–1948, Dec. 2011.

[189] B. Zhang, S. Shang, Z. Jabeen, and G. Zhang, "Involvement of ethylene in alleviation of cd toxicity by NaCl in tobacco plants," *Ecotoxicol. Environ. Saf.*, vol. 101, pp. 64–69, Mar. 2014.

[190] K. Rosén, J. Eriksson, and M. Vinichuk, "Uptake and translocation of 109cd and stable cd within tobacco plants (nicotiana sylvestris)," *J. Environ. Radioact.*, vol. 113, pp. 16–20, Nov. 2012.

[191] T. Doroszewska and A. Berbeć, "Variation for cadmium uptake among nicotiana species," *Genet. Resour. Crop Evol.*, vol. 51, no. 3, pp. 323–333, May 2004.

[192] V. Hermand, E. Julio, F. Dorlhac de Borne, T. Punshon, F. K. Ricachenevsky, A. Bellec, F. Gosti, and P. Berthomieu, "Inactivation of two newly identified tobacco heavy metal ATPases leads to reduced zn and cd accumulation in shoots and reduced pollen germination," *Metallomics*, vol. 6, no. 8, pp. 1427–1440, Aug. 2014.

[193] H. Liu, H. Wang, Y. Ma, H. Wang, and Y. Shi, "Role of transpiration and metabolism in translocation and accumulation of cadmium in tobacco plants (nicotiana tabacum l.). chemosphere, 144," pp. 1960–1965, 2016.

[194] I. D. A. Sanches, C. R. Souza Filho, and R. F. Kokaly, "Spectroscopic remote sensing of plant stress at leaf and canopy levels using the chlorophyll 680 nm absorption feature with continuum removal," *ISPRS Journal of Photogrammetry and Remote Sensing*, vol. 97, pp. 111–122, 2014.

[195] K. L. Wuensch, "Straightforward statistic for the behavioral sciences," *Journal of the American Statistical Association*, vol. 91, no. 436, p. 1750, 1996.

[196] C. Zhou, S. Chen, Y. Zhang, J. Zhao, D. Song, and D. Liu, "Evaluating metal effects on the reflectance spectra of plant leaves during different seasons in post-mining areas, china," *Remote Sensing*, vol. 10, no. 8, p. 1211, 2018.

[197] P. H. Rosso, J. C. Pushnik, M. Lay, and S. L. Ustin, "Reflectance properties and physiological responses of salicornia virginica to heavy metal and petroleum contamination," *Environ. Pollut.*, vol. 137, no. 2, pp. 241–252, Sep. 2005.

[198] Y. Li, K. Yang, F. Cheng, and C. Zhang, "Development of a new heavy metal vegetation index for improving monitoring of copper and lead concentration in corn," *Eur. J. Remote Sens.*, vol. 52, no. 1, pp. 632–639, Jan. 2019.

[199] M. B. B. Sridhar, F. X. Han, S. V. Diehl, D. L. Monts, and Y. Su, "Monitoring the effects of arsenic and chromium accumulation in chinese brake fern (pteris vittata)," *Int. J. Remote Sens.*, vol. 28, no. 5, pp. 1055–1067, Mar. 2007.

[200] Y. W. Gu, S. Li, W. Gao, and H. Wei, "Hyperspectral estimation of the cadmium content in leaves of brassica rapa chinesis based on the spectral parameters," *Acta Ecologica Sinica*, vol. 35, no. 13, pp. 4445–4453, 2015.

[201] S. W. Newete, B. F. N. Erasmus, I. M. Weiersbye, M. A. Cho, and M. J. Byrne, "Hyperspectral reflectance features of water hyacinth growing under feeding stresses ofneochetinaspp. and different heavy metal pollutants," *Int. J. Remote Sens.*, vol. 35, no. 3, pp. 799–817, Feb. 2014.

[202] T. Shi, H. Liu, Y. Chen, J. Wang, and G. Wu, "Estimation of arsenic in agricultural soils using hyperspectral vegetation indices of rice," *J. Hazard. Mater.*, vol. 308, pp. 243–252, May 2016.

[203] C. Liu, J. Guo, Y. Cui, T. Lü, X. Zhang, and G. Shi, "Effects of cadmium and salicylic acid on growth, spectral reflectance and photosynthesis of castor bean seedlings," *Plant and soil*, vol. 344, pp. 131–141, 2011.

[204] B. K. Bhattacharya, R. O. Green, S. Rao, M. Saxena, S. Sharma, K. Ajay Kumar, P. Srinivasulu, S. Sharma, D. Dhar, S. Bandyopadhyay, S. Bhatwadekar, and R. Kumar, "An overview of AVIRIS-NG airborne hyperspectral science campaign over india," *Curr. Sci.*, vol. 116, no. 7, p. 1082, Apr. 2019.

[205] Q. Du, I. Kopriva, and H. Szu, "Independent-component analysis for hyperspectral remote sensing imagery classification," *Optical Engineering*, vol. 45, no. 1, pp. 017 008–017 008, 2006.

[206] M. Huang, Q. Zhu, B. Wang, and R. Lu, "Analysis of hyperspectral scattering images using locally linear embedding algorithm for apple mealiness classification," *Comput. Electron. Agric.*, vol. 89, pp. 175–181, Nov. 2012.

[207] H. Liang and Q. Li, "Hyperspectral imagery classification using sparse representations of convolutional neural network features," *Remote Sens. (Basel)*, vol. 8, no. 2, p. 99, Jan. 2016.

[208] Y. Chen, Z. Lin, X. Zhao, G. Wang, and Y. Gu, "Deep learning-based classification of hyperspectral data," *IEEE J. Sel. Top. Appl. Earth Obs. Remote Sens.*, vol. 7, no. 6, pp. 2094–2107, Jun. 2014.

[209] G. Licciardi, P. R. Marpu, J. Chanussot, and J. A. Benediktsson, "Linear versus nonlinear PCA for the classification of hyperspectral data based on the extended morphological profiles," *IEEE Geosci. Remote Sens. Lett.*, vol. 9, no. 3, pp. 447–451, May 2012.

[210] W. Lv and X. Wang, "Overview of hyperspectral image classification," *J. Sens.*, vol. 2020, pp. 1–13, Jul. 2020.

[211] L. Zhimin, H. Panchao, H. Hong, and H. Wen, "Semi-supervised graph clustering with composite kernel and its application in hyperspectral image," *Opto-electronic Engineering*, vol. 43, no. 4, pp. 33–39, 2016.

[212] S. Priya, R. Ghosh, and B. K. Bhattacharya, "Non-Linear autoencoder based algorithm for dimensionality reduction of airborne hyperspectral data. international archives of the photogrammetry," *Remote Sensing and Spatial Information Sciences*, vol. 42, no. 3, 2019.

[213] K. Dave, T. Vyas, and Y. N. Trivedi, "Band selection technique for crop classification using hyperspectral data," *J. Ind. Soc. Remote Sens.*, vol. 50, no. 8, pp. 1487–1498, Aug. 2022.

[214] F. Mirzaei, Y. Abbasi, and T. Sohrabi, "Modeling the distribution of heavy metals in lands irrigated by wastewater using satellite images of sentinel-2," *Egypt. J. Remote Sens. Space Sci.*, vol. 24, no. 3, pp. 537–546, Dec. 2021.

[215] G. Blackburn and J. Ferwerda, "Retrieval of chlorophyll concentration from leaf reflectance spectra using wavelet analysis," *Remote Sens. Environ.*, vol. 112, no. 4, pp. 1614–1632, Apr. 2008.

[216] V. Maus, G. Camara, R. Cartaxo, A. Sanchez, F. M. Ramos, and G. R. de Queiroz, "A time-weighted dynamic time warping method for land-use and land-cover mapping," *IEEE J. Sel. Top. Appl. Earth Obs. Remote Sens.*, vol. 9, no. 8, pp. 3729–3739, Aug. 2016.

[217] F. Petitjean and J. Weber, "Efficient satellite image time series analysis under time warping," *IEEE Geosci. Remote Sens. Lett.*, vol. 11, no. 6, pp. 1143–1147, Jun. 2014.

[218] A. Kabata-Pendias, *Trace elements in soils and plants, fourth edition*, 4th ed. Boca Raton, FL: CRC Press, Aug. 2010.

[219] O. D. Adeyolanu, O. J. Kadiri, K. S. Are, and G. A. Oluwatosin, "Lead and cadmium contents in a medicinal plant/spice grown in an urban city of nigeria," *Cogent Food Agric.*, vol. 2, no. 1, Jan. 2016.

[220] A. Dutta, A. Patra, H. S. Jatav, S. S. Jatav, S. K. Singh, E. Sathyanarayana, S. Verma, and P. Singh, "Toxicity of cadmium in soil-plant-human continuum and its bioremediation techniques," *Soil Contamination-Threats and Sustainable Solutions*, p. 22, 2020.

[221] A. Stanojkovic-Sebic, R. Pivic, D. Josic, Z. Dinic, and A. Stanojkovic, "Heavy metals content in selected medicinal plants commonly used as," *Journal of Agricultural Sciences*, vol. 21, no. 3, pp. 317–325, 2015.

[222] B. A. Lajayer, M. Ghorbanpour, and S. Nikabadi, "Heavy metals in contaminated environment: destiny of secondary metabolite biosynthesis, oxidative status and phytoextraction in medicinal plants," *Ecotoxicology and Environmental Safety*, vol. 145, pp. 377–390, 2017.

[223] H. Sakoe and S. Chiba, "Dynamic programming algorithm optimization for spoken word recognition," in *Readings in Speech Recognition*. Elsevier, 1990, pp. 159–165.

[224] P. Senin, *Dynamic time warping algorithm review*, 2008.

[225] L. Zhang, L. Zhang, D. Tao, and X. Huang, "On combining multiple features for hyperspectral remote sensing image classification," *IEEE Trans. Geosci. Remote Sens.*, vol. 50, no. 3, pp. 879–893, Mar. 2012.

[226] J. Taylor, X. Zhou, N. M. Rouphail, and R. J. Porter, "Method for investigating intradriver heterogeneity using vehicle trajectory data: A dynamic time warping approach," *Trans. Res. Part B: Methodol.*, vol. 73, pp. 59–80, Mar. 2015.

[227] Y. Li, H. Chen, and Z. Wu, "Dynamic time warping distance method for similarity test of multipoint ground motion field," *Math. Probl. Eng.*, vol. 2010, pp. 1–12, 2010.

[228] K.-S. Lee, D. Jin, J.-M. Yeom, M. Seo, S. Choi, J.-J. Kim, and K.-S. Han, "New approach for snow cover detection through spectral pattern recognition with modis data," *Journal of Sensors*, vol. 2017, 2017.

[229] A. K. JHA, B. Singh, M. KUMAR, and S. KUMAR, "Behavior of cadmium in loamy sand soil ofanand," *Environment & Ecology*, vol. 28, no. 2A, pp. 1186–1189, 2010.

[230] N. K. JI, H. Soni, R. N. Kumar, and I. Bhatt, "Hyperaccumulation and mobility of heavy metals in vegetable crops in india," *Journal of Agriculture and Environment*, vol. 10, pp. 34–45, 2009.

[231] S. Singh and R. Hiranmai, "Monitoring and molecular characterization of bacterial species in heavy metals contaminated roadside soil of selected region along nh 8a, gujarat," *Heliyon*, vol. 7, no. 11, p. e08284, 2021.

[232] S. Singh and R. Yadav, "Heavy metal contamination and pollution indices in roadside soils of ahmedabad, gujarat," *Int. J. Sci. Res. Rev*, vol. 8, pp. 1839–1851, 2019.

[233] R. Khalili, S. Anvari, and M. Honarmand, "Combination of biochemical and hyperspectral remote sensing methods for detection of heavy metal pollutions in eucalyptus leaves (case study: The city of bam)." *International Archives of the Photogrammetry, Remote Sensing & Spatial Information Sciences*, vol. 40, 2015.

[234] R. Gupta, "Remote sens geol," *Heidelberg: Springer-Verlag*, vol. 10, pp. 978–973, 2003.

[235] M. Abbaszadeh and A. Hezarkhani, "Enhancement of hydrothermal alteration zones using the spectral feature fitting method in rabor area, kerman, iran," *Arab. J. Geosci.*, vol. 6, no. 6, pp. 1957–1964, Jun. 2013.

[236] F. A. Kruse, "Mineral mapping with AVIRIS and EO-1 hyperion," in *Proceedings of the 12th JPL Airborne Earth Science Workshop*, 2004.

[237] H. M. Rajesh, "Application of remote sensing and GIS in mineral resource mapping-an overview," *J. Mineral. Petrol. Sci.*, vol. 99, no. 3, pp. 83–103, 2004.

[238] F. D. Van Der Meer and S. J. De Jong, "Spectral mapping methods: many problems, some solutions," in *Proceedings of the 3rd EARSeL workshop on imaging spectroscopy*, M. Habermeyer, A. Mülle, and S. Holzwarth, Eds., Herrsching, Germany, 2003, pp. 146–162.

[239] A. A. Green, M. Berman, P. Switzer, and M. D. Craig, "A transformation for ordering multispectral data in terms of image quality with implications for noise removal," *IEEE Transactions on geoscience and remote sensing*, vol. 26, no. 1, pp. 65–74, 1988.

[240] M. K. Tripathi and H. Govil, "Evaluation of aviris-ng hyperspectral images for mineral identification and mapping," *Heliyon*, vol. 5, no. 11, p. e02931, 2019.

[241] R. Jain and R. U. Sharma, "Mapping of mineral zones using the spectral feature fitting method in jahazpur belt, rajasthan, india," *Internat. Res. Jour. Engg. Tech.,(IRJET)*, vol. 5, pp. 562–567, 2018.

[242] F. A. Kruse, A. B. Lefkoff, and J. B. Dietz, "Expert system-based mineral mapping in northern death valley, California/Nevada, using the airborne Visible/Infrared imaging spectrometer (AVIRIS)," *Remote Sens. Environ.*, vol. 44, no. 2-3, pp. 309–336, May 1993.

[243] J. W. Boardman and F. A. Kruse, "Analysis of imaging spectrometer data using N-dimensional geometry and a mixture-tuned matched filtering approach," *IEEE Transactions on Geoscience and Remote Sensing*, vol. 49, no. 11, pp. 4138–4152, 2011.

[244] E. EX, "Envi ex user's guide," 2009.

[245] A. El-Nahry and U. Altinbas, "Processing and analyzing advanced hyperspectral imagery data for identifying clay minerals. a case study," *Journal of Applied Science Research*, vol. 2, no. 4, pp. 232–238, 2006.

[246] E. Ben-Dor, S. Chabrillat, J. A. M. Demattê, G. R. Taylor, J. Hill, M. L. Whiting, and S. Sommer, "Using imaging spectroscopy to study soil properties," *Remote Sens. Environ.*, vol. 113, pp. S38–S55, Sep. 2009.

[247] F. D. Van Der Meer, H. M. Van Der Werff, F. J. Van Ruitenbeek, C. A. Hecker, W. H. Bakker, M. F. Noomen, M. Van Der Meijde, E. J. M. Carranza, J. B. De Smeth, and T. Woldai, "Multi-and hyperspectral geologic remote sensing: A review," *International Journal of Applied Earth Observation and Geoinformation*, vol. 14, no. 1, pp. 112–128, 2012.

[248] C. S. Verdel, D. Knepper, K. E. Livo, V. Mclemore, B. Penn, and R. Keller, "Mapping minerals at the copper flat porphyry, new mexico using AVIRIS data," *New Mexico Using AVIRIS Data. InAVIRIS Airborne Geoscience Workshop*, 2001.

[249] F. A. Kruse, "Comparison of AVIRIS and hyperion for hyperspectral mineral mapping," *11th JPL airborne geoscience workshop*, vol. 4, 2002.

[250] R. Jain and R. U. Sharma, "Mapping of mineral zones using the spectral feature fitting method in jahazpur belt, rajasthan, india," *India. Internat. Res. Jour. Engg. Tech*, vol. 5, pp. 562–567, 2018.

[251] S. Gates-Rector and T. Blanton, "The powder diffraction file: a quality materials characterization database," *Powder Diffr.*, vol. 34, no. 4, pp. 352–360, Dec. 2019.

[252] I. F. Macías-Quiroga, G. I. Giraldo-Gómez, N. R. Sanabria-González *et al.*, "Characterization of colombian clay and its potential use as adsorbent," *The Scientific World Journal*, vol. 2018, 2018.

[253] A. Authier, "Dynamical theory of x-ray diffraction," *International Tables for Crystallography*, pp. 534–551, 2006.

[254] X. Zhou, D. Liu, H. Bu, L. Deng, H. Liu, P. Yuan, P. Du, and H. Song, "XRD-based quantitative analysis of clay minerals using reference intensity ratios, mineral intensity factors, rietveld, and full pattern summation methods: A critical review," *Solid Earth Sci.*, vol. 3, no. 1, pp. 16–29, Mar. 2018.

[255] L. Lutterotti, M. Bortolotti, G. Ischia, I. Lonardelli, and H. Wenk, "Rietveld texture analysis from diffraction images," *Z. Kristallogr. Suppl*, vol. 26, pp. 125–130, 2007.

[256] G. K. Kome, R. K. Enang, F. O. Tabi, and B. P. K. Yerima, "Influence of clay minerals on some soil fertility attributes: A review," *Open J. Soil Sci.*, vol. 09, no. 09, pp. 155–188, 2019.

[257] R. Jing, D. Gu *et al.*, "Rapid analysis of feldspar by x-ray diffractometry rietveld refinement method," *Rock and Mineral Analysis*, vol. 36, no. 5, pp. 489–494, 2017.

[258] G. J. Churchman and D. J. Lowe, *Handbook of soil sciences*, 2nd ed., ser. Handbook of Soil Science, P. M. Huang, Y. Li, and M. E. Sumner, Eds. Boca Raton, FL: CRC Press, Nov. 2011.

[259] F. Deon, F. van Ruitenbeek, H. van der Werff, M. van der Meijde, and C. Marcatelli, "Detection of interlayered illite/smectite clay minerals with xrd, sem analyses and reflectance spectroscopy," *Sensors*, vol. 22, no. 9, p. 3602, 2022.

[260] T. Magendran and S. Sanjeevi, "Hyperion image analysis and linear spectral unmixing to evaluate the grades of iron ores in parts of noamundi, eastern india," *Int. J. Appl. Earth Obs. Geoinf.*, vol. 26, pp. 413–426, Feb. 2014.

[261] H. Govil, M. K. Tripathi, P. Diwan, and Monika, "Comparative evaluation of AVIRIS-NG and hyperion hyperspectral image for talc mineral identification," in *Data Management, Analytics and Innovation*, ser. Advances in intelligent systems and computing. Singapore: Springer Singapore, 2020, pp. 95–101.

[262] T. Mitran, K. Sreenivas, K. G. Janakirama Suresh, G. Sujatha, and T. Ravisankar, "Spatial prediction of calcium carbonate and clay content in soils using airborne hyperspectral data," *J. Ind. Soc. Remote Sens.*, vol. 49, no. 11, pp. 2611–2622, Nov. 2021.

[263] C. Gomez, P. Lagacherie, and G. Coulouma, "Continuum removal versus PLSR method for clay and calcium carbonate content estimation from laboratory and airborne hyperspectral measurements," *Geoderma*, vol. 148, no. 2, pp. 141–148, Dec. 2008.

[264] T.-T. Wong, "Performance evaluation of classification algorithms by k-fold and leave-one-out cross validation," *Pattern Recognit.*, vol. 48, no. 9, pp. 2839–2846, Sep. 2015.

[265] S. Bhattacharya, H. Kumar, A. Guha, A. K. Dagar, S. Pathak, S. Mondal, K. V. Kumar, W. Farrand, S. Chatterjee, S. Ravi *et al.*, "Potential of airborne hyperspectral data for geo-exploration over parts of different geological/metallogenic provinces in india based on aviris-ng observations," *Current Science*, vol. 116, no. 7, pp. 1143–1156, 2019.

Appendix

Appendix-1: Location of soil sampling sites along with their mineral content at Ambaji

Sr. No.	Latitude	Longitude	Kaolinite (%)	Montmorillonite (%)	Illite (%)
1	24.26677	72.54754	44	39	11
2	24.26854	72.55293	47	34	10
3	24.26852	72.56026	49	33	8
4	24.2676	72.56829	51	25	12
5	24.26116	72.54683	43	35	15
6	24.25931	72.54454	48	32	17
7	24.25154	72.5456	44	36	13
8	24.24746	72.54533	46	31	18
9	24.24489	72.54558	56	26	7
10	24.24269	72.54616	44	34	9
11	24.25673	72.55515	45	31	13
12	24.249	72.55135	54	24	11
13	24.24477	72.55107	52	25	8
14	24.24298	72.55541	41	31	18
15	24.24338	72.56036	46	25	15
16	24.24715	72.56779	49	30	10
17	24.25435	72.56608	44	35	13
18	24.24733	72.56334	54	21	8
19	24.25228	72.57009	43	37	12
20	24.26	72.57445	44	38	14
21	24.25909	72.55729	41	32	10
22	24.26082	72.55487	46	30	11
23	24.25408	72.55906	51	29	10
24	24.24544	72.57516	53	27	8
25	24.25309	72.55465	48	35	18
26	24.26214	72.55474	50	39	7
27	24.2448	72.56534	44	32	17
28	24.26416	72.57449	52	27	11
29	24.25783	72.55813	53	21	12
30	24.24764	72.55633	43	36	9

Appendix-2: Location of soil sampling sites along with their mineral content at Udaipur

Sr. No.	Latitude	Longitude	Kaolinite (%)	Montmorillonite (%)	Illite (%)
1	23.9877074	73.583408	26	39	12
2	24.0005536	73.642836	24	41	9
3	24.3828904	73.6393864	18	41	10
4	23.9572788	73.5784604	21	44	8
5	23.9885623	73.5840264	20	44	7
6	24.0849241	73.6788449	25	44	10
7	24.3837254	73.6381672	27	46	9
8	24.383517	73.6384874	24	46	14
9	24.2949081	73.6768453	21	48	12
10	23.911679	73.5559789	24	49	12
11	24.294986	73.6770684	35	51	11
12	24.02456	73.630265	36	51	10
13	23.9886511	73.5895836	31	52	14
14	23.9875073	73.5842359	30	53	13
15	23.9843413	73.5683784	30	54	15
16	24.2708276	73.574945	35	54	16
17	24.2710347	73.6752921	28	54	17
18	24.2871284	73.672907	29	55	17
19	22.2284256	73.6893145	32	55	12
20	24.2886017	73.6733503	33	57	15
21	23.9121094	73.5548898	35	57	19
22	24.2290319	73.688483	40	58	18
23	24.229335	73.6888483	31	59	22
24	24.2714899	73.6750288	39	59	20
25	24.3837694	73.6379441	43	62	22
26	24.2876344	73.6732772	42	44	11
27	24.3844076	73.6378992	39	47	15
28	24.294736	73.6769926	33	52	19
29	24.0099684	73.6559765	40	61	19
30	24.0853857	73.679396	31	50	13